

TRANSITION METAL VAPOR CRYOCHEMISTRY

WILLIAM J. POWER* and GEOFFREY A. OZIN

Lash Miller Chemical Laboratories and Erindale College,
University of Toronto, Toronto, Ontario, Canada

I. Introduction	80
II. Atomic, Diatomic, and Cluster Species.	81
A. Sc, Ti, and V Studies	83
B. Nb and Mo Studies	85
C. Co, Rh, and Ir Studies.	86
D. Ni, Pd, and Pt Studies.	89
E. Cu, Ag, and Au Studies	92
F. Bimetallic Clusters	96
III. New Cluster Techniques	101
A. Cryophotoclustering.	101
B. Selective Naked-Cluster Cryophotochemistry	103
C. Relative Extinction-Coefficient Measurements for Naked Silver Clusters by Photoaggregation Techniques.	106
D. Photonucleation Kinetic Studies	107
E. Photomanipulation of Cluster Distributions.	107
F. Photosensitive Bimetallic Aggregation	108
IV. Cluster Complexes	114
A. CO Species	115
B. O ₂ Species	118
C. C ₂ H ₂ Species	120
V. Classical Inorganic Ligands.	130
A. CO Complexes	130
B. O ₂ Complexes and Oxides	138
C. N ₂ Complexes and Nitrides	140
D. Miscellaneous Complexes	143
VI. Organometallic Complexes	145
A. Arene Complexes	145
B. Alkene and Alkyne Complexes.	149
C. Oxidative Addition Reactions	158
D. Organic Reactions.	160
E. Miscellaneous Organometallic Species	163
VII. Conclusion	166
Addendum.	166
Addendum References	168
References.	169

* Present address: Imperial Oil Limited, Sarnia, Ontario, Canada.

I. Introduction

When we were invited to write a review on an "in vogue" research topic, especially one that had previously been surveyed, there was an initial tendency to try to justify the effort. The burgeoning field of metal-vapor cryochemistry presents little difficulty in this regard, as the past two years have again witnessed continued growth of interest, impressive accomplishments, and the development of a large body of new literature. We therefore consider that a general, state-of-the-art overview of the topic examining selected, research highlights since 1976, rather than presenting comprehensive tabulations of papers, would be both timely and appropriate.

Perusal of the recent literature revealed that Timms and Turney (179) had initially evaluated the organometallic, synthetic versatility of the metal-atom technique both for main-group- and transition-metal vapors, and that Burdett (21) had comprehensively covered the metal-atom and photochemical aspects of matrix-entrapped, metal carbonyl and related complexes. A conference report on the matrix photochemistry of metal carbonyls has also appeared (191), as well as a survey of the spectroscopic aspects of metal-atom chemistry (99). A significant indicator of the impressive recognition that metal-atom and matrix chemistry have earned may be seen from the list of recent recipients of Coblentz, Corday-Morgan, and Meldola awards (3). Ozin (100) has presented a view of the "metal cluster-metal surface analogy" through the eye of matrix chemistry. Klabunde (64) has written on the organic chemistry of metal vapors, with particular emphasis on active metal slurries. The synthetic and catalytic significance of Klabunde's (64) approach to finely dispersed, metal clusters should be compared with the Wada (196) type of gas-evaporation technique and the Rieke (158) type of metal halide-alkali metal, solution-reduction method for generating ultrafine, metal particles. Complete works have now been devoted to the subject of matrix cryochemistry, as seen in a monograph by Craddock and Hinchcliffe (23) and the more comprehensive coverage of Moskovits and Ozin (91).

In its more recent phase of development, the multidisciplinary nature of metal-vapor cryochemistry is becoming evident with, for example, chemical physicists attempting to explain subtle, spectroscopic phenomena associated with matrix-entrapped, metal atomic species (75-77). A clear display of renewed physics interest in the field may be seen from a glance at the proceedings of the International Conference of Matrix Isolation Spectroscopy (*Ber. Bunsenges. Phys. Chem.*, January, 1978). In addition, matrix reactions are providing unique, syn-

thetic pathways to "experimental, chemisorption models" for theoretical chemists to calculate on, with, for example, $\text{Ni}(\text{C}_2\text{H}_4)/\text{Ni}_2(\text{C}_2\text{H}_4)$ (101) providing the basis for a GVB-CI-MO analysis (101), coordinatively unsaturated, metal carbonyl fragments being models for Hoffman and Elian's (53) stereochemical predictions, and naked metal-cluster species providing the stimulus for EHMO (2) and SCF-X α -SW (102, 113) computations for the determination of electronic, spectral, and bonding properties of small, ligand-free, metal clusters, as well as the evolution of bulk-metal properties.

Another interdisciplinary thrust, particularly from the groups of Ozin (100, 103) and Moskovits (91, 95, 96a), is the correlation of the bonding of "supercoordinatively" unsaturated, M_nL matrix-stabilized, cluster systems with that of L chemisorbed onto the corresponding bulk metal, M. It is becoming fairly evident that complexes synthesized under matrix conditions, particularly with CO, N_2 , O_2 , olefin, and acetylene ligands, may be used [with caution (96b)] as chemisorption models for evaluating localized-bonding aspects of these same ligands adsorbed on metal surfaces. Furthermore, the complexes may often be considered to be model representations for reactive intermediates involved in heterogeneously catalyzed reactions (105, 132, 136). Bimetal-vapor cocondensations and bimetallic, photoaggregation, matrix experiments (57, 78, 89, 113-116, 203) have pointed the way to an extremely promising method for securing spectroscopic and chemical data on mixed metal-cluster systems. Such data are likely to throw considerable light on a number of unanswered questions in the field of alloy and bimetallic-cluster catalysis (167).

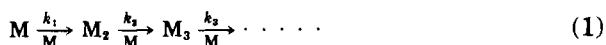
From this brief exposure to the pervasive character of metal-vapor cryochemistry and matrix-isolation spectroscopy, it is clear that a field of multidisciplinary concern is surveyed. However, in this review, we shall focus on those accomplishments of greatest interest to the inorganic community in general, while pointing out, where applicable, the relevance of the results to other branches of chemistry and physics.

II. Atomic, Diatomic, and Cluster Species

It is now fairly well established that atomic and few-atom cluster arrays can be generated and trapped in weakly interacting matrices (91), and subsequently scrutinized by various forms of spectroscopy. Up to this time, IR-Raman-UV-visible absorption and emission-esr-MCD-EXAFS-Mössbauer methods have been successfully applied to matrix-cluster samples. It is self-evident that an understanding of the methods of generating and identifying these species is a prerequisite for

their subsequent use in the synthesis of mononuclear, binuclear, or higher, cluster complexes, and so we shall briefly dwell on this point.

The problem of assigning observed atomic, and cluster-matrix, spectral features to individual species of known nuclearity was treated by Moskovits and Hulse (92), and the results were first applied to the Cr_2 (106) diatomic. In the majority of cluster experiments referred to in this Chapter, the growth-decay behavior of vibrational, or electronic, spectral features as a function of matrix-metal concentration must be analyzed, the objective being the determination of cluster nuclearity through an analysis of the deposition process. Two models were investigated, statistical and kinetic. The statistical model (92) attempted to simulate the occurrence of neighboring metal-atoms in a matrix by means of a Monte Carlo calculation, by way of the random placement of atomic reagent within the lattice confines of a face-centered-cubic network of inert-gas atoms. Counting procedures established that the concentration ratio, $[\text{M}_n]/[\text{M}]$, is roughly proportional to the metal concentration raised to the power $(n - 1)$, up to $\sim 10\%$ of total metal. The steady-state, kinetic model (92) involved metal-atom encounters in the reaction zone at the matrix surface during matrix deposition. This fluid surface-region, being quite mobile, facilitates metal-atom diffusion and aggregation, which can be expected to ensue up to the point of matrix solidification. After this point, bulk diffusion of atoms and clusters is assumed to contribute negligibly to further cluster growth. Simulation of the large number of metal-atom encounters in the semi-liquid region was achieved by assembling a set of simultaneous, linear, differential equations to describe the nucleation sequence.



Solutions were obtained, either analytically or numerically, on a computer. The quenched-reaction, kinetic model considered that the nucleation sequence of reactions evolves to some time τ_q (the quenching time) and then promptly halts. Both kinetic models yield a result having the same general form as the statistical model, namely,

$$[\text{M}_n]/[\text{M}] \propto [\text{M}_0]^{n-1}, \quad (2)$$

although Moskovits and Hulse's study (92) indicated that the quenched-reaction model fits the available experimental data slightly better than the steady-state model. Thus, the slope of a $\log ([\text{M}_n]/[\text{M}])$ versus $\log [\text{M}_0]$ plot (where $[\text{M}_0]$ is the total metal concentration) provides a convenient and direct analytical route to metal-cluster size. By similarly analyzing the nucleation sequence in the presence of various

concentrations of a reactive ligand L, the analogous relationship, namely,

$$[M_n L_m]/[ML_p] \sim [M_0]^{n-1}, \quad (3)$$

is arrived at; that is, the absorbance of a cluster complex containing n metal atoms, when normalized with respect to that of a mononuclear complex, is approximately proportional to the metal concentration raised to the power $(n - 1)$. Consequently, log-log plots for suspected, cluster species $M_n L_m$ relative to known mononuclears ML_p , as a function of the total, metal concentration provide access to cluster-size evaluation. The utility of these expressions, both for naked metal clusters and for cluster complexes, will become evident throughout this section.

A. Sc, Ti, AND V STUDIES

Ozin *et al.* (107, 108) performed matrix, optical experiments that resulted in the identification of the dimers of these first-row, transition metals. For Sc and Ti ($4s^2 3d^1$ and $4s^2 3d^2$, respectively), a facile dimerization process was observed in argon. It was found that, for Sc, the atomic absorptions were blue-shifted 500–1000 cm^{-1} with respect to gas-phase data, whereas the extinction coefficients for both Sc and Sc_2 were of the same order of magnitude, a feature also deduced for Ti and Ti_2 . The optical transitions and tentative assignments (based on EHMO calculations) are summarized in Table I.

A somewhat more detailed study of vanadium atoms and dimers has also appeared (108). Figure 1 shows the UV-visible spectra of V and V_2 as a function of vanadium concentration. Figure 2 shows a typical, metal-concentration plot illustrating the aforementioned kinetic anal-

TABLE I
OBSERVED AND CALCULATED OPTICAL SPECTRA FOR
DISCANDIUM AND DITITANIUM (107)

	Optical transition	Obs. (cm^{-1})	Calc. (cm^{-1})
Sc_2	$1\sigma_g \rightarrow 1\sigma_u$	15 100	15 492
	$1\sigma_g \rightarrow 2\sigma_u$	21 050	19 880
	$1\sigma_g \rightarrow 2\pi_u$	29 850	29 558
Ti_2	$1\sigma_g \rightarrow 1\sigma_u$	16 020	15 355
	$1\sigma_g \rightarrow 2\sigma_u$	18 310	16 654
	$1\sigma_g \rightarrow 2\pi_u$	23 250	23 307

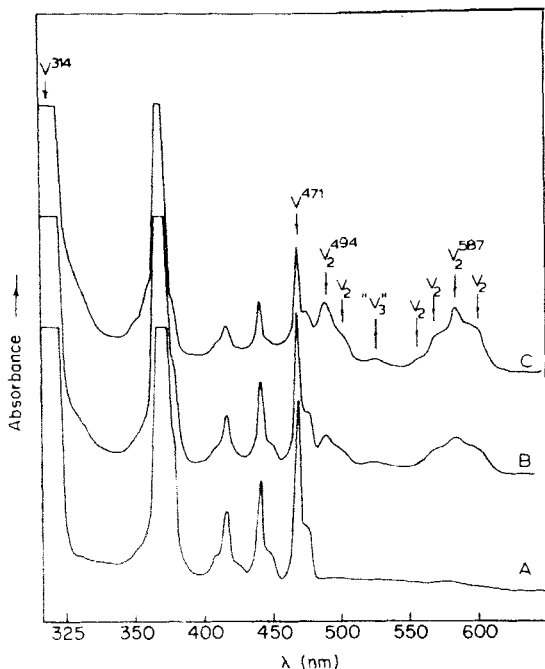


FIG. 1. The UV-visible spectrum of V in Ar matrices at 6–10 K; A, at low V concentrations, showing isolated V atoms, and B and C, at progressively higher V concentrations, showing both V atoms and the growth of V_2 molecules (108).

ysis, and identifying at least two absorptions as being associated with V_2 . The observed, metal-concentration behavior implies that the proposal of dimer formation on the matrix surface, rather than in the gas phase, is a reasonable assumption; in addition, this study was instructive in demonstrating the efficiency of matrix gases of higher molecular weight in quenching this process, that is, fewer dimers formed in Xe and Kr than in Ar under comparable, deposition conditions. The extinction coefficient ratio $\epsilon_V/\epsilon_{V_2}$ was found to be roughly 3.0, in agreement with the results of other studies (91).

Vanadium atom depositions were further studied in alkane matrices (109) in an effort to observe the influence of other low-temperature, matrix environments on the optical spectra and clustering properties of metal atoms. Thus, vanadium atoms were deposited with a series of normal, branched, and cyclic alkanes over a wide range of temperature. The atomic spectra were somewhat broadened compared to those in argon, but the matrix-induced, frequency shifts from gas-phase values were smaller. As shown in Fig. 3, these shifts decrease with in-

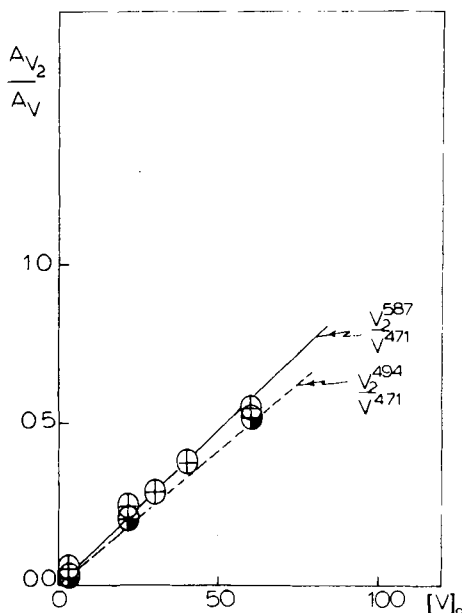


FIG. 2. A plot of the absorbances of typical lines attributed to V_2 , relative to that of a V resonance absorption as a function of the V metal deposition rate at constant Ar deposition rate (108).

creasing chain-length for n -alkanes. In general, under similar experimental conditions, alkane matrices are more efficient than argon for the isolation of atoms over diatomic, and higher, nuclearity clusters, and the isolation efficiency increases with increasing chain-length of the n -alkane matrix-material up to decane. These data may prove useful in tailoring the production of mononuclear complexes for those metals for which dimerization is particularly facile, e.g., Co and Rh. In addition, the higher-temperature, diffusion properties observed for vanadium atoms in these supports may permit the design of specific, metal-atom syntheses which, although kinetically impeded in noble-gas matrices (4.2–40 K), may well proceed in higher-temperature, alkane supports (40–300 K). The potential application of such ideas is unbounded, limited only by the imagination of the metal-atom chemist.

B. Nb AND Mo STUDIES

By use of quantitative, metal-atom, matrix-cocondensation techniques and the kinetic analysis previously discussed, the dimeric spe-

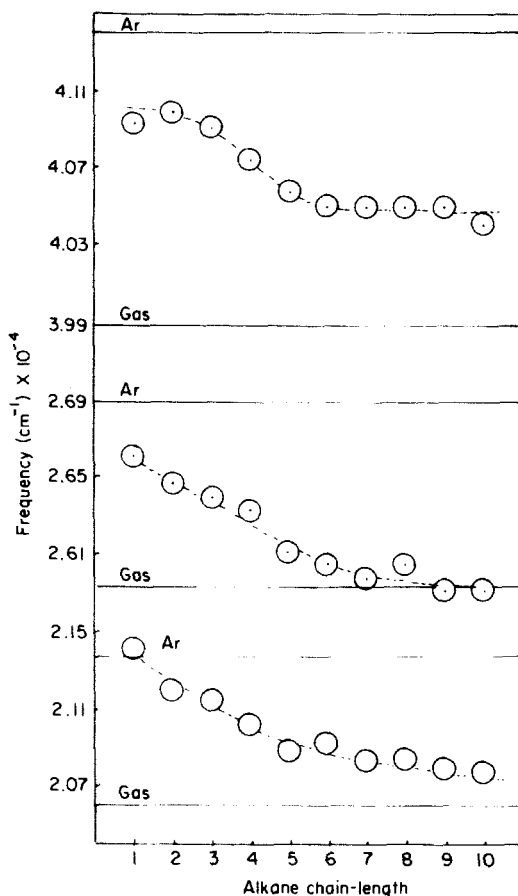


FIG. 3. Frequencies of three representative vanadium atom absorptions in different open-chain C_nH_{2n+2} matrices (where $n = 1-10$), compared to gas-phase and argon-isolated atomic vanadium (109).

cies Nb_2 and Mo_2 were generated (110) and their optical spectra (200–700 nm) established. The spectral assignments of Nb_2 and Mo_2 are summarized in Table II, where they are also compared with their first-row congeners V_2 and Cr_2 . Interestingly, EHMO and $X\alpha$ calculations suggest that a closed-shell configuration for Nb_2 and Mo_2 (at the bond distances listed in Table II) would lead to formally high-order, “pentuple” and “sextuple” bonds, respectively.

C. Co, Rh, AND Ir STUDIES

The metal concentration, matrix, and temperature effects that favor clustering of the cobalt group of metal atoms have been assessed by

Ozin, Hanlan, and Power, using optical spectroscopy (49, 121). In view of the marked temperature-effect observed for the cobalt system, we shall focus on this cluster system here. Evidence for cobalt-atom aggregation at the few-atom extreme first came from a comparison of the optical data for Co:Ar $\approx 1:10^4$ mixtures recorded at 4.2 and 12 K (see Fig. 4). A differential of roughly 8 K in this cryogenic-temperature regime was sufficient to cause the dramatic appearance of an entirely new set of optical absorptions in the regions 320–340 and 270–280 nm (see Fig. 4). Matrix variation, from Ar, to Kr, to Xe, helped clarify atom–cluster, band-overlap problems (see Fig. 5).

The effect of deposition temperature on the clustering ability of Co atoms to form small, cobalt clusters was most revealing in terms of optical assignments, as well as activation-energy considerations. A series of runs with Co:Ar $\approx 1:10^4$ deposited at 4.2, 12, 20, 25, 30, and 35 K (see Fig. 4) nicely demonstrated the gradual progression from isolated Co atoms to mixtures of Co/Co₂ to mixtures of Co/Co₂/Co₃. The most

TABLE II
OBSERVED AND CALCULATED OPTICAL SPECTRA FOR
V₂, Cr₂, Nb₂, AND Mo₂ (110)

	r _e (pm)	D _e (eV)	Assignment	Spectra (nm)	
				Obs.	Calc. ^a
V ₂ ,	190	0.99	1σ _g → 2σ _u	494	521
			1σ _g → 1σ _u	558	558
			1σ _g → 2π _u	^b	350
			2σ _g → 2π _u	588	607
			1π _u → 3σ _g	^b	350
Cr ₂ ,	180	2.65 ^c	1σ _g → 2σ _u	456	494
			1σ _g → 2π _u	340	309
			2σ _g → 2π _u	^b	389
			1π _u → 3σ _g	260	261
Nb ₂ ,	220	1.52	1σ _g → 2σ _u	660	612
			1σ _g → 2π _u	420	512
			1π _u → 3σ _g	280	269
Mo ₂ ,	210	3.45 ^c	1σ _g → 2σ _u	512	500
			1σ _g → 2π _u	308	362
			2σ _g → 2π _u	^d	458
			1π _u → 3σ _g	232	186

^a Only electric-dipole- and spin-allowed electronic transitions in the proximity of the observed transitions are tabulated. ^b Anticipated overlap with atomic absorptions.

^c Note that, because of the different approximations inherent in EH and Xα MO calculations, these assignments do not correlate exactly with those presented in Table VI.

^d The predicted 2σ_g → 2π_u transition at 458 nm and 1δ_g → 2π_u at 490 nm are either too weak to be observed, or accidentally coincident with the Mo₂ absorption at 512 nm.

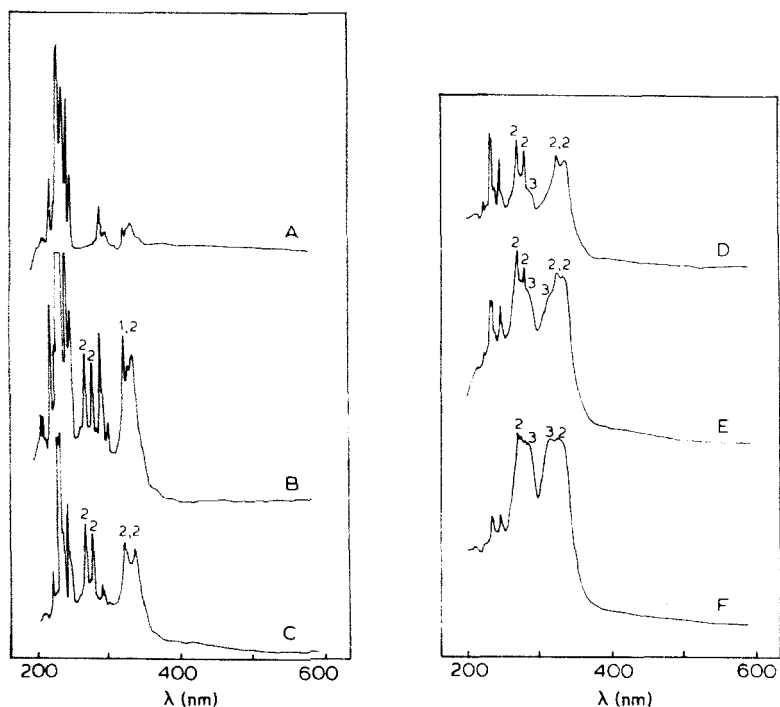


FIG. 4. The ultraviolet-visible absorption spectra of Co:Ar $\approx 1:10^4$ mixtures deposited at (A) 4.2 K, (B) 10–12 K, (C) 20 K, (D) 25 K, (E) 30 K, and (F) 35 K, showing the progression from isolated Co atoms to Co/Co₂ and Co/Co₂/Co₃ mixtures (49, 154).

dramatic realization of the presence of the third Co species is seen in the 35 K deposition (see Fig. 4), where the strongest, Co atomic-resonance lines have intensities close to zero, while almost equal absorbances of Co₂ and Co₃ remain. A large number of experiments at various temperatures and cobalt-concentration matrices were performed, and these generally supported the contention of *three* distinguishable, small, cobalt-cluster species ascribed to Co/Co₂/Co₃. Preliminary, spin-unrestricted, SCF-X α -SW calculations (148) of the optical spectrum for Co₂ were found to agree quite well with the observed spectra, as may be seen by reference to Table III.

Iridium, the heaviest element of the cobalt group, was found to display the least tendency towards cluster formation at 10–12 K (49), which, as already mentioned, was quite facile for Co and Rh (49). Considering the plethora of sharp, well-defined, atomic-resonance lines observed for Ir (see Fig. 6) compared to those of Co and Rh, the remarkably impressive correlation with the representation of the gas-

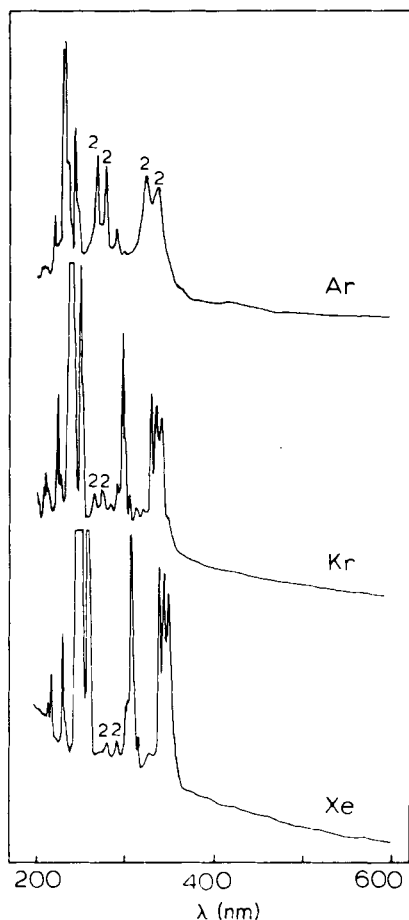


FIG. 5. Correlation of the UV-visible spectra of Co atoms and Co₂ molecules isolated in Ar, Kr, and Xe matrices under identical conditions of temperature and gas and metal deposition rates (49, 154).

phase, atomic-emission spectrum reported by Gruen *et al.* (48) and Moore (90) is interesting. Attempts to generate diiridium or higher iridium clusters in Ar, Kr, and Xe have thus far proved unsuccessful (49).

D. Ni, Pd, AND Pt STUDIES

The optical spectra of the nickel-triad metals have been reinvestigated (111) in Ar, Kr, and Xe matrices, and, although the data for Ni and Pt atoms correlated well both with previous studies and with the

TABLE III
OBSERVED AND CALCULATED (SCF-X α -SW MO) OPTICAL
SPECTRUM OF DICOBALT,^a Co₂ (148)

Obs. (nm)				Calc. (nm) ^b	Assignment ^{c,d}
Ar	Kr	Xe	CH ₄		
340 ^e	321	—	345	353 } 355 }	2 $\sigma_g^+ \rightarrow 2\pi_u$ 1 $\sigma_g^+ \rightarrow 2\pi_u$
320	312	328	325	324	1 $\sigma_u^+ \rightarrow 3\sigma_g^+$
280 ^e	284	290	283	305	1 $\sigma_g^+ \rightarrow 2\sigma_u^+$
270	274	279	274	247 } 252 }	1 $\sigma_g^+ \rightarrow 2\pi_u$ 1 $\pi_u \rightarrow 3\sigma_g^+$

^a Cobalt-cobalt bond-length, 232 pm. ^b 2 $\sigma_g^+ \rightarrow 2\sigma_u^+$, calculated at 484 nm, which is in the region of extremely weak absorptions, possibly associated with Co₂. ^c Ground-state configuration (1 σ_g)²(1 π_u)⁴(1 δ_g)⁴(2 σ_g)²(1 σ_u)⁴(1 π_g)². ^d Preliminary values obtained from ground-state transition-energies; the detailed, spin-unrestricted, transition-state calculation will be reported later (148). ^e Narrow-band, continuous photoexcitation in these bands causes photobleaching of all of the dicobalt absorptions.

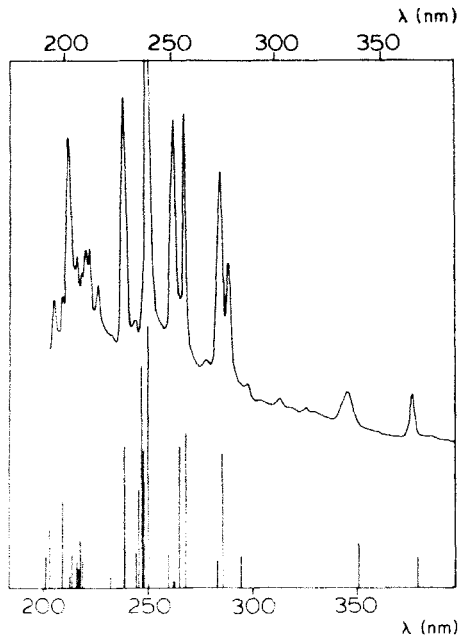
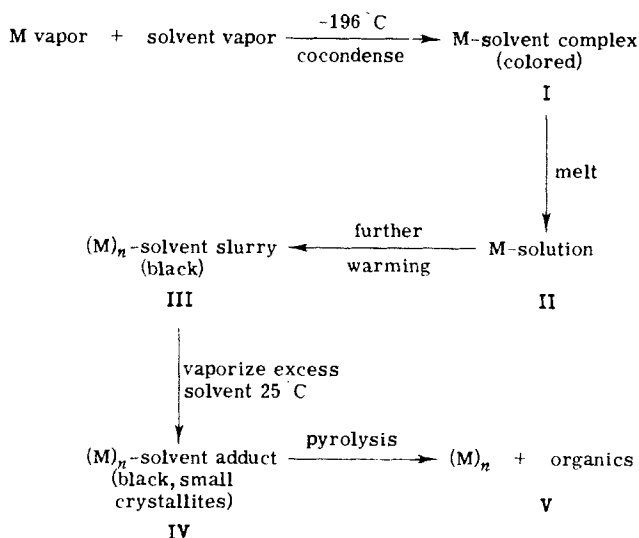


FIG. 6. Optical spectrum of Ir atoms isolated in solid Ar at 10–12 K, compared to the gas-phase atomic transitions of Ir. The stick heights correspond to reported oscillator strengths of gaseous Ir atoms (49).

gas-phase, atomic spectra, the results for Pd were inconsistent with earlier reports (82). It was found that the absorbances originally assigned to Pd atoms at wavelengths greater than 250 nm were actually associated with dinitrogen complexes of Pd (an atmospheric-impurity problem), and the authentic, optical spectrum of Pd atoms was found at higher energy ($\lambda < 250$ nm). Interestingly, shifts in the optical spectra of these metals as a function of inert-gas matrix suggested that Xe is not quite so "inert" as Ar or Kr. The spectral changes on passing from Ar, to Kr, to Xe, are much more drastic for Pd and Pt than for Ni, and it is possible that these metals, being somewhat more polarizable than Ni ("soft," in the Pearson sense), may be considered to be forming a "weak complex" with Xe. Such a weak, bonding interaction had been postulated by Turner and Perutz (192), who, on photodissociating $\text{M}(\text{CO})_6$ to $\text{M}(\text{CO})_5$, found (by UV-visible spectroscopy) that the matrix interacted with the metal atom at the vacant coordination-site. Thus, it is at times necessary to exercise caution in regard to the meaning of the word "inert."

The UV-visible spectra of Ni_2 and Ni_3 have also been identified in argon matrices (93); Ni_2 absorbed at 377, 529, and 410 nm, with vibronic structure on the first two bands, and with spacing of ~ 330 cm^{-1} , and Ni_3 absorbed at 420 and 480 nm, the latter band showing vibrational spacing of ~ 200 cm^{-1} . Higher-nuclearity clusters were observed, but not characterized. After prolonged warm-up of these matrices, nickel colloid was formed (93).

The metal-atom technique and its application in the formation of cluster species has been extended to the clustering of nickel atoms in organic media (66), in that codeposition of metal vapors with certain organic solvents allows the formation of very reactive, high-surface-area, metal slurries (67). The mechanism suggested for the formation of these nickel clusters, summarized in Scheme 1, is made up of a number of discrete stages, beginning with weak complex-formation. The nature of the clusters formed depends on the solvent used and their surface areas range from 45–400 m^2/g (compared to 80–100 m^2/g for Raney Ni) (66). A more detailed study of the reaction of nickel atoms with pentane (68) showed that, during warm-up, the nickel clusters react with the organic compound to yield a "pseudo-nickel organometallic" that has Ni:C:H ratios of 2–5:1:2, is thermally stable to $>200^\circ\text{C}$, and is an extremely active, hydrogenation catalyst. It was suggested (68) that the reaction occurs at $<-100^\circ\text{C}$, probably by oxidative addition to C–H and C–C bonds, to afford the "pseudo complexes." Catalytic studies (69) showed that a Ni-toluene product is also a hydrogenation catalyst, and that Ni-THF is fairly unreactive,



SCHEME 1 (66)

either as a hydrogenation or an olefin-isomerization catalyst. It is informative to contrast Klabunde and Davis's studies (69) with those of Rieke *et al.* (159), who produced similar reactive slurries by the reduction of a metal salt in an ethereal or hydrocarbon solvent with an alkali metal. These nickel-triad slurries were found to insert readily into R-X bonds, a reaction known in metal-atom chemistry for many years (168).

E. Cu, Ag, AND Au STUDIES

Copper clusters containing two to four atoms have been formed (94) in argon and methane, whereas large, colloidal-copper particles resulted in dodecane matrices (94). The authors suggested that the "birth" of the band structure of copper is clearly visible on passing from the dimer to the tetramer, with Cu_4 already possessing many of the features of the bulk metal (94).

Considerable effort has been expended on Ag atoms and small, silver clusters. Bates and Gruen (10) studied the spectra of sputtered silver atoms (a metal target was bombarded with a beam of 2-keV, argon ions produced with a sputter ion-gun) isolated in D_2 , Ne, and N_2 . They found that an inverse relationship between Z_{eff} of the metal atom and the polarizability of rare-gas matrices (as determined from examination of

spin-orbit coupling and crystal-field parameters) could be extended to include silver atoms in D_2 and N_2 matrices, thereby allowing a detailed evaluation of atom-matrix interactions. The correlation breaks down for Ne, presumably because the size of a substitutional site and the polarizability of Ne are such as to cause multiple-site occupation. They also reported (10) data for Ag_2 , which has now been studied in detail in the gas phase (18) [although some of the Ag_2 assignments were confused with unsuspected Ag_3 , also present in the matrix (112)].

Ozin and Huber (112) synthesized and characterized very small silver particles, Ag_n ($n = 2-5$) by conventional deposition methods, as well as by a novel technique that they have termed "cryophotoaggregation." This study will be discussed in detail in Section III. Of interest here is a study of silver atoms and small, silver clusters entrapped in ice and high-molecular-weight paraffin ($n-C_{22}H_{46}$, $n-C_{32}H_{66}$) matrices (146) (see Figs. 7 and 8, and Tables IV and V). Besides the intriguing, multiple-site (solvation) occupancy of atomic silver in ice matrices, and their thermal and photochemical interconvertibility, their extremely

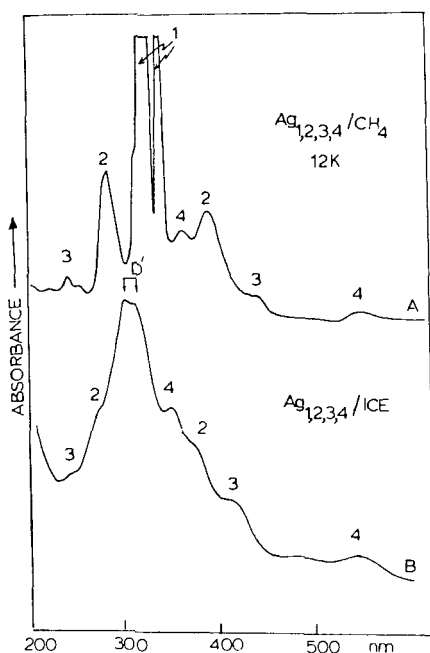


FIG. 7. The optical spectra obtained on depositing (A) silver vapor with methane at 10–12 K at $Ag:CH_4 \approx 1:10^3$, and (B) silver vapor with water vapor at 10–12 K at $Ag:H_2O \approx 1:10^3$, brief warming to 77 K, and recooling to 10–12 K for spectral recording (146).

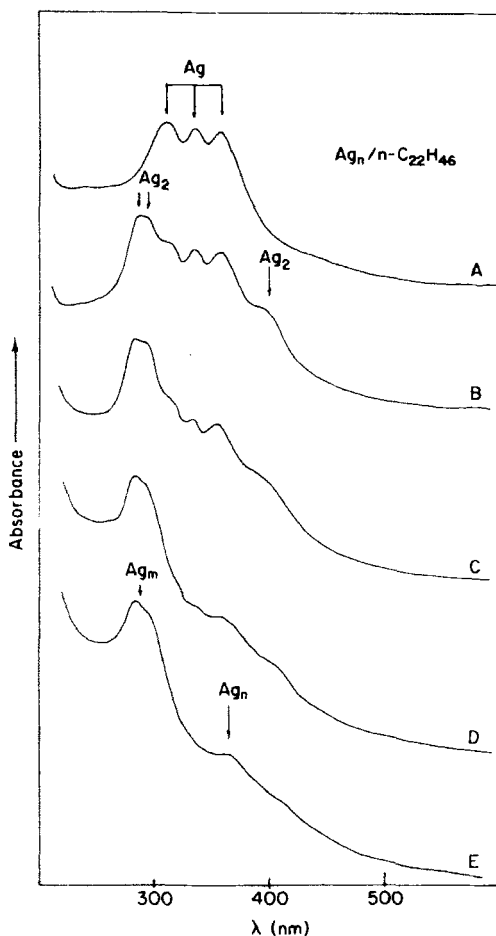


FIG. 8. The optical spectra obtained on depositing silver vapor with $n\text{-C}_{22}\text{H}_{46}$ vapor at 10–12 K, and (A) $\text{Ag}: n\text{-C}_{22}\text{H}_{46} \approx 1:10^4$, (B) $\text{Ag}: n\text{-C}_{22}\text{H}_{46} \approx 1:10^3$, and (C)–(E) showing the progress of annealing (B) at 30, 40, and 80 K, respectively (146).

high, bulk diffusion–aggregation behavior ($0.5 T_{\text{mp}}$) is a most noteworthy feature in terms of potential, supported-cluster, catalyst fabrication (146). In contrast, the glassy, open structures of the silver atom–wax-quenched, condensed films, having considerable chain-mobility built in, even at cryogenic temperatures, resulted in a matrix having poor trapping ability for atoms on deposition, and surprisingly low, bulk diffusion–aggregation temperatures ($0.1 T_{\text{mp}}$) during matrix annealing (146). Aside from inhomogeneous band-broadening effects of the silver, atomic and cluster, optical absorptions in ice and wax matrices, it is

TABLE IV
THE OPTICAL SPECTRA OF $\text{Ag}_{1,2,3,4}$ IN ICE AND METHANE MATRICES
AT 10–12K (146)

Ice matrices (nm)	Methane matrices (nm)	Ag_n cluster assignments in ice
542	528	Ag_4
412	428–418	Ag_3
375–385	380	$\text{Ag}_2 + \text{Ag}$ (site A')
353	360	$\text{Ag}_4 + \text{Ag}$ (site B')
333	333	Ag (site C')
316	320	Ag (site D') + Ag (site C')
301	310	Ag (site D')
270	278	Ag_2
245	252–238	Ag_3

significant to note the relatively minor frequency-perturbations on passing from an environment that could be regarded as a nonpolar paraffin to a highly dipolar, ice lattice (146). While discussing the synthesis of small silver particles, brief mention should be made of the isolation of Ag_8 molecules (165), formed within cubes of eight Ag^+ ions in fully Ag^+ -exchanged zeolite A that had been dehydrated under vacuum at elevated temperatures. A crystal structure is shown in Fig. 9.

Techniques other than UV-visible spectroscopy have been used in matrix-isolation studies of Ag; see, for example, some early ESR studies by Kasai and McLeod (56). The fluorescence spectra of Ag atoms isolated in noble-gas matrices have been recorded (76, 147), and found to show large Stokes shifts when optically excited via a $^2\text{S}_{1/2} \rightarrow ^2\text{P}_{1/2,3/2}$ atomic transition which is threefold split in the matrix by spin-orbit and vibronic interactions. The large Stokes shifts may be explained in terms of an excited state silver atom-matrix cage complex; in this

TABLE V
OPTICAL SPECTRA OF Ag ATOMS AND Ag_2 DIMERS IN METHANE AND
HIGH-MOLECULAR-WEIGHT PARAFFIN WAX ($n\text{-C}_{22}\text{H}_{46}$, $n\text{-C}_{32}\text{H}_{66}$)
MATRICES (146) AT 10–12 K

CH_4	$n\text{-C}_{22}\text{H}_{46}$	$n\text{-C}_{32}\text{H}_{66}$	Assignment
380	390	390	Ag_2
333	357	360	Ag
320	334	338	Ag
310	312	315	Ag
278	298 } 284 }	300 } 284 }	Ag_2
			Ag_2

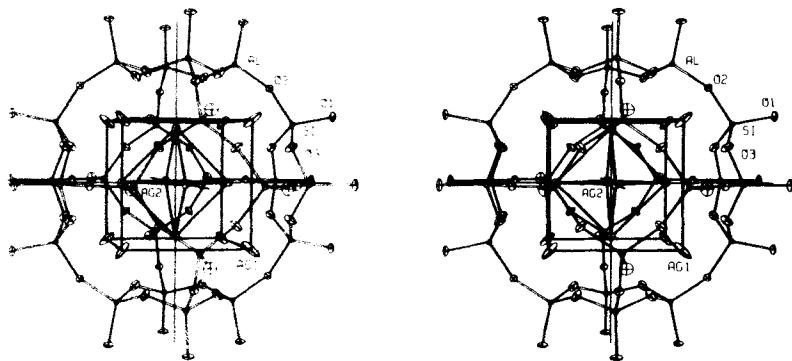


FIG. 9. A stereoview of a sodalite unit containing an octahedral Ag_6 molecule within a cube of eight Ag^+ ions is shown, using ellipsoids of 20% probability. The ions at $\text{Ag}(3)$ occupy 8-ring sites and are not shown (165).

way, the ensuing photoaggregation observed by Ozin and Huber (112) may be rationalized (see later). Raman data have also been gathered for Ag_2 and Ag_3 (163) in solid Kr, a number of bands being observed below 220 cm^{-1} . The two strongest, at 194 and 120 cm^{-1} , were assigned to Ag_2 and Ag_3 , respectively, and the authors speculated that the observation of only one band for Ag_3 suggests that the trimer is linear, in agreement with previous MO calculations (5). However, laser-Raman investigations of this system unveiled unsuspected, laser photoaggregation and resonance Raman-fluorescence complications that have necessitated a re-evaluation of the silver-cluster, vibrational assignments (164).

Theoretical analyses (75–77) of the matrix-induced changes in the optical spectra of isolated, noble-metal atoms have also been made. The spectra were studied in Ar, Kr, and Xe, and showed a pronounced, reversible-energy shift of the peaks with temperature. The authors discussed the matrix influence in terms of level shift-differences, as well as spin-orbit coupling and crystal-field effects. They concluded that an increase in the matrix temperature enhances the electronic perturbation of the entrapped atom, in contrast to earlier prejudices that the temperature dilation of the surrounding cage moves the properties of the atomic guest towards those of the free atom.

F. BIMETALLIC CLUSTERS

In 1977, a number of groups independently demonstrated that matrix-isolation methods could be used for generating, isolating, and

spectroscopically probing small, bimetallic clusters. For example, Zmbova *et al.* (203) formed AuLi via the simultaneous vaporization of Au and Li from separate Knudsen cells. They monitored the product by IR spectroscopy in various matrix supports (see Fig. 10). The vibrational frequencies for AuLi were found to be strongly dependent on the kind of matrix gas used and are split into two components for both isotopomers, Au⁷Li (A) and Au⁶Li (B), in all cases (multiple trapping site effect). Using an empirical relationship, they estimated the gas phase frequencies $\nu_{\text{Au-}^6\text{Li}}$ at $746 \pm 10 \text{ cm}^{-1}$, and $\nu_{\text{Au-}^7\text{Li}}$ at $705 \pm 10 \text{ cm}^{-1}$, with $k_{\text{AuLi}} = 1.90 \pm 0.03 \text{ mdyn/100 pm}$.

Simultaneous with this work, Ozin and co-workers were independently investigating other bimetallic combinations. When Cr and Mo were cocondensed (133) together in Ar, using the apparatus shown in Fig. 11, a controlled pathway to CrMo was found. This molecule had previously been observed in the gas phase (30) from flash photolysis of a mixture of Cr(CO)₆ and Mo(CO)₆ vapors. The molecule was identified (UV-visible spectroscopy) by a series of Cr/Mo/Ar concen-

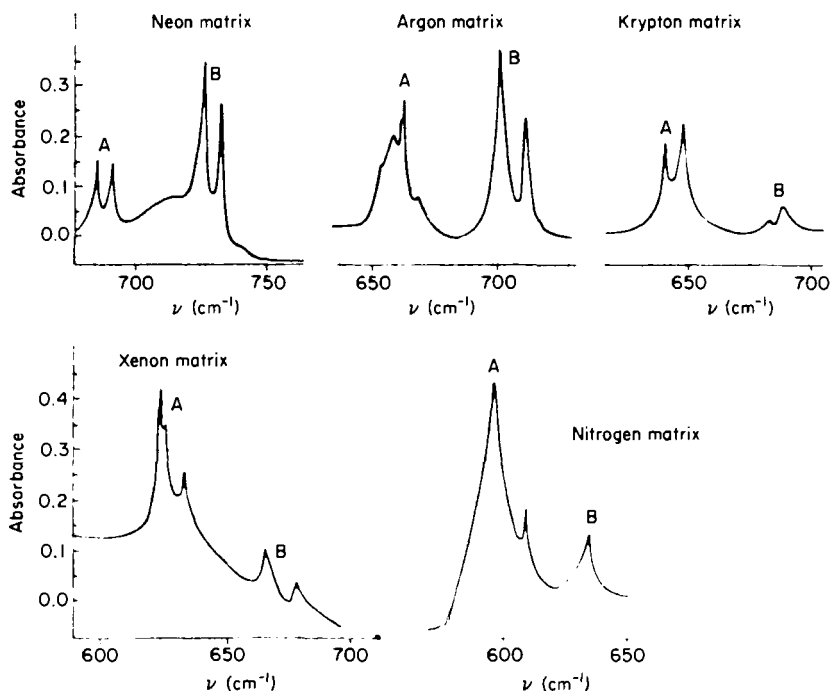


FIG. 10. IR absorption spectra of the species AuLi in various matrices (203).

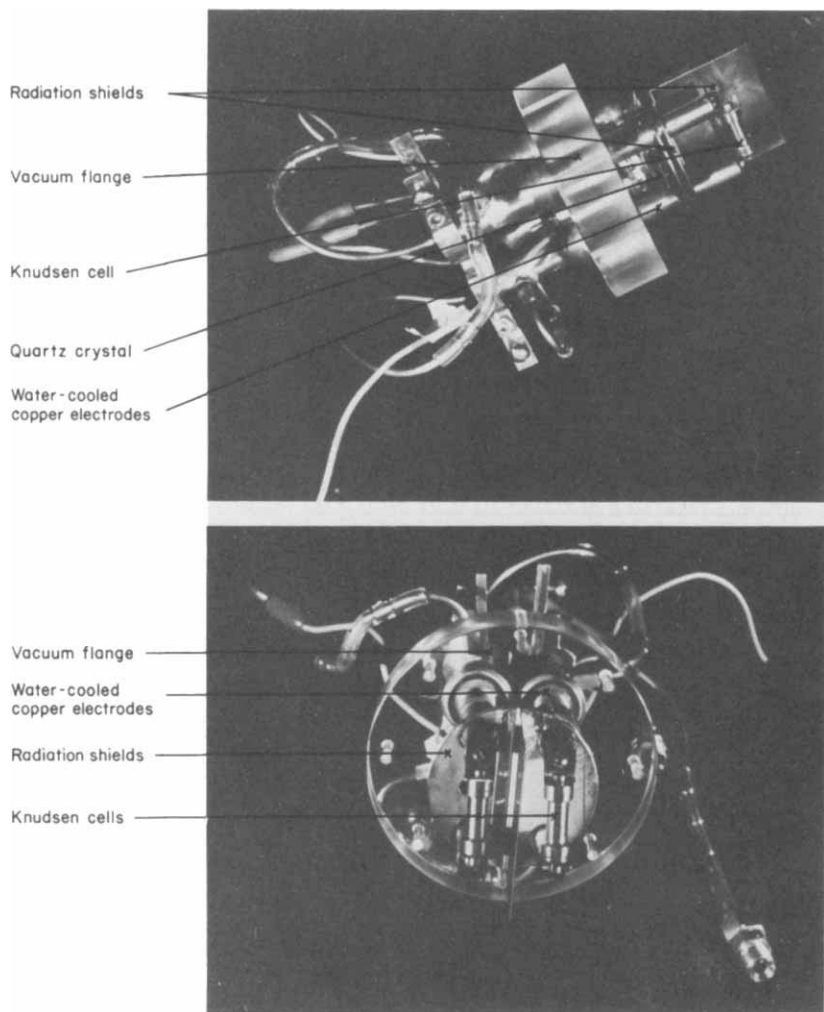


FIG. 11. Photograph of the four-electrode, vacuum flange and dual, quartz crystal, microbalance assembly, (A) side view, and (B) front view, used for mixed Cr atom, Mo atom matrix depositions with simultaneous monitoring of the individual metal flows. (The resolution of the microbalance is $\sim 10^{-8}$ g) (113).

tration experiments; the spectra of Cr_2 , Mo_2 , and CrMo are summarized in Table VI, along with assignments based on SCF- $X\alpha$ -SW calculations (113). Interestingly, there is a close correspondence between the energies of the observed transitions of CrMo and those cal-

culated under the assumption that

$$\nu_{\text{CrMo}} = 0.5(\nu_{\text{Cr}_2} + \nu_{\text{Mo}_2}). \quad (4)$$

Such an averaging effect of the transition energies of CrMo relative to Cr₂ and Mo₂ is intuitively understandable, as the electronic ground-states of Cr and Mo atoms are both $ns^1(n-1)d^5$ and those of Cr₂ and Mo₂ are both considered to be $1\sigma_g^2 1\pi_u^4 2\sigma_g^2 1\delta_g^4$. Furthermore, the Cr 4s, 3d and the Mo 5s, 4d atomic orbitals, considered to be the main contributors to the metal-metal bonding in Cr₂/CrMo/Mo₂ are known to have similar energies. Further discussion of these bimetallics formed by cryophotoclustering methods will be found in Section III.

Montano (89) developed matrix Mössbauer spectroscopy to the point of being able to identify FeMn, FeCo, FeNi, and FeCu bimetallics. In these combinations, an increase in the electron density at the ⁵⁷Fe nu-

TABLE VI
ELECTRONIC TRANSITIONS OF Cr₂, CrMo, AND Mo₂, AS CALCULATED
BY THE SCF-X α -SW METHOD^{a,b} (113)

Transition	Molecule	Calc. ^c	Exptl.
1 $\delta_g \rightarrow 1\delta_u$	Cr ₂	12.7	
	Mo ₂	14.4	
2 $\sigma_g \rightarrow 1\sigma_u$	Cr ₂	24.9	21.7
2 $\sigma \rightarrow 3\sigma$	CrMo	22.0	20.6
2 $\sigma_g \rightarrow 1\sigma_u$	Mo ₂	21.8	19.4
2 $\sigma_g \rightarrow 2\sigma_u$	Cr ₂	28.8	29.4
2 $\sigma \rightarrow 4\sigma$	CrMo	28.0	31.1?
2 $\sigma_g \rightarrow 2\sigma_u$	Mo ₂	30.1	32.5
1 $\pi_u \rightarrow 1\pi_g$	Cr ₂	32.0	^d
1 $\pi \rightarrow 2\pi$	CrMo	31.9	^d
1 $\pi_u \rightarrow 1\pi_g$	Mo ₂	40.1	^d
1 $\sigma_g \rightarrow 1\sigma_u$	Cr ₂	36.5	38.0
1 $\sigma \rightarrow 3\sigma$	CrMo	38.1	40.3
1 $\sigma_g \rightarrow 1\sigma_u$	Mo ₂	45.4	43.1
1 $\sigma_g \rightarrow 2\pi_u$	Cr ₂	40.2	^e
	Mo ₂	47.1	^e

^a Band positions are given in $\text{cm}^{-1} \times 10^3$. The calculated values were obtained by using the relation $1 \text{ eV} = 8.06548 \times 10^3 \text{ cm}^{-1}$. ^b See footnote c in Table II. ^c Explicit predictions of the singlet (spin-allowed) transitions, except for the $1\delta_g \rightarrow 1\delta_u$ and $1\pi_u \rightarrow 1\pi_g/1\pi \rightarrow 2\pi$ excitations, where the predictions are of the average transition-energy to the four singlet-states arising from the excited, orbital configuration. ^d Either too weak to be observed or obscured by free atom absorptions. ^e Could possibly be associated with the weak bands observed at 268 nm for Cr₂ and 226 nm for Mo₂, respectively. If this is, in fact, true, the weak band at $\sim 255 \text{ nm}$ for CrMo could be the corresponding $1\sigma \rightarrow 3\pi$ transition.

cleus was observed on going from Cu to Ni, with the FeNi molecule having the weakest bond. In FeNi, the quadrupole splitting of the Mössbauer spectrum is half the value of Fe₂, indicating a different, orbital ground-state for FeNi. By contrast, FeCo is more strongly bound, this being reflected in a more positive, isomer shift. A typical spectrum is shown in Fig. 12.

Kasai and McLeod (57, 58) also studied a series of bimetallic diatomics, AgM (M = Mg, Ca, Sr, Be, Zn, Cd, or Hg), by ESR spectroscopy. For all of these species, the hyperfine coupling to the Ag nucleus was found to be isotropic. It was shown that the unpaired electron resides in an orbital resulting essentially from an anti-bonding combination of the valence s orbitals of the Ag and M atoms. A typical spectrum is shown in Fig. 13.

Some macroscale, bimetal-vapor, cryochemical reactions involving group IA/IB-ammonia cocondensations have pointed the way to solvated, transition-metal anions of the type M⁻. Thus, in sharp contrast to the Li/Au/Ar, 10–12 K, matrix reactions of Zmbova *et al.* (203) that led to the IR detection of molecular ^{6,7}LiAu, Lagowski and Peer (79b) discovered that simultaneous M/Au/NH₃ cocondensations at 77 K (M = Li, K, Rb, or Cs) resulted in solutions at -65°C that display gradual loss of the 1850-nm, solvated-electron absorption, with concomitant growth of an intense, UV absorption in the range of 277 to 289 nm, having ϵ in the range of 1.8 to 7×10^4 L mol⁻¹ cm⁻¹. The

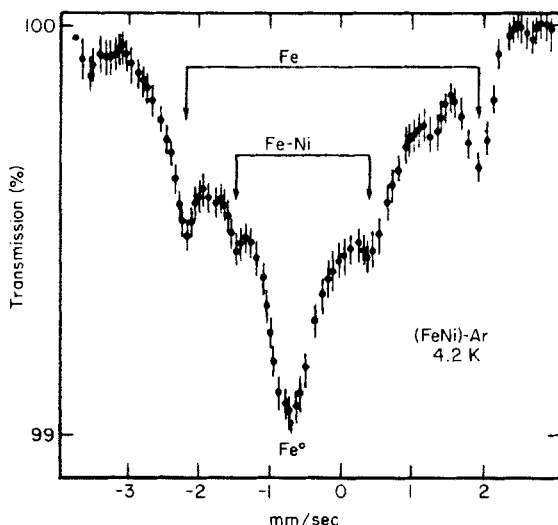


FIG. 12. Mössbauer spectrum of an argon matrix containing iron and nickel (89).

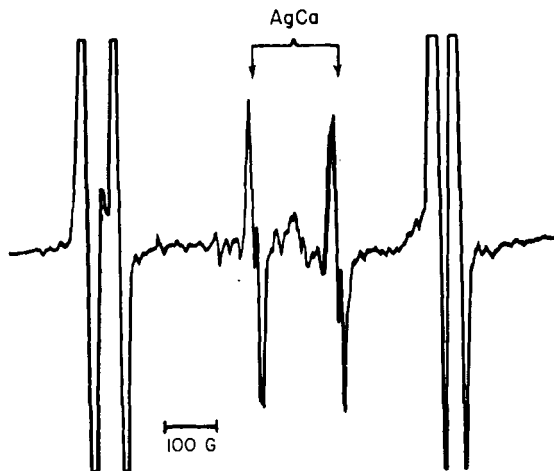


FIG. 13. ESR spectrum of AgCa generated in an argon matrix (58).

chemical behavior of these gold solutions, and the large extinction- and temperature-coefficients of the gold-related band, indicated the presence of a solvated, gold anion Au_x^- . In view of the results of a Zintl type of potentiometric titration that favored an Au_x^- stoichiometry, together with small, alkali-cation effects, and UV-absorption extinction coefficients approximately the same as that of the solvated electron, Lagowski and Peer (79b) promoted the idea of the existence of a $5d^{10}6s^2 \text{Au}^-$ solvated, gold anion.

III. New Cluster Techniques

Cryophotochemical techniques have been developed that (i) allow a controlled synthetic approach to mini-metal clusters (112), (ii) have the potential for "tailor-making" small, bimetallic clusters (mini-alloy surfaces) (114, 116), (iii) permit the determination of relative extinction-coefficients for naked-metal clusters (149), and (iv) allow naked-cluster, cryophotochemical experiments to be conducted in the range of just a few atoms or so (112, 150, 151).

A. CRYOPHOTOCLUSTERING

The cryophotoaggregation phenomenon was first observed for Ag atoms (112) entrapped in Ar at 10–12 K (see Fig. 14). The trick essentially involves narrow-band, continuous irradiation into the

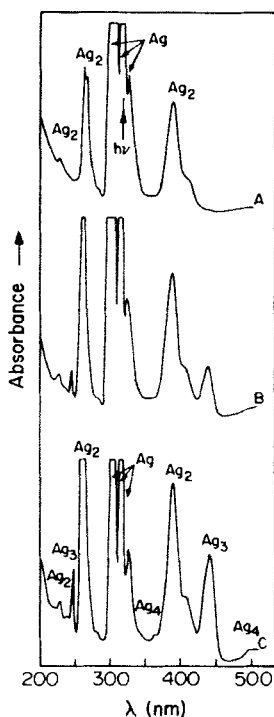


FIG. 14. UV-visible spectra of $\text{Ag}/\text{Ag}_2/\text{Ar}$ generated from $\text{Ag}:\text{Ar} \approx 1:10^3$ depositions: (A) at 10–12 K; (B) after 15-min, 10–12 K photolysis at 315 nm; (C) after an additional 45-min, 10–12 K photolysis at 315 nm, showing the decay of atomic Ag and the concomitant growth of Ag_2 and Ag_3 (112).

atomic-resonance absorptions of matrix-entrapped, metal atoms. In the silver system, photoclustering was initiated by excitation of any one of the components of the $^2\text{S}_{1/2} \rightarrow ^2\text{P}_{1/2,3/2}$ atomic resonance. It may be envisaged that, following atomic excitation, some nonradiative, electronic-to-lattice, phonon energy transfer, local warming and softening of the surrounding matrix-cage, atom photomobilization (bulk diffusion), and subsequent photoaggregation to diatomic and higher metal clusters may occur. Cluster sizes were found to be dependent on the metal concentration, the matrix material, the matrix temperature, the excitation wavelength, and the light-intensity. Controlled photoaggregation up to Ag_5 has been observed in this way (112), and the process appears to be amenable to analysis by conventional, solid-state, diffusion theory (149). Cluster size-determination appears to be tractable by these methods (see later) (112, 149).

FIG. 15. The optical spectrum of Cu:Ar $\approx 1:10^4$ at 10–12 K, (A) showing isolated Cu atoms and Cu₂ molecules; (B), (C) photoaggregation as the result of two 30-min irradiations in the resonance lines of Cu atoms at 302 nm, (D) photodissociation of Cu₂ resulting from a 30-min irradiation at the 370-nm band of Cu₂. The features marked "a" are thought to arise from secondary trapping sites of Cu₂. Note the scale change between 325 and 400 nm (150).

growth of Cu_3 , and yet *decay* of Cu_2 , under these matrix-concentration conditions (150). Similar effects have been observed for Ag_2 (150). The Cu_2 and Ag_2 visible cryophotochemistry observed may be rationalized in terms of a highly selective, matrix-induced, photodissociation step for which a mechanism involving formation of an excited Cu (Ag) atom-matrix cage complex has been proposed. SCF-X α -SW MO calculations for Cu_2 (and Ag_2) (150) confirmed that the wavelengths used for the photoexcitations are essentially those of the electronic transitions from the main bonding to the main antibonding orbital (i.e., $s\sigma_g \rightarrow s\sigma_u$), thus providing a description of the excited states that is useful in accounting for the observed photochemistry (112, 150) (see Table VII).

Selective, trisilver, cryophotochemical transformations have also been observed that involve HOMO-LUMO visible excitation (420–440 nm, depending on the matrix support) (151). A typical series of optical traces that depict the outcome of Ag_3/Kr , 423-nm excitation at 10–12 K is illustrated in Fig. 16. These data show that Ag_3 absorptions at 423/247 nm may be selectively photoannihilated simultaneously with the

TABLE VII
CALCULATED AND EXPERIMENTAL ELECTRONIC SPECTRA OF Cu_2
AND Ag_2 ($\text{cm}^{-1} \times 10^3$) (150)

Transition	Calculated ^a	Experimental			
		Gas ^b	Ar	Kr	Xe
Cu ₂					
1π _g → 2σ _u	24.1 (0.02)	20.4	25.0	25.0	25.0
2σ _g → 2σ _u	26.5 (0.32)	21.7	27.0	27.0	27.8
1π _g → 2π _u	35.2 (0.15)		38.2	37.0	35.1
2σ _g → 2π _u	37.2 (1.02)		41.7/42.4	41.5/42.0	40.5/41.0
1δ _g → 2π _u	39.5 (0.13)		43.1	42.7	41.7
1σ _g → 2σ _u	39.8 (0.36)		44.8	44.0	43.1
1σ _u → 3σ _g	43.7 (0.03)				
Ag ₂					
2σ _g → 2σ _u	22.0 (0.64); 25.7 (0.63)	23.0	24.3/25.8	25.6	25.6
2σ _g → 2π _u	33.2 (1.33); 33.6 (1.37)	37.6	37.8/38.3	35.5/37.0	34.5/35.3
1π _g → 2σ _u	43.5 (0.03); 45.6 (0.04)	40.2	44.1	45.0	46.1

^a All spin- and dipole-allowed transitions below 48 and $51 \text{ cm}^{-1} \times 10^3$ for Cu_2 and Ag_2 , respectively. For Ag_2 , the first value is for 284 pm and the second for 247 pm. Oscillator strengths are given in parentheses. ^b 0 \rightarrow 0 transitions, from "Spectroscopic Data Relating to Diatomic Molecules," Pergamon Press, New York, 1970, for Cu_2 , and from *J. Mol. Spectrosc.* **69**, 25 (1978) for Ag_2 . The weak $B \leftarrow X$ and $D \leftarrow X$ bands of Ag_2 at 35.8 and $39.0 \text{ cm}^{-1} \times 10^3$, believed to be due to forbidden transitions, are omitted.

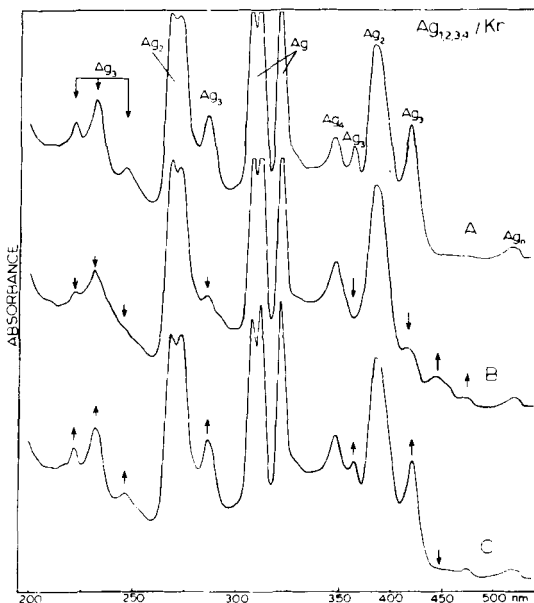


FIG. 16. The UV-visible spectra of $\text{Ag}_{1,2,3,4}/\text{Kr}$ mixtures ($\text{Ag}/\text{Kr} \approx 1/10^2$) at 10–12K: (A) After a 30-min irradiation centered at the atomic resonance absorption lines. (B) The outcome of a 10-min, 423-nm Ag_3 irradiation, showing major decay of the bands associated with Ag_3 (indicated by arrows) and the appearance of two new bands near 450 nm. (C) The result of a 5-min, 25K bulk thermal annealing period, showing regeneration of the original Ag_3 spectrum and loss of the new band near 445 nm (151).

growth of a new band-system around 450 nm. A number of aspects of this selective, photobleaching phenomenon are significant. Firstly, certain absorptions of the original, Ag_3 , optical spectrum in Kr (233 and 223 nm) displayed only slight changes on 423-nm, Ag_3 photoexcitation. Secondly, the absorptions associated with other silver species, $\text{Ag}_{1,2,4}$, co-trapped with Ag_3 remained essentially unchanged with respect to Ag_3 photoexcitation. Thirdly, higher silver-cluster absorptions belonging to $\text{Ag}_{5,6}$ remained spectroscopically invisible. Fourthly, in the densely packed, cluster-overlap region (330–370 nm), where at least one Ag_3 absorption was suspected, concomitant decay of the 368-nm absorption to disappearance, along with the photobleaching of the 423/247 nm Ag_3 absorptions just listed, were observed. Finally, it was discovered that this highly discriminative photobleaching of *part* of the Ag_3 optical spectrum could be approximately reversed by 25K thermal annealing, while leaving the other Ag_n spectral lines largely unaffected (see Fig. 16).

In brief, one possible rationale for the 423-nm, Ag_3/Kr photochemistry may be formulated in terms of a photoisomerization process whereby a specific, Ag_3 , geometrical isomer (for example, linear) is selectively excited to an electronic state that allows conversion into, and trapping of, a metastable, geometric isomer (for example, nonlinear) of Ag_3 , all localized within the matrix cage. It would appear at this stage that an alternative explanation, in terms of the formation of $\text{Ag}_2 + \text{Ag}$ (just outside the matrix cage) and re-formation of Ag_3 on annealing, is unlikely, in view of the prior knowledge that the $\epsilon_2:\epsilon_1$ and $\epsilon_3:\epsilon_1$ extinction-coefficient ratios are very close to unity in Kr matrices (149). Therefore, a primary, $\text{Ag}_3 \rightarrow \text{Ag}_2 + \text{Ag}$, photodissociative step should have been detected through substantial variations in the intensity of the Ag and Ag_2 bands, but this was not found in practice (see ref. 151 for further details).

C. RELATIVE EXTINCTION-COEFFICIENT MEASUREMENTS FOR NAKED SILVER CLUSTERS BY PHOTOAGGREGATION TECHNIQUES

Low-temperature, photoaggregation techniques employing ultraviolet-visible absorption spectroscopy have also been used to evaluate extinction coefficients relative to silver atoms for diatomic and triatomic silver in Ar and Kr matrices at 10–12 K (149). Such data are of fundamental importance in quantitative studies of the chemistry and photochemistry of metal-atom clusters and in the analysis of metal-atom recombination-kinetics. In essence, simple, mass-balance considerations in a photoaggregation experiment lead to the following expression, which relates the decrease in an atomic absorption to increases in diatomic and triatomic absorptions in terms of the appropriate extinction coefficients.

$$(A'_1 - A''_1) = 2 \epsilon_1/\epsilon_2(A'_2 - A''_2) + 3 \epsilon_1/\epsilon_3(A'_3 - A''_3) \quad (5)$$

It is prearranged in this analysis that M_4 and higher clusters are not produced in significant proportions. The symbol A'_n represents the absorbance due to M_n at time t' , A''_n is the absorbance due to M_n at time t'' , and ϵ_n represents the molar extinction coefficient for M_n . Dilute conditions and short irradiation times yield ϵ_1/ϵ_2 directly, whereas longer irradiation times allow solving for ϵ_1/ϵ_3 . However, the advantage of the photoaggregation method is that only one deposition is needed for each ϵ_1/ϵ_2 or ϵ_1/ϵ_3 determination, so that the method is much more convenient and considerably more accurate, as mass balance of the total metal is maintained after each irradiation, thus eliminating the need for multiple, quantitative depositions.

The relative extinction-coefficients for $\text{Ag}_{1,2,3}$ determined by photoaggregation procedures were found not to be strongly matrix-dependent (see Table VIII). Moreover, the results for Ag_2 were in good agreement with those obtained by quantitative, metal-atom deposition-techniques.

D. PHOTONUCLEATION KINETIC STUDIES

Kinetic studies of the cryophotoclustering process are now in progress. Preliminary results indicate that, under certain conditions, the rates of formation of diatomic and triatomic silver may usefully be approximated by simple, second-order kinetics (149). A simple analysis predicts that the slope of a $\log[\text{Ag}_n]/[\text{Ag}]$ versus $\log(t)$ plot, where Ag_n and Ag represent absorbances, and t represents the irradiation time, should have a value close to 1.0 for $n = 2$, and 2.0 for $n = 3$ (149). A typical plot is shown in Fig. 17. The observed slopes, 0.9/1.0 and 2.1/2.2, support the Ag_2 and Ag_3 assignments for the run indicated in Fig. 18, and correlate exactly with earlier assignments based on Ag-atom concentration experiments.

E. PHOTOMANIPULATION OF CLUSTER DISTRIBUTIONS

It has also been demonstrated that cryophotoaggregation experiments involving matrix-entrapped silver atoms can possibly be tailored to the point of generating almost pure disilver clusters, as well as cluster distributions that are inaccessible by conventional, deposition and bulk-annealing procedures (152). By carefully selecting the silver concentration and matrix support, it may be arranged that substantial conversion of Ag atoms into Ag_2 occurs, with only slight conversion losses to Ag_3 or higher silver clusters. Figure 19 demonstrates this remarkable, atom-diatom photoredistribution-reaction, where a Kr matrix

TABLE VIII
RELATIVE EXTINCTION COEFFICIENTS^{a,b} FOR Ag_2 AND Ag_3

	Peak height	Peak area
$\epsilon_1^{315}/\epsilon_2^{380} (\text{Ar})$	0.8 ± 0.2	0.40 ± 0.05
$\epsilon_1^{315}/\epsilon_3^{345} (\text{Ar})$	1.2 ± 0.5	0.60 ± 0.30
$\epsilon_1^{323}/\epsilon_2^{270} (\text{Kr})$		0.43 ± 0.05

^a The corresponding wavelengths (in nm) in Ar and Kr matrices are indicated as superscripts. The uncertainty limits represent estimated upper and lower bounds.

^b Determined by photoaggregation procedures (149).

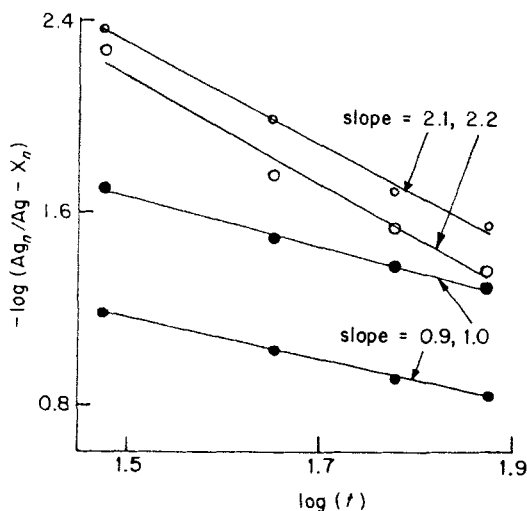


FIG. 17. Kinetic plots showing a linear dependence on irradiation time (305 nm) of the absorbance ratios $\text{Ag}_2^{263\text{nm}}:\text{Ag}^{300\text{nm}}$ and $\text{Ag}_2^{390\text{nm}}:\text{Ag}^{300\text{nm}}$ (○) and a linear dependence on the square of the irradiation time of the absorbance ratios $\text{Ag}_3^{245\text{nm}}:\text{Ag}^{300\text{nm}}$ and $\text{Ag}_3^{340\text{nm}}:\text{Ag}^{300\text{nm}}$ (●), as predicted from the simple kinetic analysis. The quantities X_n were chosen in order to shift the $\text{Ag}_2:\text{Ag}$ vs. t and $\text{Ag}_3:\text{Ag}$ vs. t^2 plots through the origin (149).

containing dominant amounts of Ag_2 has been produced. The potential of the method for generating very narrow distributions of Ag_2/Ag_3 in the absence of Ag_1 has been realized in cyclooctane matrices (see Fig. 20), and of $\text{Ag}_2/\text{Ag}_3/\text{Ag}_4$, with very little Ag_1 , in methane matrices (see Fig. 21). The ramifications of these kinds of experiments in terms of the spectroscopy of individual clusters and the possible fabrication of highly potent and selective diatom and diatom-triatom cluster catalysts are clearly considerable.

F. PHOTOSELECTIVE BIMETALLIC AGGREGATION

We have already shown how simultaneous codeposition of two metals in inert-gas matrices can lead to the formation of mixed-metal dimers. As in the case of silver, it was found that irradiation into the atomic absorptions of Cr or Mo results in formation of their respective dimers and trimers (114). In addition to this, however, irradiation into the atomic resonances of the two metals in the presence of each other results (114) in formation of the mixed-metal species CrMo , Cr_2Mo , and CrMo_2 . It would seem that selective irradiation into the 300–400-nm bands of atomic Cr or Mo excites the $3d^54p^1$, $3d^44s^14p^1$, or $4d^55p^1$,

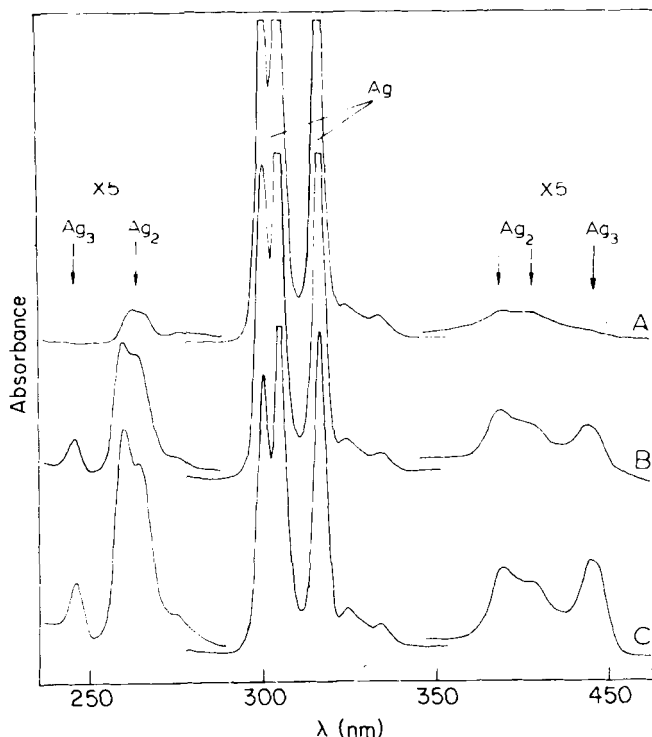


FIG. 18. UV-visible spectra of $\text{Ag}_{1,2,3}/\text{Ar}$ mixtures ($\text{Ag}:\text{Ar} \approx 1:10^3$) at 10–12K. Note the growth of Ag_2 and Ag_3 clusters and loss of Ag atoms as a result of 305 nm, Ag atom excitation. Spectra A, B, and C represent irradiation times of 0, 1, and 4 min, respectively (149).

$4d^45s^15p^1$ states, respectively, which subsequently decay and transfer energy to the surrounding, matrix cage. It seems likely, therefore, that part, or all, of the electronic energy of these states is channeled into lattice vibrational-energy and translational energy of the caged atoms, the results being photoinduced, bulk diffusion and aggregation, to afford the mixed-cluster species observed. This concept points to the likelihood of localized excitation, matrix cage-softening, and short-range, bulk diffusion, rather than of extensive matrix-softening. Further evidence in support of this possibility stems from consecutive (instead of simultaneous) deposition of Mo and Cr, followed by selective, atomic excitation. Under these conditions, formation of mixed-metal species was not observed.

The selectivity of the photochemical events was demonstrated in a more detailed study of the Cr/Mo system (115). Starting with matrices

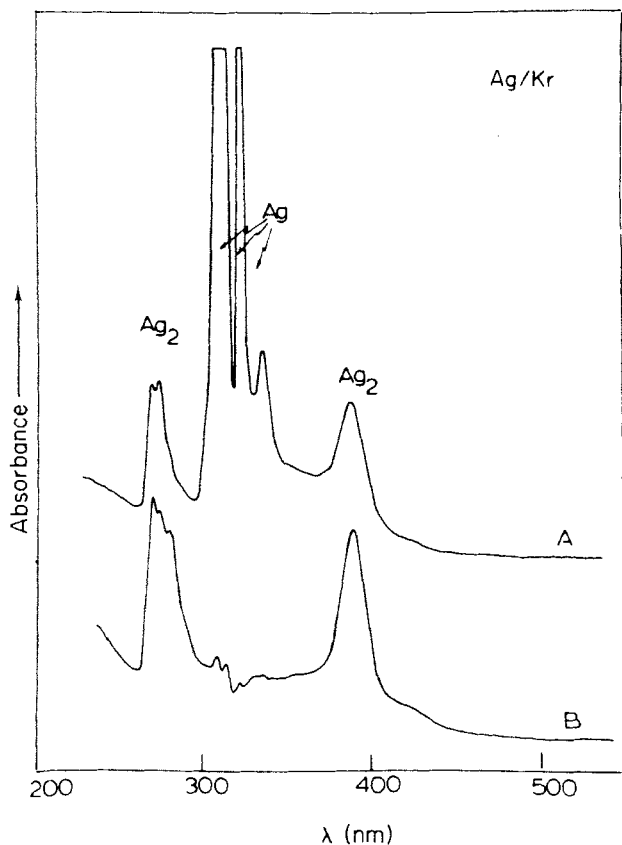


FIG. 19. The optical spectrum of the products of a $\text{Ag}:\text{Kr} \approx 1:10^4$ cocondensation reaction, (A) after deposition at 10–12 K, and (B) after 60-min, narrow-band (8 nm), 325-nm continuous irradiation from an Oriel 500-W xenon lamp–Schoeffel monochromator assembly (152).

(Kr or Ar at 12 K) that clearly displayed the characteristic absorptions of Cr, Mo, Cr_2 , Mo_2 , CrMo , Cr_3 , Cr_2Mo , CrMo_2 , and Mo_3 , the concept of photoselectivity could be explored as follows. Upon irradiation at 295 nm (Mo atoms), major decay of Mo absorptions was observed, and selective growth of CrMo , CrMo_2 , Mo_2 , and Mo_3 occurred. Only a slight decay of Cr was noticed; this was probably the result of formation of CrMo , while Cr_2 and Cr_3 remained approximately unchanged. This and similar results obtained upon 335-nm (Cr atom) irradiation (where the behavior of the metals is interchanged) argue strongly in favor of selective photoexcitation and photomobilization of the irradiated species.

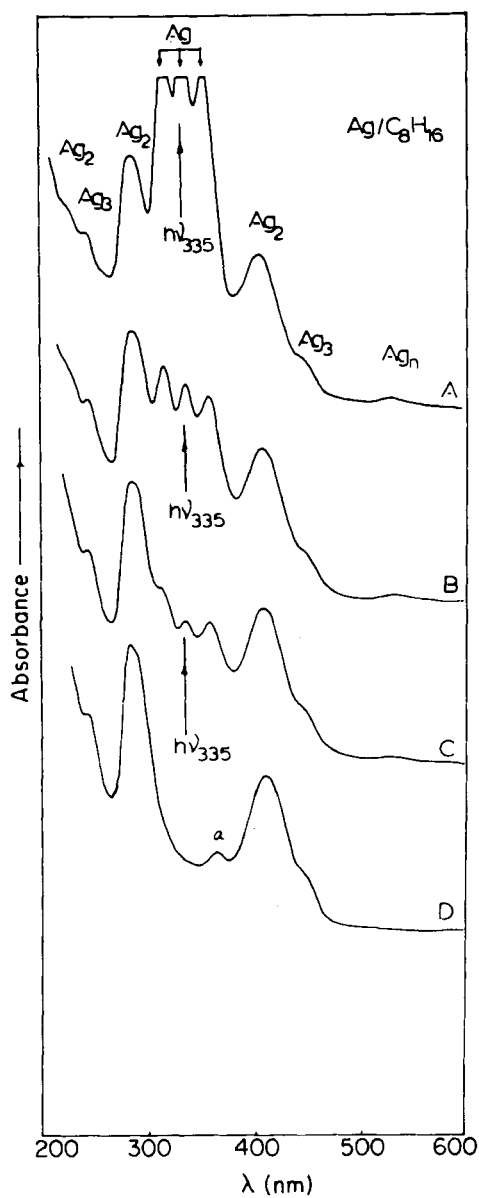


FIG. 20. The optical spectrum of the products of a $Ag:C_8H_{16}$ (cyclooctane) $\approx 1:10^3$ cocondensation reaction, (A) after deposition at 10–12 K, and (B)–(D) after 15-, 30-, and 60-min, narrow-band (8 nm), 335-nm, continuous excitation (152).

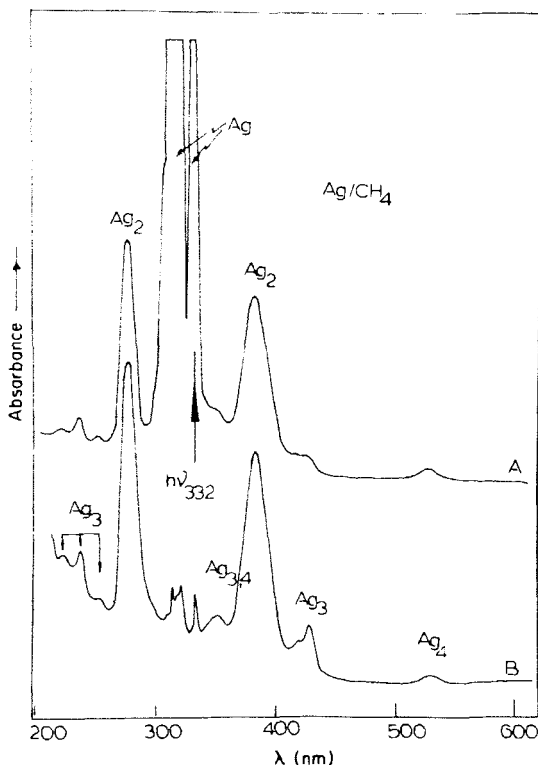


FIG. 21. The optical spectrum of the products of a $\text{Ag}:\text{CH}_4 \approx 1:10^3$ cocondensation reaction, (A) after deposition at 10–12 K, and (B) after 30-min, narrow-band (8 nm), 332 nm, continuous irradiation (152).

This behavior is illustrated in Fig. 22, and summarized schematically in Fig. 23. It is also noteworthy that nonselective photonucleation may also be arranged by irradiation into Cr/Mo overlap regions (350 nm), upon which, growth of all of the cluster species expected was observed, concomitant with the decay of both the Cr and the Mo resonances (115).

The photoaggregation technique has been extended to the Ag/Cr system (116), where the naked, bimetallic species AgCr and Ag_2Cr can be selectively photogenerated, and identified, in the presence of the unimetallic, parent clusters, with photoselectivity reminiscent of that of the Cr/Mo system (115). A typical trace is shown in Fig. 24.

From these early successes, it is evident that this new photochemical technique is likely to find a wide range of applications in the continuing quest to thoroughly understand the electronic, geometric, chemi-

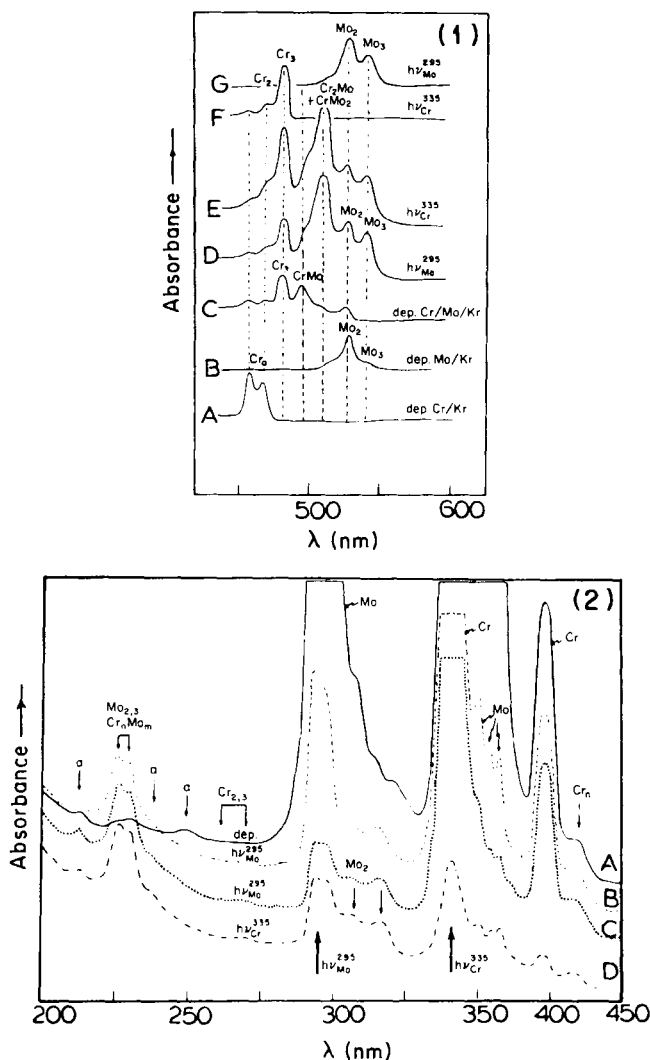


FIG. 22. (1) The low-energy optical spectra of (A) Cr:Kr \approx 1:10³, (B) Mo:Kr \approx 1:10³, and (C) Cr:Mo:Kr \approx 1:1:10³ mixtures, all deposited at 10–12 K, showing the characteristic absorptions of Cr_2 , Cr_3 , CrMo , Cr_2Mo , CrMo_2 , Mo_2 , and Mo_3 ; (D) the result of 10-min, $h\nu_{\text{Mo}}^{295}$ photolysis of sample (C); (E) the result of 5-min, $h\nu_{\text{Cr}}^{335}$ photolysis of sample (D); (F) the result of 3-min, $h\nu_{\text{Cr}}^{335}$ photolysis of sample (A); (G) the result of 30-min, $h\nu_{\text{Mo}}^{295}$ photolysis of sample (B). (2) (A) The high-energy, optical spectra of Cr:Mo:Kr = 1:1:10³ mixtures deposited at 10–12 K, showing the known absorptions of Cr, Mo, Cr_2 , Mo_2 , and Mo_3 ; (B) and (C), the result of 50- and 130-min $h\nu_{\text{Mo}}^{295}$ photolysis of sample (A); and (D) the result of a further, 22-min, $h\nu_{\text{Cr}}^{335}$ photolysis of sample (C). Note that the bands labeled "a" could be associated with mixed clusters Cr_nMo_m (115).

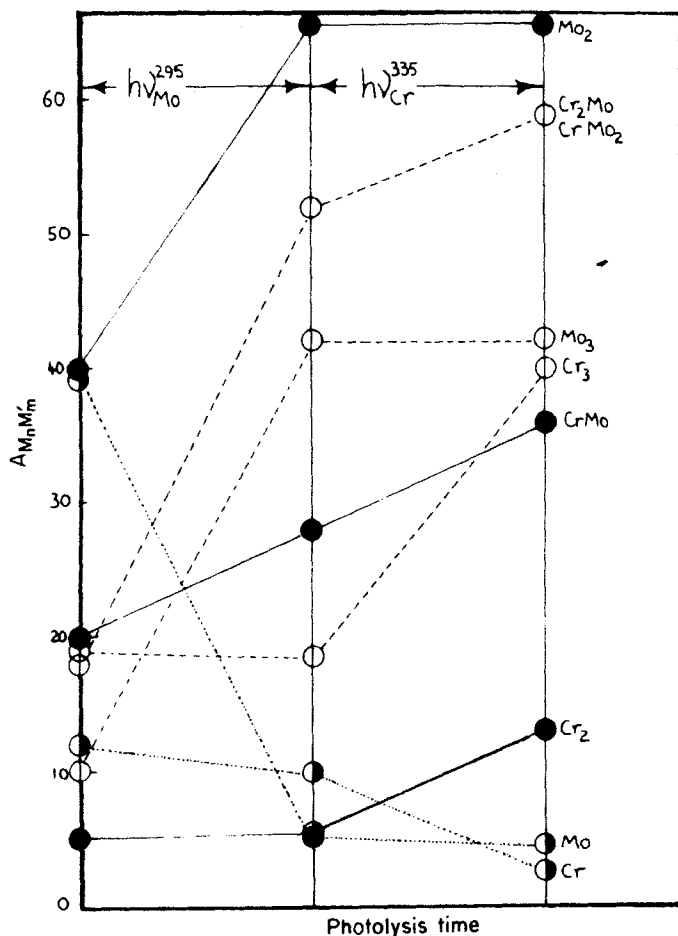


FIG. 23. A schematic representation of the photoselectivity experiments involving (Cr:Mo:Kr \approx 1:1:10⁹ mixtures deposited at 10–12 K and then sequentially subjected to $h\nu_{\text{Mo}}^{295}$ and $h\nu_{\text{Cr}}^{335}$ photolyses. Note that the Cr and Mo atom absorbances are recorded on a scale that is 1/10th that used for the Cr_nMo_m clusters (115).

sorptive, and catalytic properties of unimetallic and bimetallic clusters as a function of size and composition.

IV. Cluster Complexes

Strictly speaking, a cluster complex, as generally considered in organometallic chemistry, consists of a framework of more than two transition-metal atoms. However, in this Section, we shall ignore tra-

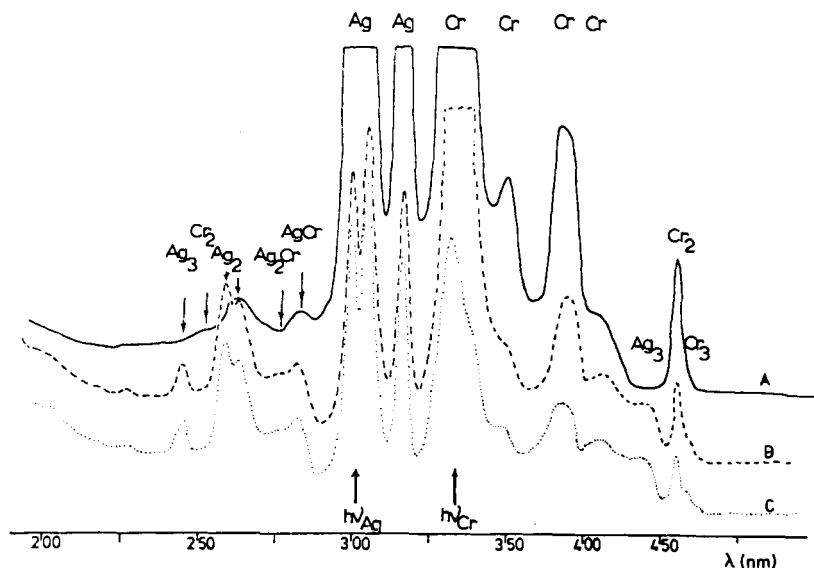


FIG. 24. The UV-visible spectra of a Cr:Ag:Ar $\approx 1:1:10^3$ mixture (A) deposited at 10–12 K, showing Cr, Ag, Cr₂, Ag₃ and AgCr; (B) after Ag atom 305-nm photoexcitation, showing the growth of Ag₃, Ag₂, AgCr, and Ag₃Cr; and (C) after Cr atom 350-nm photoexcitation and 30-min relaxation time, showing the growth of Cr₃ and AgCr (116).

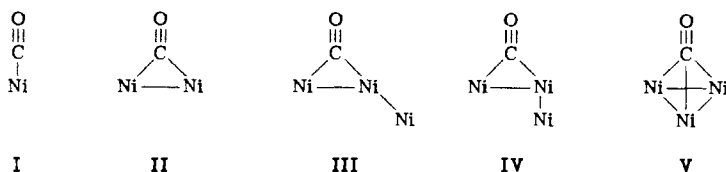
dition, and arbitrarily include dimer species, as they constitute a logical extension of the discussion presented in Sections II and III.

One of the major attractions in the metal-atom synthesis of dimer and cluster species is the ability to isolate highly unsaturated species, M_nL_m , that may then be considered to be models for chemisorption of the ligand, L, on either a bare, or a supported, metal surface (100). It is quite informative to compare the spectral properties of these finite cluster-complexes to those of the corresponding, adsorbed surface-layers (100), in an effort to test localized-bonding aspects of chemisorption, and for deciphering UPS data and vibrational-energy-loss data for the chemisorbed state. At times, the similarities are quite striking.

A. CO SPECIES

Nickel cluster carbonyls containing up to three nickel atoms were formed by cocondensing monatomic nickel vapor with CO in Ar at cryogenic temperatures (95) as an extension of DeKock's (26) earlier work on mononuclear nickel carbonyls. By using considerably higher metal:matrix ratios, "low-coverage," CO chemisorption models were formed; these clusters included monocarbonyls having two-center, and

three-center, bridge-bonded CO, as well as linear CO. The structures illustrated, including three forms of $\text{Ni}_3(\text{CO})$, were assigned on the



basis of (a) metal-concentration studies, using the kinetic analyses (92) already discussed, (b) mixed $^{12}\text{CO}/^{13}\text{CO}$ isotope experiments, and (c) normal-coordinate analyses of the vibrational data. The complexity of the spectra obtained is illustrated in Fig. 25, and the spectra of the various monocarbonyls were assigned as in Table IX. Observation of three forms of $\text{Ni}_3(\text{CO})$ implies the presence of three forms of Ni_3 in the matrix. Considering MO calculations (2) that suggested that the stable form of Ni_3 is linear, the other trinuclear forms might be a kinetic consequence of the low temperature at which the complexes were synthesized.

The carbonyl clusters provide an interesting set of models for the chemisorption of CO on nickel. It is very interesting that, for the $\text{Ni}_n(\text{CO})$ assignments, a plot of ν_{CO} versus $1/n$ for the three-center-bonded CO moieties extrapolates to 1950 cm^{-1} for $n = \infty$ (the "chemi-

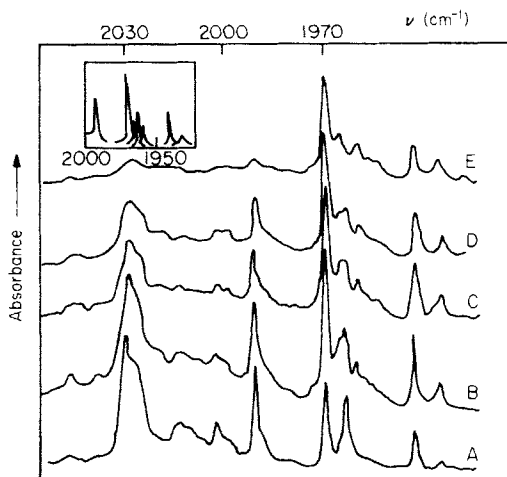


FIG. 25. Portions of the IR spectra of the products of the cocondensation of Ni atoms with CO/Ar (1:250). A through E refer to increasing, total-metal concentration. The inset is a curve-resolved version of spectrum B (95).

TABLE IX
 ν_{CO} STRETCHING FREQUENCIES FOR
 VARIOUS Ni_nCO SPECIES (95)

Complex	$\nu_{\text{CO}}(\text{cm}^{-1})$	Notation
NiCO	1996	I
Ni_2CO	1973	II
Ni_3CO	1969	III
Ni_3CO	1963	IV
Ni_3CO	1938	V

sorbed" limit), which corresponds to the center of the spectrum of CO on Ni (95). A different extrapolation, from NiCO , to Ni_3CO , to Ni_nCO , yields a value (1905 cm^{-1}) close to that observed for low-coverage, chemisorbed CO on Ni. Such convergence behavior suggests that CO interacting with bulk nickel bonds in a manner similar to that found in stable, metal carbonyls and, moreover, supports the proposal that both terminal- and multi-center-bonded CO occur on nickel surfaces.

Moskovits and Hulse (96) also investigated the interaction of CO with small, copper clusters of known size. Species absorbing at 2128, 2117, 2103, and 2011 cm^{-1} were found, from metal-concentration studies and mixed-isotope experiments, to be associated with finite complexes of stoichiometry Cu_2CO , Cu_3CO , Cu_4CO , and CuCO , the last having been identified previously (117). Annealing the matrix containing these species to 32 K results in the formation of a larger, copper carbonyl cluster species ($\nu_{\text{CO}} = 2090 \text{ cm}^{-1}$) of indeterminate stoichiometry, the IR spectrum of which closely resembles that of CO chemisorbed on bulk copper (155). A ν_{CO} trend similar to that of Ni_nCO (95) was found for Cu_nCO on extrapolating to $n = \infty$, implying that the bonding of CO to Cu [and other transition metals (95)] is localized. The fact that the CO stretching-frequency of Cu_4CO lies close to that of CO chemisorbed on Cu (155) suggested that four copper atoms provide a good model for the bulk-copper surface.

In this context, it is noteworthy that the IR spectrum of bridge-bonded $\text{Rh}_2(\text{CO})_8$ [generated from $\text{Rh}(\text{CO})_4$ matrix-dimerization reactions and Rh/CO matrix-concentration studies (153)] shows bands in the terminal region at 2060, 2043, and 2038 cm^{-1} , and in the bridge region at 1852 and 1830 cm^{-1} , that are *very close to the proposed, terminal-bridged, chemisorbed, CO species on clean Rh films and supported Rh clusters* (4, 34, 50, 162) (see Table X). Moreover, the matrix, ν_{CO} frequency observed for RhCO (2013 cm^{-1}) (154) falls between the ν_{CO} values for the proposed terminal and bridge sites of chemisorbed CO on

TABLE X
CO CHEMISORPTION DATA FOR SUPPORTED RHODIUM SAMPLES (154)

Rh/SiO ₂ (Guerra ^a)	Rh/Al ₂ O ₃			Assign- ment	Rh ₂ (CO) ₆ (Ozin ^e)	Assign- ment
	(Garland ^b)	(Rothschild ^c)	(Arai ^d)			
2080	2095	2100	2108	Rh(CO _{chemis}) ₂	2060	ν CO _i
2020–1990 ^f	2027	2030	2065		2043	ν CO _i
2065–2040	2062–2045	2000	2040	Rh(CO _{chemis}) ₂	2038	ν CO _i
1900–1890	1925	1900–1850	1860	Rh ₂ (CO _{chemis})	1852	ν CO _b
					1830	ν CO _b

^a Ref. (48b). ^b Ref. (34). ^c Ref. (162). ^d Ref. (4). ^e Ref. (153). ^f May be partially a SiO₂-CO species.

both supported and unsupported Rh. Both of these sets of data point to a localized description for CO chemisorbed on Rh, and provide additional evidence for the surface vibrational-assignments.

A kinetic study (118) of the controlled formation of a diatomic species, according to the equation



has been conducted at temperatures ranging from 30 to 37 K. The kinetics of the reaction appear to be diffusion-controlled in solid CO matrices, with the diffusion coefficient of Ag(CO)₃ found to have a value of $7 \times 10^{-16} \text{ cm}^2/\text{sec}$ at 35 K; the activation energy of the diffusion process was calculated to be 1.9 kcal/mol. The dinuclear carbonyl was found to be unstable, even at these cryogenic temperatures, decomposing, presumably, to silver dimers, or higher clusters, or both. The study is interesting, in that it presented a mechanism (bimolecular, diffusion-controlled reaction) for the formation of a binuclear cluster-species in an annealed matrix, and, moreover, illustrated the feasibility of matrix kinetics studies involving highly reactive intermediates.

B. O₂ SPECIES

The interaction of small, well defined, rhodium clusters, Rh₂ and Rh₃, with O₂ has been investigated (120) by matrix infrared, and UV-visible, spectroscopy, coupled with metal/O₂ concentration studies, warm-up experiments, and isotopic oxygen studies. A number of binuclear O₂ complexes were identified, with stoichiometries Rh₂(O₂)_n, $n = 1-4$. In addition, a trinuclear species Rh₃(O₂)_m, $m = 2$ or 6, was identified. The infrared data for these complexes, as well as for the mononuclear complexes Rh(O₂)_x, $x = 1-2$ (119), are summarized in Table XI. Metal-concentration plots that led to the determination of

TABLE XI
OBSERVED INFRARED SPECTRA FOR $\text{Rh}_x(\text{O}_2)_y$ SPECIES FORMED
IN O_2 AND O_2/Ar MATRICES (120)

Obs.		Designation	Assignment [see ref. (120)]
O_2 matrices	O_2/Ar matrices		
1266	1278 } 1268 }	D'_1	$\text{Rh}_2(\text{O}_2)$
1130	1126	T	$\text{Rh}_3(\text{O}_2)_2$ or 6
1120sh	1115		$\text{Rh}_3(\text{O}_2)_n?$
	1081	D_3	$\text{Rh}_2(\text{O}_2)_3$
1075	1076	D_4	$\text{Rh}_2(\text{O}_2)_4$
1038	1048	M_2	$\text{Rh}(\text{O}_2)_2$
	922	D_1	$\text{Rh}_2(\text{O}_2)$
	908	M_1	$\text{Rh}(\text{O}_2)$
	902	D_2	$\text{Rh}_2(\text{O}_2)_2$
	890	D_3	$\text{Rh}_2(\text{O}_2)_3$

the metal nuclearity in some of these complexes are illustrated in Fig. 26.

The compound $\text{Rh}_2(\text{O}_2)_4$ may be regarded as the metal-metal-bonded dimer of the parent monomer $\text{Rh}(\text{O}_2)_2$, presumably formed by a mechanism similar to that described for $\text{Ag}_2(\text{CO})_6$ (118). The lower-stoichiom-

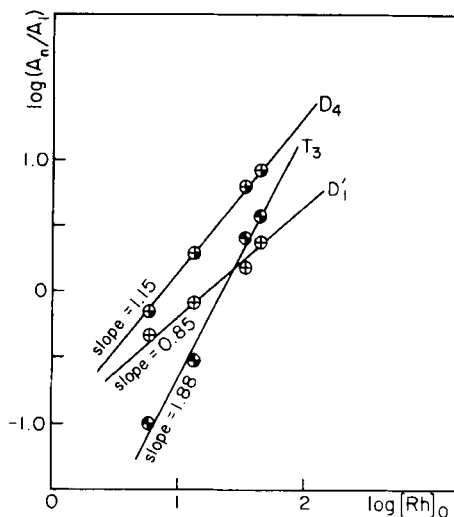
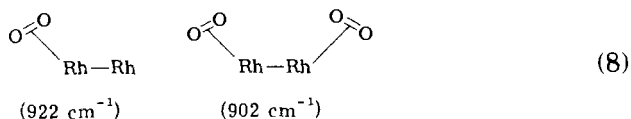


FIG. 26. A log-log plot of the ratio of the absorbances of lines attributed to $\text{Rh}_x(\text{O}_2)_y$ species to that of a $\text{Rh}(\text{O}_2)_2$ reference absorption as a function of the total rhodium concentration $[\text{Rh}]_0$ at constant dioxygen deposition-rate (120).

etry binuclears may be visualized as deriving from $\text{Rh}_2(\text{O}_2)_4$ by successive O_2 stripping. In addition, it would appear that $\text{Rh}_3(\text{O}_2)_m$ is also derived from $\text{Rh}(\text{O}_2)_2$, and, hence, it is probably best formulated as a triangular cluster, $\text{Rh}_3(\text{O}_2)_6$, but this has not been confirmed. All of these dioxygen complexes show $\nu_{\text{O-O}}$ (see Table XI) in the range normally expected for coordinated $\text{O}_2^{\delta-}$, where $1 \leq \delta \leq 2$. There is, however, another binuclear complex, $\text{Rh}_2(\text{O}_2)$, having $\nu_{\text{O-O}} = 1275\text{--}1265\text{ cm}^{-1}$, that evidently has much less charge transferred from the dirhodium site to the dioxygen, and, hence, the O_2 is more weakly coordinated. Interestingly, no evidence for bridging dioxygen was found, although the latter complex, with its weak $\text{Rh}_2 \cdots \text{O}_2$ interaction, has been proposed as a model for "physisorbed" O_2 on bulk Rh in a manner such as that depicted.



Although there is a severe paucity of vibrational data for the molecular form of O_2 chemisorbed on rhodium surfaces, it is possible to visualize the dinuclear and trinuclear complexes as models for the associative chemisorption of O_2 on rhodium. The $\nu_{\text{O-O}}$ values of the complexes $\text{Rh}_2(\text{O}_2)_{1,2}$ show little



perturbation from $\text{Rh}(\text{O}_2)$ (908 cm^{-1}), and, hence, it may be argued that they might be useful "low- and high-coverage" models, respectively. The small frequency-shift on passing from one to two coordinated dioxygens, and the similarity to the mononuclear, imply minimal, nearest-neighbor, dioxygen-coupling effects and minimal perturbation effects of adding a second Rh atom. Such minor, intraligand shifts with metal stoichiometry are also noted with such ligands as C_2H_4 (101) and, as already mentioned, CO (95, 96). Insensitivity of this type argues, for these simple molecules, in favor of localized bonding to metal surfaces.

C. C_2H_4 SPECIES

A wide range of ethylene complexes, both mononuclear and higher cluster in nature, have been synthesized, and studied, by the metal atom-matrix technique. In this Section, we shall focus on the reactions

of Co (121), Ni (101, 123), and Cu (122, 124) with ethylene and, although this Section deals mainly with dimer and cluster species, we shall also include, at this point, a discussion of the mononuclear complexes of these metals. To a large extent this is necessary, as, in order to characterize the clusters, it is first essential to identify the mononuclears. In addition, the spectral trends on progressing from one, to two, to more, metal atoms are quite informative.

The cryochemical reaction of copper atoms with C_2H_4 and C_2H_4/Ar mixtures at 10–12 K, using copper-concentration conditions (94) that favor mononuclear reaction-products, gives rise (124) to three highly colored, binary, copper–ethylene complexes, $Cu(C_2H_4)_n$, $n = 1-3$. These stoichiometries were confirmed by vibrational and electronic spectroscopy, taken in conjunction with metal and ligand concentration experiments and $^{12}C_2H_4/^{13}C_2H_4$ mixed-isotope, concentration studies. These complexes are less stable than the analogous nickel species (123), with $Cu(C_2H_4)_3$ being converted into $Cu_2(C_2H_4)_m$ (m not defined) at low temperatures (122), whereas $Ni(C_2H_4)_3$ is stable to $0^\circ C$ (199). This instability is considered to be, in part, a manifestation of their paramagnetic character and tendency toward dimerization, as well as their inherent, thermal lability. These mononuclear species all display intense visible and ultraviolet absorptions that monotonically red- and blue-shift, respectively, with increasing olefin stoichiometry. The visible transitions have been assigned, by $X\alpha$ calculations (148), as metal-to-ligand charge-transfer involving a mainly localized, metal s-electron, whereas the ultraviolet transitions may be considered to be metal-to-ligand charge-transfer involving mainly localized metal d-electrons. The optical results are summarized in Table XII.

Quantitative Cu/C_2H_4 concentration experiments and controlled annealing of matrices containing $Cu(C_2H_4)_{2or3}$ in the 30–45K range show convincing evidence for a transformation to a dinuclear species, $Cu_2(C_2H_4)_m$ where m was not defined. Such a transformation is well il-

TABLE XII
ULTRAVIOLET SPECTRAL DATA^a FOR $M(C_2H_4)_m$ AND $M_2(C_2H_4)_m$
(WHERE $M = Co, Ni, \text{ OR } Cu$, AND $m = 1 \text{ OR } 2$) (121)

Complex	Co	Ni	Cu
$M(C_2H_4)$	375	320	382
$M(C_2H_4)_2$	~280 ^b	280	276
$M_2(C_2H_4)$	240	240	240
$M_2(C_2H_4)_2$	225		

^a Units in nm. ^b Appears as a broad shoulder on the 240-nm absorption of $Co_2(C_2H_4)$.

illustrated by the UV-visible spectra shown in Fig. 27. Although the shifts in the optical spectra between mononuclears and dinuclears are large, the IR spectra do not show such a large effect of metal nuclearity, with $\nu_{C=C}$ shifts of only a few cm^{-1} . This behavior is reminiscent of the effects of Rh cluster size in rhodium-dioxygen complexes (119, 120), where the ν_{O-O} shifts vary little on moving from one to three Rh atoms.

These binuclear copper-ethylene complexes do not show very great thermal stability as discrete species. Rather, on warming of matrices containing these complexes to > 50 K, ethylene dissociation and controlled copper-clustering occur, and, at < 104 K, very small Cu_n species ($n < \sim 10$) may be observed in pure C_2H_4 . The data did not, however, permit an unambiguous, size-frequency determination of the distribution of the Cu_n species; a mixture of species is evidently present. In dilute $\text{C}_2\text{H}_4/\text{Ar}$ mixtures, such clustering is even more pronounced. Optical monitoring of these decomposition reactions is shown in Fig. 28.

Nickel atoms have also been allowed to react with C_2H_4 under cryogenic conditions (101, 123). Depending on the metal-concentration conditions and the deposition temperature, either mononuclear species, $\text{Ni}(\text{C}_2\text{H}_4)_n$, $n = 1-3$ (123), or multinuclear species, $\text{Ni}_2(\text{C}_2\text{H}_4)_m$, $m = 1-2$, and $\text{Ni}_3(\text{C}_2\text{H}_4)_l$, may be isolated. Unlike the copper complexes, these species are all colorless; the mononuclear ethylene complexes each dis-

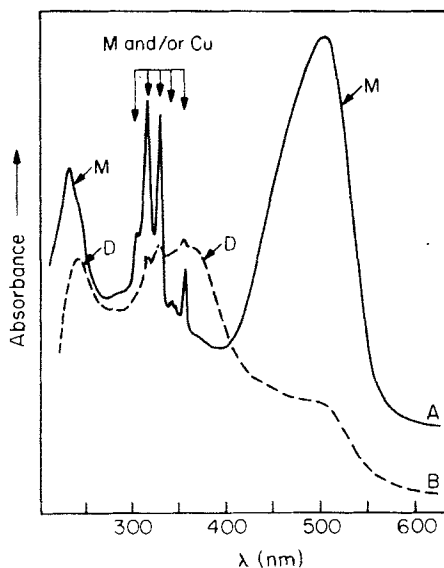


FIG. 27. The UV-visible spectrum of the products of the $\text{Cu}:\text{C}_2\text{H}_4 \approx 1:10^4$ cocondensation reaction (A) at 10–12K, showing $\text{Cu}(\text{C}_2\text{H}_4)_3$ (M), and (B) after warm-up to 50 K, showing the growth of the 365/240 nm absorptions of $\text{Cu}_2(\text{C}_2\text{H}_4)_m$ (D) (122).

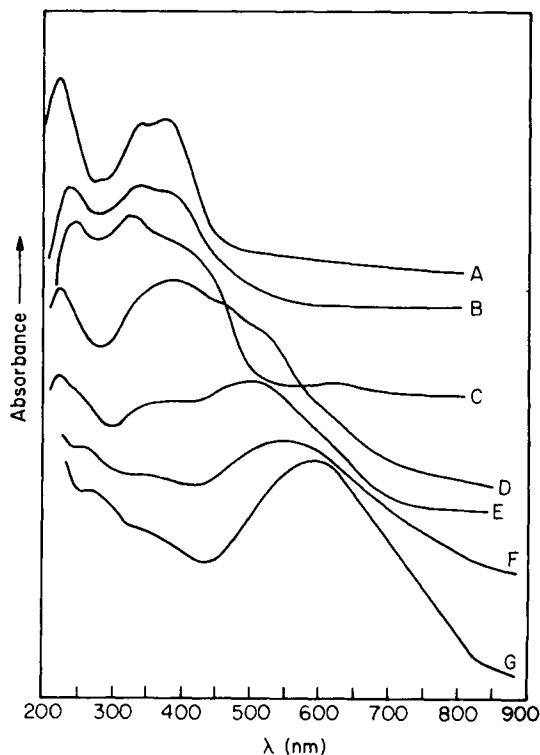


FIG. 28. The optical spectra of the products of the decomposition of $\text{Cu}_2(\text{C}_2\text{H}_4)_m$ (A)–(C) warmed from 50 to 100 K from pure C_2H_4 matrices; (D)–(G) warmed from 45 to 70 K from concentrated C_2H_4 : Ar \approx 1 : 10 matrices, showing the temperature–time evolution of “growing” copper clusters in the size regime less than 1.0 nm (122).

play one UV absorption that blue-shifts with increasing ethylene stoichiometry. The optical spectra, as with copper, show drastic changes on going from one nickel atom to two in an ethylene complex, but, once again, the IR spectra show only minor shifts in the $\nu_{\text{C}=\text{C}}$ and δ_{CH_2} modes (see Table XIII). [It should be mentioned that all of the ethylene complexes discussed in this Section yielded vibrational spectra consistent with their formulation as π -complexes (83). No evidence was found for di- σ -type species.] The spectroscopic data are summarized in Tables XII and XIII.

GVB–CI MO calculations have been performed on $\text{Ni}(\text{C}_2\text{H}_4)$ and $\text{Ni}_2(\text{C}_2\text{H}_4)$ (39, 101) in an effort to determine the electronic effects responsible for the shifts in the UV spectra and the nature of the bonding interactions between Ni and C_2H_4 . In essence, the two major points of interest in this Ni/ C_2H_4 study were (1) the minimal perturbation of

TABLE XIII
COMPARISON OF HRELS^a FOR C₂H₄ ON Ni(111) WITH Ni_n(C₂H₄)
CHEMISORPTION MODELS (121)

HRELS C ₂ H ₄ /Ni(111) (Ibach, Demuth, Lehwald ^b)	Ni(C ₂ H ₄) Ar/10–12K (Ozin, Power, Huber ^c)	Ni ₂ (C ₂ H ₄) Ar/10–12K (Ozin, Power, Upton, Goddard ^d)	Assignment
2940	2963	2880, 2908	νCH_2
2690 ^e			νCH_2^f
1500 ^f	1499	1488	$\nu\text{C}=\text{C}$
1430	^g	^g	δCH_2
1090	1160	1208, 1180	$\rho_w\text{CH}_2$
880	902	910	$\rho_r\text{CH}_2$
440	376	416 or 446 ^h	νNiC

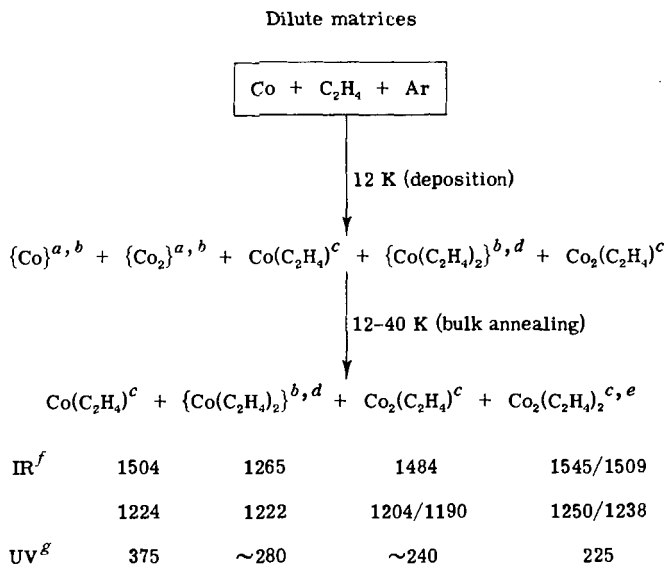
^a HRELS = high-resolution, electron-energy-loss spectroscopy. ^b *Surf. Sci.* (in press). ^c Ref. (123). ^d Ref. (101). ^e Softened νCH_2 surface-mode. ^f Weak band observed around 1500 cm⁻¹; could be a surface-dipole-forbidden, $\nu_{\text{C}=\text{C}}$ mode. ^g Hidden under intense δCH_2 mode of free C₂H₄ in the matrix. ^h One of these bands belongs to Ni₂(C₂H₄)₂.

the coordinated, ethylene intraligand, vibrational spectrum on placing the second nickel atom on Ni(C₂H₄), and (2) the observation of a UV transition for Ni(C₂H₄) at 320 nm that blue-shifts to 243 nm on passing to Ni₂(C₂H₄). In chemisorption terms, the perturbation of the electronic structure of a π -bonded, C₂H₄ moiety on a single, nickel-atom site by a neighboring Ni atom is observed.

To be brief, the calculations showed that, for both complexes, the ethylene geometry was only weakly perturbed, with R(CC) = 132 pm and R(NiC) = 207 pm. The C–H bonds were found to have a bend-back angle of only 2°. Upon coordination of the second nickel atom, the Ni–C₂H₄ binding-energy increased from 14.2 kcal for Ni(C₂H₄) to 27.2 kcal for Ni₂(C₂H₄). The GVB–CI transition-state calculations permitted making of tentative assignments for the optical spectra, and it was suggested that these excitations might best be described as MLCT [actually, Ni (3d → 4p), but with some mixing of 4p_y with π^* of C₂H₄]. The blue shift on going from Ni(C₂H₄) to Ni₂(C₂H₄) results from the greater stabilization of the 3d levels in the binuclear. The minimal, geometrical perturbation of the coordinated ethylene as a function of nickel cluster-size is, as mentioned, reflected in the insensitivity of the intraligand, vibrational spectra.

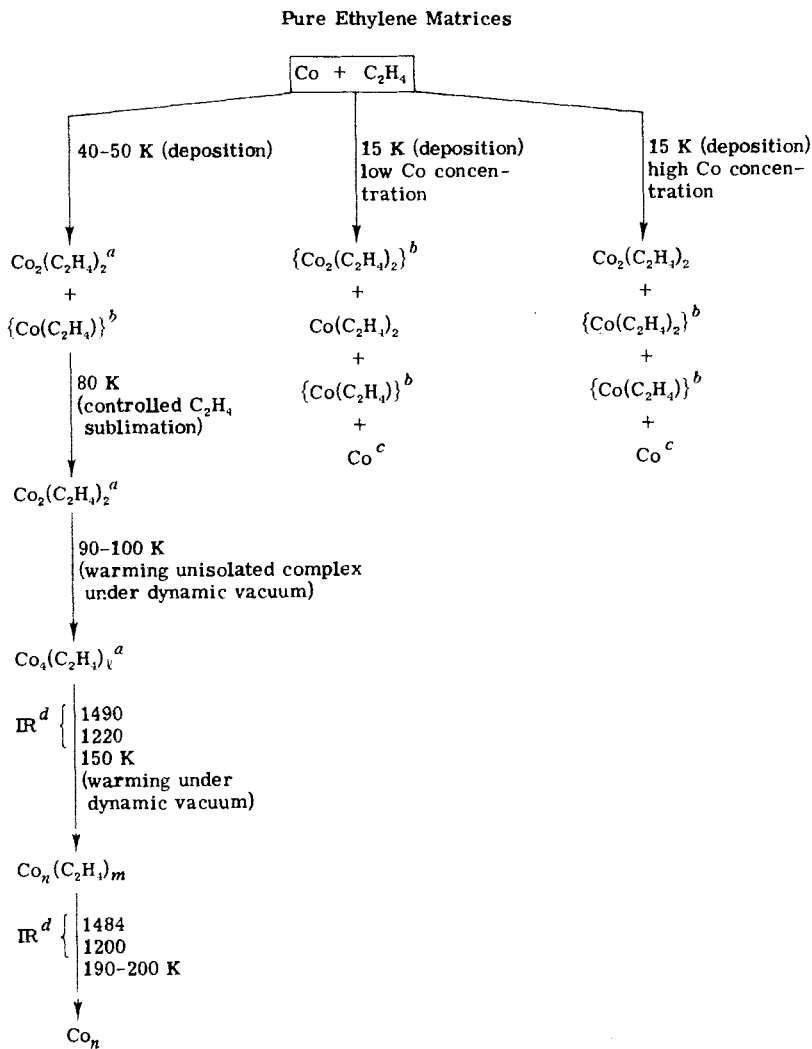
Cobalt atom reactions with ethylene were also studied (121). By using techniques similar to those described for Cu (122) and Ni (101), it has proved possible to synthesize a novel series of mononuclear and binuclear cobalt–ethylene complexes, Co(C₂H₄)_l, *l* = 1, or 2, and

$\text{Co}_2(\text{C}_2\text{H}_4)_m$, $m = 1$, or 2, as well as a suspected tetranuclear species $\text{Co}_4(\text{C}_2\text{H}_4)_n$. The routes to these complexes are summarized in Schemes 2 and 3, which also include the optical and vibrational data pertinent to the complexes. The formation of the dinuclear species was facilitated by the ready formation of Co_2 in Ar matrices, as shown by Hanlan (49). With respect to the mononuclears, the lack of evidence for a species of stoichiometry $\text{Co}(\text{C}_2\text{H}_4)_3$ reported by Timms and Piper (186) is interesting, as is, in this system, the stability of $\text{Co}_2(\text{C}_2\text{H}_4)_2$ at 80 K in the absence of any matrix (i.e., C_2H_4 pumped off under dynamic vacuum). Warming this complex to 100K resulted in its dimerization to $\text{Co}_4(\text{C}_2\text{H}_4)_n$, which further clustered at 150 K; the final product decomposed [presumably, to Co_n , similar to the Cu system (122)] at 190 K [coincidentally, the decomposition temperature reported for $\text{Co}(\text{C}_2\text{H}_4)_3$ (186)]. The conversion from $\text{Co}_2(\text{C}_2\text{H}_4)_2$ to $\text{Co}_4(\text{C}_2\text{H}_4)_n$ is shown in Fig. 29.



^a Seen in UV-visible. ^b The braces indicate minor products under these reaction conditions. ^c $^{12}\text{C}_2\text{H}_4/^{13}\text{C}_2\text{H}_4/(\text{Ar})$ isotopic confirmation. ^d Seen in 1/20-1/50 range; highly dependent on deposition conditions. No isotopic confirmation (see text). ^e Predominates at high Co concentrations and after 35 K, bulk annealing experiments. ^f Units in cm^{-1} . ^g Units in nm.

SCHEME 2. Dilute matrices (121).



^a ¹²C₂H₄/¹³C₂H₄ isotopic confirmation. ^b Braces indicate minor products under these reaction conditions. ^c Seen in UV-visible spectrum. ^d Units in cm⁻¹

SCHEME 3. Pure ethylene matrices (121).

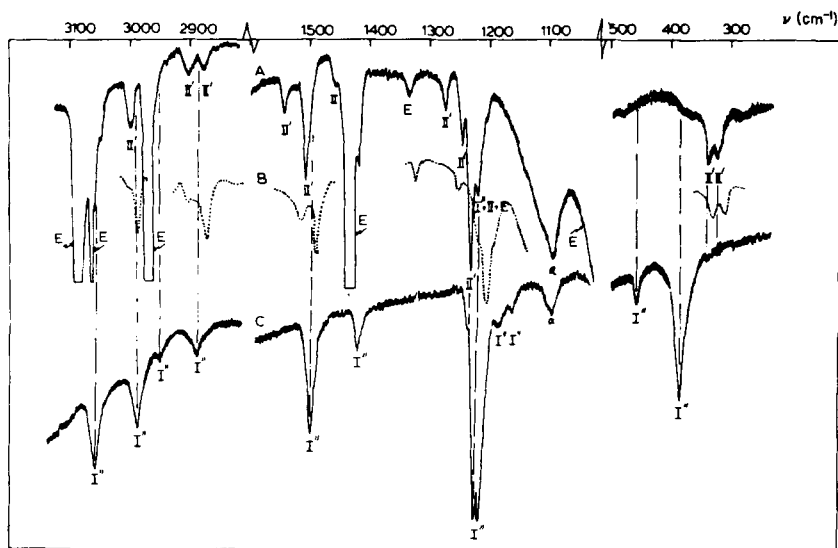


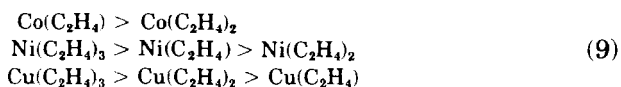
FIG. 29. The matrix IR spectra of Co atoms (A) deposited with $^{12}\text{C}_2\text{H}_4$ at 40–50 K, (B) deposited with $^{13}\text{C}_2\text{H}_4$ (91%) at 40–50 K, and (C) the spectrum obtained after controlled, $^{12}\text{C}_2\text{H}_4$ sublimation at 75–80 K from the matrix in (A) and further warming to 90–100 K, showing the transformation $\text{Co}_3(\text{C}_2\text{H}_4)_2$ to $\text{Co}_4(\text{C}_2\text{H}_4)_n$, where I = $\text{Co}(\text{C}_2\text{H}_4)$; II = $\text{Co}(\text{C}_2\text{H}_4)_2$; I' = $\text{Co}_2(\text{C}_2\text{H}_4)$; II' = $\text{Co}_3(\text{C}_2\text{H}_4)_2$; II'' = $\text{Co}_4(\text{C}_2\text{H}_4)_n$; E = unreacted C_2H_4 (121).

At this stage, it need hardly be said that the optical spectra for these complexes show a more significant dependence on olefin stoichiometry and metal nuclearity than the vibrational spectra. The exception to this statement is the noticeably large sensitivity of the $\nu_{\text{M}-\text{C}}$ modes both to metal-cluster size and the nature of the metal. For example, on passing from $\text{Ni}(\text{C}_2\text{H}_4)$ to $\text{Ni}_2(\text{C}_2\text{H}_4)_{1,2}$, the observed $\nu_{\text{Ni}-\text{C}}$ stretching modes shift from 376 to 416 and 446 cm^{-1} , respectively; in the case of $\text{Co}_2(\text{C}_2\text{H}_4)_2$ and $\text{Co}_4(\text{C}_2\text{H}_4)_n$, the observed $\nu_{\text{Co}-\text{C}}$ modes shift from 332, 314, to 384, 460 cm^{-1} . The higher frequencies for the nickel complexes are in line with the correspondingly greater thermal stabilities with respect to the cobalt complexes.

At this point, it seems appropriate to consider the Co-, Ni-, and Cu-ethylene system as a whole, both to rationalize any spectral trends as a function of metal, and to evaluate the use of these complexes as localized-bonding models for chemisorption of C_2H_4 .

In spite of the general insensitivity of the intraligand, vibrational modes to cluster size, there are a few specifics worth mentioning, particularly with respect to $\nu_{\text{C}=\text{C}}$ (ignoring effects of coupling with δ_{CH_2}

modes). The first point relates to the observed $\nu_{C=C}$ orderings



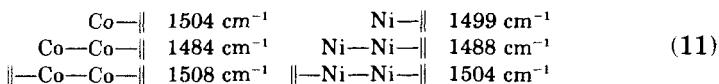
The amonotonic order for Co and Ni, compared to the monotonic order for Cu, may best be rationalized in terms of a finite, positive $k_{C=C, C=C}$ interaction force constant for Co and Ni, rather than as the outcome of amonotonicity in the principal $k_{C=C}$ force-constants.

A second significant point concerning the $\nu_{C=C}$ is the order



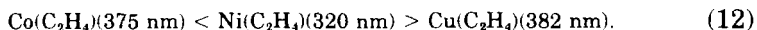
which is consistent with the GVB-CI idea that the main bonding interaction for these complexes is $\pi(\text{C}_2\text{H}_4) \rightarrow \sigma(\text{sp})\text{M}$ bonding.

Some other interesting parallels in the $\nu_{C=C}$ frequencies are the following.



The red shift from $\text{M}(\text{C}_2\text{H}_4)$ to $\text{M}_2(\text{C}_2\text{H}_4)$ is probably the result of lessened π -charge density on the ligand in the dimer; with charge density polarized (GVB-CI) away from the ethylene, it can more closely approach the metal atom, with subsequent, greater π -donation and, hence, a lower $\nu_{C=C}$. The subsequent blue-shift on adding the second C_2H_4 ligand most probably arises from increased, charge-repulsion effects between the π -electron densities of the ethylenes and the mainly s-s charge-density localized in the metal-metal bond. This would result in weaker π -bonding, which is manifested in the increased $\nu_{C=C}$.

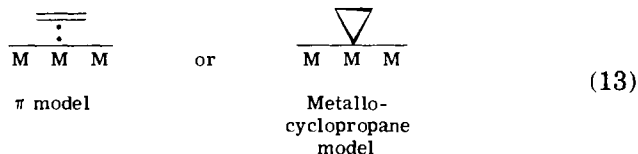
The order of the UV transitions is as follows:



Assuming that the $\text{Ni}(\text{C}_2\text{H}_4)$ transition is MLCT ($d \rightarrow p$), a metal-localized, $d \rightarrow p$ energy ordering in $\text{M}(\text{C}_2\text{H}_4)$ of the form $\text{Co} < \text{Ni} > \text{Cu}$ must be accounted for. In terms of effective nuclear charge-orbital penetration arguments, the $d \rightarrow p$ gap would initially be expected to take on the order $\text{Co} < \text{Ni} < \text{Cu}$. This is evidently an oversimplification, and account must be taken of the effect of a monotonically increasing, $\pi(\text{C}_2\text{H}_4) \rightarrow \sigma(\text{sp})\text{M}$, charge donation from C_2H_4 to the metal; this will clearly have an effect opposite to Z^* /penetration effects alone, and could well account for the "anomalously" low energy of the $d \rightarrow p$ excitation observed for $\text{Cu}(\text{C}_2\text{H}_4)$, and the resulting, amonotonic, $d \rightarrow p$, metal-localized ordering, $\text{Co} < \text{Ni} > \text{Cu}$.

The utility of any or all of these complexes as models for the chemisorption of ethylene on the pertinent metals is best illustrated by reference to Table XIII, which compares the vibrational data of C_2H_4 on the Ni(111) surface (27) to that of $Ni_2(C_2H_4)$ (101) and $Ni(C_2H_4)$. The similarity of the data presented indeed suggests that these matrix-isolated species may be regarded as such models. The spectrum of chemisorbed C_2H_4 consists of a broad band at 2940 cm^{-1} that would correspond to bands observed in the $3050\text{--}2875\text{ cm}^{-1}$ region of the finite-cluster species. The crucial, $\nu_{C=C}$ stretching modes of π -bonded ethylene seem relatively insensitive to cluster size or ethylene stoichiometry; this suggests that the δ_{CH_2} modes around 1200 cm^{-1} and the ν_{M-C} modes around $450\text{--}300\text{ cm}^{-1}$ are likely to be most informative in terms of localized-bonding discussions. In particular, it would appear that increasing the cluster size from $1 \rightarrow 2 \rightarrow 4$ causes a monotonic blue-shift of ν_{M-C} towards the value observed for the corresponding, ethylene-chemisorption mode, being already reasonably close for 2 to 4 metal-atom clusters. Broadly speaking, this would imply that it is possible to represent π -chemisorbed ethylene by a finite, cluster-ethylene complex of this nuclearity.

At this time, there is no obvious way of ascertaining whether or not matrix-isolated complexes are the best models for the interaction of small molecules with metal surfaces, clean or supported. Throughout the previous section, we gave an indication of the similarities of the spectra obtained in the two distinct types of experiments, and, although the correspondences are striking, there is no readily accessible, one-to-one correlation. It is, however, evident that the general idea is sound, and, if nothing else, the synthesis of such model complexes should serve to alert the surface and heterogeneous catalyst chemist to the availability of such organometallic data. Nevertheless, it must be borne in mind that the vibrational data for such "chemisorption models" as $M(C_2H_4)_n$ and $M_2(C_2H_4)_m$ can only be used as a guide to an understanding of the geometric and electronic structures of the π -chemisorbed form of ethylene on metal surfaces. The same idea applies to the other molecules under investigation. The clear distinction, for instance, between π -coordination and metallocyclopropane



bonding found for $Ni(C_2H_4)$ may not persist for the metal surface,

owing to the effect of long-range interactions with other metal atoms on and near the surface. Indeed, the type of bonding could depend on the surface site and may be radically modified for sites at edges or corners, rather than on plateaus (174, 175).

An indication of growing interdisciplinary interest in the field is illustrated in a review on new perspectives in surface chemistry and catalysis by Roberts (160), who discussed the interaction of N_2 with iron surfaces. In so doing, he referred to the $Fe_n(N_2)_m$ matrix Mössbauer work of Barrett and Montano (7), which showed that molecular nitrogen only bonds to iron when the latter is present as a dimer. As the chemisorption studies (161) indicated that N_2 is absorbed on single-atom sites, Roberts suggested (160), of the matrix data (7), "if this is correct, then our assignment of the N(1s) peak at 405 eV to end-on chemisorbed N_2 will require further investigation." Other reviews that consider matrix-isolation techniques for chemisorption simulation are collected in footnote a.

V. Classical Inorganic Ligands

Both the metal-atom and matrix techniques have many applications (91) in the study of complexes having such classical, inorganic ligands as CO, N_2 , O_2 , or phosphines. From a metal-atom point of view, novel complexes have been synthesized that have not been readily accessible via normal, chemical-synthesis techniques. The entrapment of such species permits both a rationalization of their spectroscopic and chemical properties and an evaluation of their stability.

A. CO COMPLEXES

Two separate publications (125, 126) described the synthesis of a number of carbonyl complexes of vanadium. The mononuclear species $V(CO)_n$, $n = 1-6$, have all been identified by using CO matrix-dilution experiments and mixed ^{12}CO - ^{13}CO isotope experiments while main-

^a 1. The Characterization and Properties of Small Metal Particles. Y. Takasu and A. M. Bradshaw, *Surf. Defect. Prop. Solids* p. 401 (1978). 2. Cluster Model Theory. R. P. Messmer, in "The Nature of the Chemisorption Bond" G. Ertl and T. Rhodin, eds. North-Holland Publ., Amsterdam, 1978. 3. Clusters and Surfaces. E. L. Muetterties, T. N. Rhodin, E. Band, C. F. Brucker, and W. R. Pretzer, Cornell National Science Center, Ithaca, New York, 1978. 4. Determination of the Properties of Single Atom and Multiple Atom Clusters. J. F. Hamilton, in "Chemical Experimentation Under Extreme Conditions" (B. W. Rossiter, ed.) (Series, "Physical Methods of Organic Chemistry"), Wiley (Interscience), New York (1978).

taining mononuclear metal-concentration conditions. The geometries of the carbonyls were assigned (126) as follows: $V(CO)_5$, D_{3h} ; $V(CO)_4$, D_{4h} or T_d ; $V(CO)_3$, D_{3h} ; and $V(CO)_2$, three isomers, C_{2v} , C_{2h} , and $D_{\infty h}$. These geometries have been compared with theoretical predictions (21a, 54). An interesting point concerning $V(CO)$ was the anomalously high, ν_{CO} stretching-frequency (1904, 1890, and 1868 cm^{-1} in Ar, Kr, and Xe, respectively) when compared to $Fe(CO)$, $Co(CO)$, $Ni(CO)$, and $Cu(CO)$ (1898, 1954, 1996, and 2010 cm^{-1} , respectively) (127). Molecular-orbital calculations suggested that the high ν_{CO} can be taken as strong evidence that the predicted Jahn-Teller instability of the molecule resulted in the formation of a nonlinear monocarbonyl.

The "saturated" species $V(CO)_6$ and $V_2(CO)_{12}$ were directly synthesized (28, 125) in CO, and CO-doped rare-gas, matrices by standard, metal-atom techniques. $V(CO)_6$ was investigated by IR and UV-visible spectroscopy, and $V_2(CO)_{12}$ by IR spectroscopy. The distortion indicated for $V(CO)_6$ in pure CO was found to persist in Ne, Ar, Kr, and Xe matrices, but with a magnitude of the same order as, or less than, a matrix-site splitting, as seen by comparison with regular O_h $M(CO)_6$ complexes in solid, noble-gas matrices. The polarizability-frequency plots suggested that the larger splitting in CO results from a matrix split superimposed on a genuine, molecular distortion. As shown in Fig. 30, two binuclear complexes could be generated in pure CO matrices, one of which (D_1) is more thermally stable than the other (D_2). By quantitative, V-concentration studies, the nuclearity was confirmed. From warm-up studies and isotope experiments, and by comparison with the isoelectronic, complex anion $[V_2(CO)_8(CN)_4]^{4-}$ (156), the more stable dimer D_1 was formulated as $(OC)_5V(\mu CO)_2V(CO)_5$, containing two equivalent, vanadium atoms and two bridging, CO groups.

The matrix UV-visible data for $M(CO)_6$ ($M = Ti, V$, or Cr) and $M(N_2)_6$ ($M = Ti, V$, or Cr) (128) have been obtained, and the ligand field and charge-transfer spectra analyzed and assigned. These data are summarized in Table XIV. Charge transfer from the ligand, N_2 or CO, was observed, with the former at lower energy. The interpretation of the data implied that N_2 is a weak ligand compared to CO, with both σ -donation and π -acceptance being less. A molecular-orbital analysis indicated that the lower the first-order energy of the acceptor orbital and the better its overlap, the greater the degree of back-donation in the ground state and the higher the energy of the charge-transfer, excited state. In this way, the lower-energy charge-transfer to N_2 compared to CO may be rationalized. In addition, $10D_q$ for N_2 is lower than for CO and, in these complexes, is relatively insensitive to the metal.

The magnetic circular dichroism (MCD) spectrum of matrix-isolated

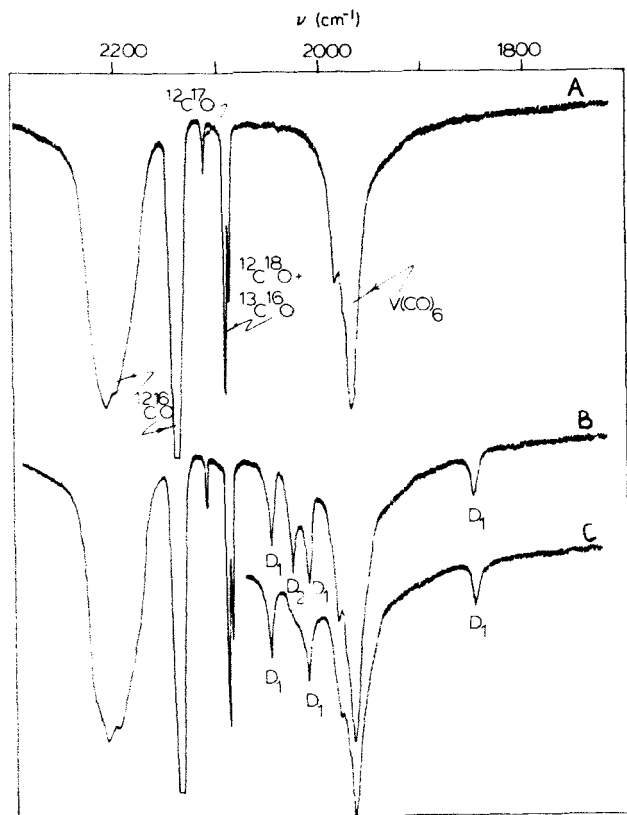


FIG. 30. IR spectra of the cocondensation reaction of V atoms with CO at 6–10 K: (A) at low V concentrations; (B) at high V concentrations; (C) at the same concentrations as (B), but after warming to 35 K (125).

$V(CO)_6$ generated by cocondensing presynthesized $V(CO)_6$ with N_2 at 10 K has been observed (44, 45). As suggested in a metal-atom study (125), the results indicated that a static, Jahn–Teller distortion is present. Matrix MCD also proved useful in confirming the predicted paramagnetism of $Fe(CO)_4$ (45) (produced by photolysis of $Fe(CO)_5$). In addition, matrix MCD was used to detect such paramagnetic species as MnO_2Cl_2 in the presence of MnO_3Cl (45).

Nonmetal-atom, matrix-isolation spectroscopy has proved useful in structure and isomer determination of stable, metal carbonyls. $Fe(CO)_4(NO)$ was investigated (157) in low-temperature matrices with ^{13}CO enrichment, and it was demonstrated that the IR spectrum is consistent with C_{2v} symmetry (trigonal bipyramid with an equatorial NO), in agreement with X-ray studies (55). The work resolves the dis-

TABLE XIV
LIGAND FIELD AND CHARGE-TRANSFER TRANSITION-ENERGIES FOR $M(N_2)_6$
AND $M(CO)_6$ (WHERE $M = Ti, V, Cr$) (128)

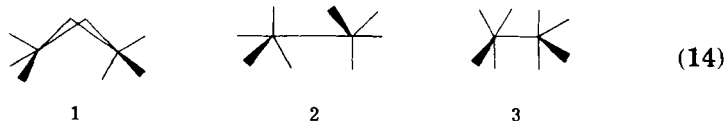
	M = Ti	M = V	M = Cr	
$M(N_2)_6$				
d-d	20 833 24 096	19 455 23 585	20 576 23 474	
Charge transfer	26 738	26 740 29 155	27 397	$t_{2g} \rightarrow t_{1u}$ CT1(N_2)
	30 581	31 646 33 557	32 680 34 602	$t_{2g} \rightarrow t_{2u}$ CT2(N_2)
		35 461	40 000	$t_{2g} \rightarrow t_{2g}^*$ (?)
$M(CO)_6$				
d-d	27 174 29 762	25 840 30 478	31 350 ^a	
Charge transfer	33 898	32 154 33 784 37 453	35 780 ^a	$t_{2g} \rightarrow t_{1u}$ CT1(CO)
	38 023	40 650 44 248	44 480 ^a	$t_{2g} \rightarrow t_{2u}$ CT2(CO)
			51 280 ^a	$t_{2g} \rightarrow t_{2g}^*$

^a H.B. Gray and N.A. Beach, *J. Am. Chem. Soc.* **85**, 2922 (1963).

parity between previous solution IR studies, where C_{3v} symmetry and an axial NO were suggested (55, 177), and the X-ray studies (55).

A partially oriented (using polarized, visible photolysis) sample of $Fe(CO)_5$ in solid CO at 20 K has been prepared (193). It was subsequently found that *no change* in the polarization properties of the system occurred during several hours of spectroscopic observation. It was concluded that the fluxionality of $Fe(CO)_5$ had been quenched under these conditions, as, were this not the case, maintenance of polarization for more than a fraction of a second would be impossible.

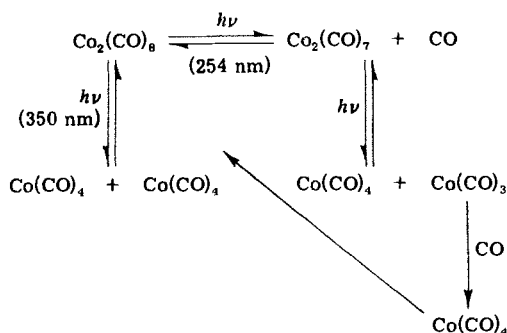
$Co_2(CO)_8$ has also been studied in low-temperature matrices (19, 20), the photochemical behavior of which led to the identification of three isomeric forms of the dimer complex (19). Two of these are the accepted forms, 1 and 2, whereas the third has no bridging, CO ligands. The structure most



compatible with the IR spectrum of the third isomer (3) was D_{2d} , in which the Co-Co bond axis lies in the plane of the trigonal, bipyramidal arrangement at each metal. Moreover, the isomers were found to be readily interconvertible: the nonbridged, D_{3d} isomer is transformed into the bridged form in hexane matrices, with $\Delta G^\ddagger = 6.4 \pm 0.4$ kcal/mol at 84 K. A separate study (17), using high temperatures and pressures, also showed the existence of a third isomer of $\text{Co}_2(\text{CO})_8$.

On photolyzing $\text{Co}_2(\text{CO})_8$ in the matrix (20), a number of photoproducts could be observed. The results of these experiments are summarized in Scheme 4, which illustrates the various species formed. Of particular interest is the formation of $\text{Co}_2(\text{CO})_7$ on irradiation of $\text{Co}_2(\text{CO})_8$ in CO (254 nm), as this species had not been characterized in the metal-atom study of Hanlan *et al.* (129). Passage of $\text{Co}_2(\text{CO})_8$ over an active, cobalt-metal surface before matrix isolation causes complete decomposition. On using a less active catalyst, the IR spectrum of $\text{Co}(\text{CO})_4$ could be observed. An absorption due to a second decomposition product, possibly $\text{Co}_2(\text{CO})_6$, was also noted.

Using Ag atom cocondensations, as well as other standard, matrix-characterization techniques, the silver carbonyls $\text{Ag}(\text{CO})_n$, $n = 1-3$, and $\text{Ag}_2(\text{CO})_6$ were synthesized (130). An illustration of the ^{12}CO - ^{13}CO stoichiometry confirmations for the mononuclears is shown in Fig. 31. When $\text{Ag}(\text{CO})_3$ is synthesized in pure CO, the vibrational data are consistent with a slightly distorted, trigonal planar structure. However, this is a matrix effect, because, in Ar, Kr, or Xe, a D_{3h} structure is observed. The esr spectrum of $\text{Ag}(\text{CO})_3$ in CO/Ar matrices supports this description ($g_{\parallel} = 2.012$ and $g_{\perp} = 1.995$), whereas the corresponding, optical spectra are consistent with that expected for a D_{3h} species having a $^2A_2''$ ground-state. Unlike the analogous, Cu complex, $\text{Ag}_2(\text{CO})_6$ could not be synthesized from the matrix reaction of Ag



SCHEME 4

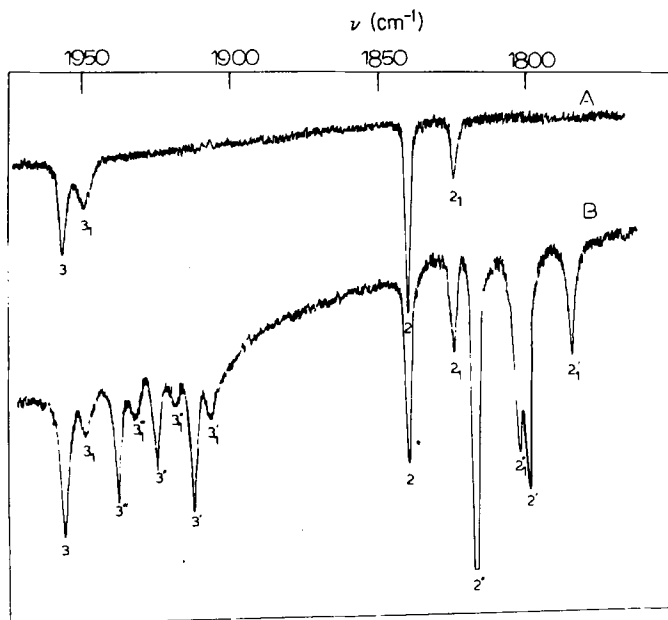


FIG. 31. The matrix IR spectrum of the products of the cocondensation reaction of Ag atoms with (A) $^{12}\text{C}^{16}\text{O}:\text{Ar} = 1:100$, and (B) $^{12}\text{C}^{16}\text{O}:^{12}\text{C}^{18}\text{O}:\text{Ar} \approx 1:1:250$ matrices at 10–12K, showing $\text{Ag}(\text{CO})_3$ and $\text{Ag}(\text{CO})_2$ (where 2 and 3 = site 1; 2_1 and 3_1 = site 2) (130).

and CO at high silver concentrations. However, as already discussed, $\text{Ag}(\text{CO})_3$ dimerizes in CO matrices at 30–35 K, to yield $\text{Ag}_2(\text{CO})_6$ (118).

Binary gold carbonyls $\text{Au}(\text{CO})_{1,2}$ have also been synthesized (131), and characterized by using ^{12}CO – ^{13}CO isotopic substitution. The IR data for $\text{Au}(\text{CO})_2$ in rare gas matrices favor a linear $D_{\infty h}$ structure. Detailed investigation of the complexes revealed a variety of interesting site-effects and matrix-induced frequency-shifts. However, unusual, vibrational-isotope patterns were observed for the product formed in $^{12}\text{C}^{16}\text{O}/^{13}\text{C}^{16}\text{O}$, $^{12}\text{C}^{16}\text{O}/^{12}\text{C}^{18}\text{O}$, and $^{12}\text{C}^{16}\text{O}/^{13}\text{C}^{18}\text{O}$ mixtures, as shown in Fig. 32. Ten distinct, mixed isotopic molecules were observed, containing nonequivalent carbonyl ligands. These data could be interpreted in terms of an isocarbonyl(carbonyl)gold complex, $(\text{OC})\text{Au}(\text{OC})$, a linkage isomer of bis(carbonyl)gold. A further, spectroscopic difference is illustrated in the optical spectra (see Fig. 33), which show a large shift in one particular UV absorption and a small shift in the intense, visible absorption. It would seem that the existence of the isocarbonyl may be a consequence of the head-to-tail, orientational requirements of the CO molecules in the fcc lattice of crystalline CO, rather than of an inher-

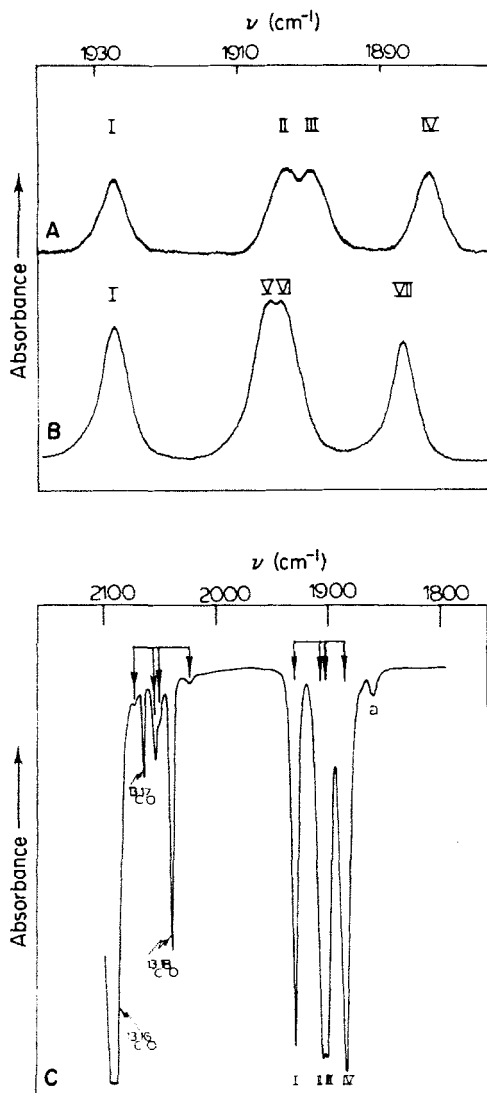
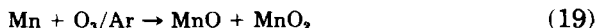
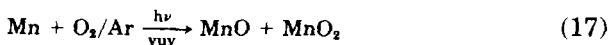


FIG. 32. Matrix IR spectrum of Au atoms deposited with (A) a $^{12}\text{C}^{16}\text{O}:^{13}\text{C}^{16}\text{O} \approx 1:1$ mixture, and (B) a $^{12}\text{C}^{16}\text{O}:^{12}\text{C}^{18}\text{O} \approx 1:1$ mixture at 6–10 K, showing the presence of the seven, distinct, mixed isotopic molecules $\text{Au}(^{12}\text{C}^{16}\text{O})(^{16}\text{O}^{12}\text{C})$ (I), $\text{Au}(^{12}\text{C}^{16}\text{O})(^{16}\text{O}^{13}\text{C})$ (II), $\text{Au}(^{13}\text{C}^{16}\text{O})(^{16}\text{O}^{12}\text{C})$ (III), $\text{Au}(^{13}\text{C}^{16}\text{O})(^{16}\text{O}^{13}\text{C})$ (IV), $\text{Au}(^{12}\text{C}^{16}\text{O})(^{18}\text{O}^{12}\text{C})$ (V), $\text{Au}(^{12}\text{C}^{18}\text{O})(^{16}\text{O}^{12}\text{C})$ (VI), and $\text{Au}(^{12}\text{C}^{18}\text{O})(^{18}\text{O}^{12}\text{C})$ (VII). Curve C is the same as curve A, but with a complete scan after a long deposition-time, showing the quartet isotopic pattern associated with the weak, high-frequency absorptions at 2072, 2054, 2050, and 2024 cm^{-1} (note that, under these conditions, weak absorptions due to traces of free $^{13}\text{C}^{17}\text{O}$ and $^{13}\text{C}^{18}\text{O}$ in the commercial $^{12}\text{C}^{16}\text{O}/^{13}\text{C}^{16}\text{O}$ mixture were observed in the 2100- cm^{-1} region) (131).

and the other after warm-up to 40–45 K, were observed. The corresponding IR spectra only show weakly perturbed CO₂ lines, and, hence, the low-temperature species is probably Au(CO₂), with a weak gold–CO₂ interaction. The warm-up product was not characterized. In a similar way, Ag atoms reacted with CO₂ to form a single compound best formulated as Ag(CO₂) (133), a weak π -complex.

B. O₂ COMPLEXES AND OXIDES

Manganese atoms were cocondensed with O₂, N₂O, or O₃, to afford MnO, MnO₂, MnO₃, and MnO₄ (197). The actual reactions involved were



The compounds formed were studied by esr spectroscopy, with the magnetic parameters being used to determine the geometries. MnO₂ is linear, whereas MnO₃ is trigonal planar (D_{3h}), and MnO₄ is distorted tetrahedral with C_{3v} symmetry.

In a preliminary report (1), Fe atoms were reacted with O₂, leading to formation of Fe(O₂), a cyclic isosceles (C_{2v}) species, as suggested by mixed isotope experiments. Reaction of Fe atoms with N₂O resulted in formation of FeO. A feature at 887 cm⁻¹, assigned to a Fe/N₂ complex, is probably erroneous, and may be an iron nitride species. In the same triad, the MCD spectrum of matrix-entrapped OsO₄ was studied (46). The spectrum was found to be similar to that of MnO₄⁻ in a solid lattice, and was assigned accordingly.

The Rh/O₂ system (119, 120) has already been discussed with particular reference to the multinuclear species. To summarize, at low Rh concentrations, the species Rh(O₂)_{1and2} can be isolated. The optical spectra of Rh(O₂)₂ and Pd(O₂)₂ were compared (see Fig. 34), and the spectral shifts interpreted in light of qualitative, MO considerations. The absence of any visible absorption argues against an M²⁺(O₂)₂ formulation, and the UV-spectral shifts are consistent with a LMCT assignment. Thus, although the π and π^* O₂ levels remain at about the same energy in the two complexes, the metal d-orbitals stabilize on going from Rh to Pd. Hence a transition from a low-lying, O₂ π orbital

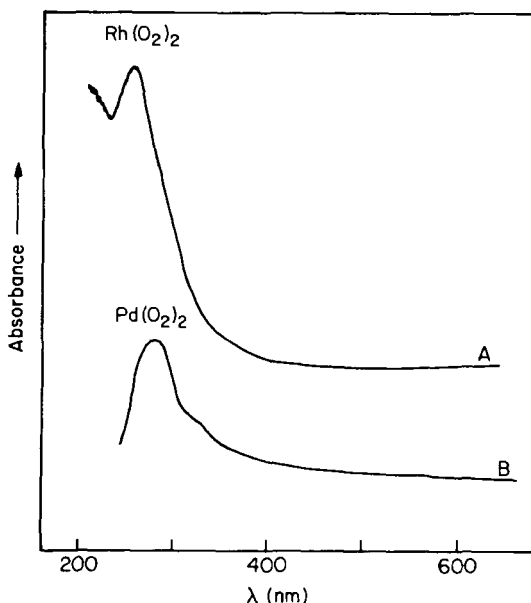


FIG. 34. UV-visible spectrum of the products formed when (A) Rh atoms, and (B) Pd atoms are cocondensed with $^{16}\text{O}_2$ at 10–12 K and $M : ^{16}\text{O}_2 \approx 1 : 10^5$ (119).

to a vacancy in the upper $M\text{—O}_2$ levels would red-shift in the observed order (119, 120).

A number of investigations of the copper-group oxides and dioxygen complexes have been reported. The electronic spectra of CuO , AgO , and AuO were recorded in rare-gas matrices (9), and it was found that the three oxides could be formed effectively by cocondensation of the metal atoms with a dilute, oxygen matrix, followed by near-ultraviolet excitation. The effective wavelengths for CuO or AgO formation were $\lambda \geq 300$ nm and for AuO was $\lambda \geq 200$ nm. In addition, the laser fluorescence spectrum of CuO in solid Ar has been recorded (97).

The metal-atom reactions of Cu (98), Ag (134), and Au (135) with O_2 provided interesting results, especially when these were compared with the results from the nickel triad (137). As shown by standard matrix-techniques, Ag forms two O_2 complexes that are best formulated as Ag^+O_2^- and Ag^+O_4^- , based on the absence of visible absorptions and the similarity of the IR spectra to those of Cs^+O_2^- and Cs^+O_4^- (3a,b). The UV absorptions for $\text{Ag}(\text{O}_2)$ and $\text{Ag}(\text{O}_4)$, at 275 and 290 nm, respectively, could be associated with the O_2^- and O_4^- anions. The shifts in the IR spectra on going from $\text{Ag}(\text{O}_2)$ to $\text{Ag}(\text{O}_4)$ also argue against an $(\text{O}_2)\text{Ag}(\text{O}_2)$ formulation for the latter complex, being in the opposite sense to those observed for $\text{Pd}(\text{O}_2)_1$ and 2 (137). In contrast, whereas

Cu^+O_2^- may be formulated in the same way, $\text{Cu}(\text{O}_2)_2$ is best regarded as a bis(dioxygen) species [actually, $\text{Cu}^{2+}(\text{O}_2^-)_2$ (98)], rather than as a complex of O_4^- . The geometry of Ag^+O_4^- could not be determined from the spectroscopic data; however, the results of MO calculations on Na^+O_4^- (3a, 3b) favored a puckered, five-membered ring. These differences between Cu, Ag, and Au may possibly be explained by noting that the unfavorably high, second ionization-potential for Ag might preclude the formation of an Ag(II) dioxygen complex. This argument is somewhat strengthened by the fact that gold forms only $\text{Au}(\text{O}_2)$ (135). The green color of $\text{Au}(\text{O}_2)$ suggests a zero-valent, gold formulation, where the high, first-ionization potential of Au (9.22 eV) precludes oxidation to Au(I) under cryogenic reaction-conditions ($\text{IP}_{\text{Cu}} = 7.72$, $\text{IP}_{\text{Ag}} = 7.57$ eV).

On cocondensing Ag atoms with mixed CO/ O_2 matrices (136), a new species (OC)Ag(O_2) was observed, most probably containing O_2 bound in a side-on fashion ($^{16}\text{O}_2/^{18}\text{O}_2$ isotope data). The appearance of the carbonyl stretching-mode (2165 cm^{-1}) in a region above that of free CO (2138 cm^{-1}), and the O_2 stretching mode at about the frequency of the superoxide anion (1110 cm^{-1}), when taken in conjunction with an observed UV absorption (285 nm) close to that of free O_2^- and the absence of any visible absorption, provided convincing evidence in favor of the tight, ion-pair formulation (OC)Ag $^+(\text{O}_2^-)$, in which the silver atom may be considered to act as a strong σ -acceptor, and yet a weak π -donor with respect to CO. The (OC)Ag $^+(\text{O}_2^-)$ complex, unlike the peroxy-formate product of the Au/CO/ O_2 system (132), does not act as a precursor to CO_2 .

Work has also been conducted that involved the investigation, via infrared spectroscopy, of matrix-isolated, plutonium oxides (40), with the appropriate precautions being taken because of the toxicity of plutonium and its compounds. A sputtering technique was used to vaporize the metal. The IR spectra of PuO and Pu O_2 in both Ar and Kr matrices were identified, with the observed frequencies for the latter (794.25 and 786.80 cm^{-1} , respectively) assigned to the ν_3 stretching-mode of Pu $^{16}\text{O}_2$. Normal-coordinate analysis of the Pu O_2 isotopomers, Pu $^{16}\text{O}_2$, Pu $^{18}\text{O}_2$, and Pu $^{16}\text{O}^{18}\text{O}$ in Ar showed that the molecule is linear. The PuO molecule was observed in multiple sites in Ar matrices, but not in Kr, with Pu ^{16}O at 822.28 cm^{-1} in the most stable, Ar site, and at 817.27 cm^{-1} in Kr. No evidence for Pu O_3 was observed.

C. N_2 COMPLEXES AND NITRIDES

Titanium atoms have been cocondensed with CO and N_2 matrices (138) and the products identified as $\text{Ti}(\text{CO})_6$ and $\text{Ti}(\text{N}_2)_6$. The IR data

for the two species indicated that they are structurally related, and are subject to a Jahn–Teller distortion. The 40-cm^{-1} split observed for the $T_{1u} \nu_{CO}$ stretching-mode in solid CO is retained in noble-gas matrices, a fact that, coupled with the linear, Buckingham plots (see Fig. 35) for both components, supports the designation of an inherent, molecular distortion for $\text{Ti}(\text{CO})_6$ [and $\text{Ti}(\text{N}_2)_6$], rather than a matrix effect. However, the magnitude of the distortion is probably quite small, as the electronic spectra of both species display the gross features expected for low-spin, d^4 octahedral complexes (128).

Under similar reaction-conditions, the vanadium species $\text{V}(\text{N}_2)_6$ (139) has been isolated. In addition, a species $\text{V}_2(\text{N}_2)_n$ (n probably = 12) was observed (139). The metal nuclearity was established by the standard, metal-concentration techniques. A comparison of the optical spectra of $\text{V}(\text{N}_2)_6$ and $\text{V}(\text{CO})_6$ (128) suggested that these molecules have very similar, electronic properties, and the data clearly established that N_2 is a strong, field ligand in its bonding properties. Interestingly, atomic V could be isolated in N_2 matrices from 8–12K co-

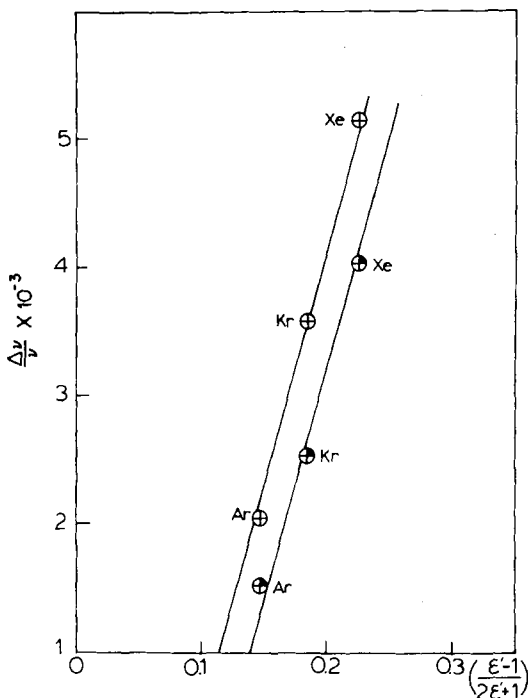
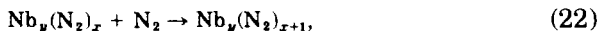


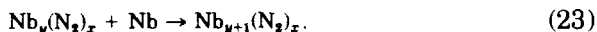
FIG. 35. Buckingham plot for both components of the doublet splitting of $\text{Ti}(\text{CO})_6$ in Ar, Kr, and Xe matrices (138).

depositions, and yet $V(N_2)_6$ is preferentially formed at 20–25 K; this demonstrated the subtle temperature-dependence of product yield when direct syntheses are performed with metal atoms.

Dinitrogen has also been reacted with atomic Nb (produced from a sputtering source) (47), a number of $\nu_{N\equiv N}$ stretching-modes being observed. The spectra were too complicated to permit full, stoichiometric and structural identification, but $Nb(N_2)$ and a D_{4h} square-planar $Nb(N_2)_4$ were tentatively assigned. The authors deduced a number of conclusions. (1) Geometrical isomers exist for the higher stoichiometries, e.g., D_{3h} and C_{2v} for $Nb(N_2)_3$. (2) Both "sideways" and "end-on" bonding of N_2 to Nb result in more than one absorption peak, even for the lower stoichiometry species, such as $Nb(N_2)$. (3) There is an unusually strong interaction between the complexes and the matrix environment, resulting in multiple sites and, hence, multiple absorptions. (4) Some of the complexes are multinuclear. (5) Some of the complexes contain a ligand other than N_2 (perhaps a CO impurity). (6) The warm-up data can be explained by such reactions as



rather than



Clearly, more work needs to be done with this system.

The products of the cocondensation of Cr atoms with N_2 at 10–12 K have been investigated (29) using IR and UV-visible spectroscopy, and the products of similar N_2 /Ar depositions were monitored by IR spectroscopy. From ligand-concentration experiments and annealing studies, six mononuclear species, $Cr(N_2)_n$ ($n = 1-6$) were identified. It was suggested that $Cr(N_2)$ and $Cr(N_2)_2$ are linear, with $C_{\infty v}$ and $D_{\infty h}$ symmetries, respectively. $Cr(N_2)_3$ is probably C_{2v} , whereas $Cr(N_2)_4$ is either T_d or D_{4h} . $Cr(N_2)_5$ is a tetragonal pyramid, C_{4v} , whereas $Cr(N_2)_6$ is O_h . The optical spectra supported the contention (29, 139) that N_2 is a strong field-ligand having an observed $10Dq$ of $28,800\text{ cm}^{-1}$ in $Cr(N_2)_6$. The optical spectra and assignments had been previously discussed (128).

The reaction of plutonium metal with N_2 in a sputtering device (41) resulted in the observation of matrix-isolated, plutonium nitride species. The species observed were PuN and PuN_2 , the latter being a linear species.

This section on N_2 complexes concludes with a brief mention of a Mössbauer study of the Fe/N_2 system (8). The N_2 stoichiometries were

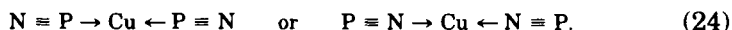
not determined, but it was found that N_2 reacts only with the Fe dimer. The ^{57}Fe isomer shift suggested less σ -donation or π -backbonding, or both, in the identified iron-nitrogen complex than in stable, dinitrogen compounds.

D. MISCELLANEOUS COMPLEXES

A number of other metal atom-matrix studies have appeared in the literature, with such typical inorganic ligands as NO and H. In the following Section, we shall briefly summarize some of these results.

A Japanese group reacted iron vapor with nitric oxide at 77 K (6). Two different species were observed, with ν_{NO} at 1800 and 1720 cm^{-1} , that were assigned as NO species adsorbed on oxidized and metallic iron, respectively. Although no evidence was presented as to the nuclearity of the products, the authors considered the species to be models for the chemisorption of NO on iron surfaces.

Timms and Atkins (181) reacted the novel ligand, PN (180) (generated by pyrolyzing P_3N_3), with a number of different metal atoms. With Cu, a bis(PN) complex was formed, although it was not possible to distinguish between the two isomers



MO calculations (86) suggested that coordination through phosphorus may be more probable. Au atoms also formed a $Au(PN)_2$ species in Kr. These Cu and Au species are straw-colored; in contrast, Ag atoms and PN form an intensely blue matrix, with IR bands suggesting the presence of two species, assigned as $Ag(PN)$ and $Ag_2(PN)_2$, the latter having bridging, PN ligands (suggested by the much lower ν_{PN} , the 150- cm^{-1} shift being similar to the shifts observed between terminal and bridging CO ligands). Reactions with Co, Ni, or Pd atoms also yielded complexes, although the stoichiometries were not elucidated.

Iron atoms have been reacted with various phosphine ligands. Verkade *et al.* (194) reacted Fe with $P(OMe)_3$ on a macro-scale, both by cocondensing the two simultaneously, and by depositing Fe onto a cooled solution of the ligand. The product isolated from the reaction mixture was $Fe[P(OMe)_3]_5$, which could also be synthesized by the sodium amalgam reduction of $FeCl_2$ in the presence of an excess of the ligand. Another complex, $Fe[P(OCH_2)_3CCH_2CH_3]_5$, was synthesized by cocondensing Fe atoms with 1,5-COD in a static reactor precharged with the phosphine ligand. Yields were, however, quite low (<20%) in the metal-atom reactions. King and co-workers (63) reacted Fe vapor with aminodifluorophosphines, to form $Fe[(CH_3)_2NPF_2]_3$ in 14% yield.

In addition, a similar reaction resulted in a 1% yield of $\text{Fe}[\text{CH}_3\text{N}(\text{PF}_2)_2]_4$.

The iron complex $\text{Fe}[\text{P}(\text{OC}_6\text{H}_5)_3]_2[(\text{C}_6\text{H}_4\text{O})\text{P}(\text{OC}_6\text{H}_5)_2]_2$ has been synthesized by metal-atom evaporation-techniques (190). The complex is, formally, the result of two ortho-oxidative, C-H additions, accompanied by loss of a molecule of H_2 .

Ytterbium atoms have been reacted with thermally generated hydrogen or deuterium atoms, with the resultant formation of YbH and YbD (198). The IR ν_{YbH} stretching-frequency was observed at 1214.9 cm^{-1} . In addition, Yb atom and YbH absorption and emission spectra were observed. The magnetic parameters of YbH were determined from the esr spectra of the $^2\Sigma$ molecules (with Yb nuclear spin $I = 0$ and $I = \frac{1}{2}$) to be $g_{\parallel} = 1.9953$, $g_{\perp} = 1.9402$, $A_{\parallel}(\text{H}) = 226\text{ MHz}$, $A_{\perp}(\text{H}) = 224\text{ MHz}$, $A_{\perp}[^{171}\text{Yb} (I = \frac{1}{2})] = 5.266\text{ GHz}$, $A_{\parallel}[^{171}\text{Yb} (I = \frac{1}{2})] = 5.724\text{ GHz}$. The hyperfine parameters indicated that the spin density is less than 20% on the hydrogen, and that the bonding is largely Yb^+H^- .

Another study (200) presented IR data for a number of hydride and deuteride species. Using matrix-isolation spectroscopy in conjunction with a hollow-cathode, sputtering source (the apparatus for which is shown in Fig. 36), the IR-active vibrations of the diatomic hydrides and deuterides of aluminum, copper, and nickel were observed. The vibra-

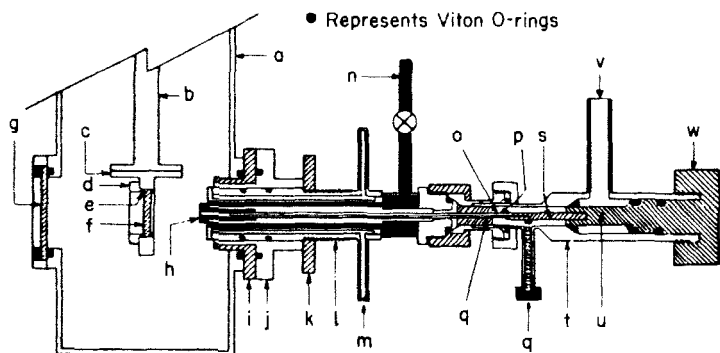


FIG. 36. Cross-sectional view of a matrix-isolation, hollow-cathode, sputtering device. See ref. (200) for explanation of components. The letters indicate the following: (a) vacuum chamber; (b) Cryogenic Technology, Inc., Model 21 closed-cycle, helium refrigerator; (c) OFHC-copper-deposition plate-holder; (d) OFHC-copper retaining ring; (e) indium gaskets; (f) KCl or CsI deposition plate; (g) quartz window; (h) metal cathode; (i) Teflon spacer; (j) flange; (k) brass, threaded ring; (l) cathode support; (m) water-cooled tubes; (n) gas-flow inlet; (o) quartz tube; (p) platinum-wire anode; (q) Teflon plug; (r) spring-loaded electrode; (s) brass rod; (t) modified, glass stopcock; (u) stopcock valve; (v) discharge-gas inlet; (w) stopcock knob.

tions at 14 K in an Ar matrix were AlH, 1593; AlD, 1158; CuH, 1882; CuD, 1356; NiH, 1906; and NiD, 1374 cm^{-1} . Interestingly, the compounds were produced only when hydride or deuteride atoms were formed in the discharge; on codeposition of the metals with molecular H_2 , hydrides were not observed. Spectra of molecular hydrides and deuterides of Ti, V, Zr, Nb, Mo, and W were also isolated (200), but, because of spectral complications, the compound stoichiometries were not reported.

VI. Organometallic Complexes

It is in the synthesis of organometallic complexes that the metal-atom technique shows its greatest utility. From metal vapors, many complexes may be synthesized on a macroscale that are difficult, if not impossible, to prepare by standard, wet-chemical techniques (64, 65). In this section, we shall illustrate the vast potential that the method has in this area, although, to be sure, it is evident throughout this entire review.

A. ARENE COMPLEXES

Chromium atoms have been reacted at 77 K with a mixture of benzene and pentafluorobenzene (84), to give a 22% yield of the sandwich complex $[(\text{C}_6\text{H}_6)\text{Cr}(\text{C}_6\text{F}_5\text{H})]$; this was the starting point in an interesting series of reactions (85). The complex is readily lithiated at -78°C , with subsequent conversion into $[(\text{C}_6\text{H}_6)\text{Cr}(\text{C}_6\text{F}_5\text{X})]$, where $\text{X} = \text{SiMe}_3$, CO_2Li , CMe_2OH , $(\eta\text{-C}_5\text{H}_5)\text{Fe}(\text{CO})_2$, or $(\eta\text{-C}_5\text{H}_5)\text{Fe}(\eta\text{-C}_5\text{H}_4\text{CHOH})$. In a similar way, the complexes 1,2,3,5-tetrafluorochromarene, 1,2,4,5-tetrafluorochromarene, 2,3,4,5,6-pentafluoro-1,1'-dimethylchromarene, and 1,1'-dimethylchromarene (85) were obtained. [Chromarene was the authors' name for $(\text{C}_6\text{H}_6)_2\text{Cr}$, the derivatives being named by analogy with ferrocene (85).]

Benzene, benzene- d_6 , and fluorobenzene were found (170, 171) to react with chromium, cobalt, iron, and nickel atoms on codeposition in the neat ligand at 77 K, or in argon matrices at 10–12 K. IR studies of the products indicated that the initial reaction of these transition-metal atoms with an aromatic system is π -complex formation. Studies of ligand concentration-effects showed that the chromium-atom reaction is approximately second-order with respect to benzene, yielding the previously known (182) complex $(\text{C}_6\text{H}_6)_2\text{Cr}$, whereas, with the other metals, the reaction is first-order, yielding $\text{M}(\text{C}_6\text{H}_6)$, $\text{M} = \text{Co}$, Fe , or Ni . The absence of $\text{Cr}(\text{C}_6\text{H}_6)$ is probably a reflection of (a) the fact that the

M:L ratio in this particular study was not sufficiently low to permit isolation of $\text{Cr}(\text{C}_6\text{H}_6)$, or (b) the exceedingly high lability of the complex. Stoichiometries were determined by mixed $\text{C}_6\text{H}_6/\text{C}_6\text{D}_6$ or $\text{C}_6\text{H}_6/\text{C}_6\text{H}_5\text{F}$ depositions, an example of which is shown in Fig. 37. The IR shifts of some modes of $\text{M}(\text{C}_6\text{H}_6)$ ($\text{M} = \text{Co}, \text{Fe}, \text{or Ni}$) and $\text{Cr}(\text{C}_6\text{H}_6)_2$, tabulated in Table XV, indicated that the relative bond-strengths of the metal-arene bonds are $\text{Cr} > \text{Fe} > \text{Co} > \text{Ni}$. Evidence for binuclear or higher cluster complexes, or both, was observed, but these species were not characterized. Manganese atoms were found not to react with benzene under the conditions studied, possibly as a result of manganese cluster-formation.

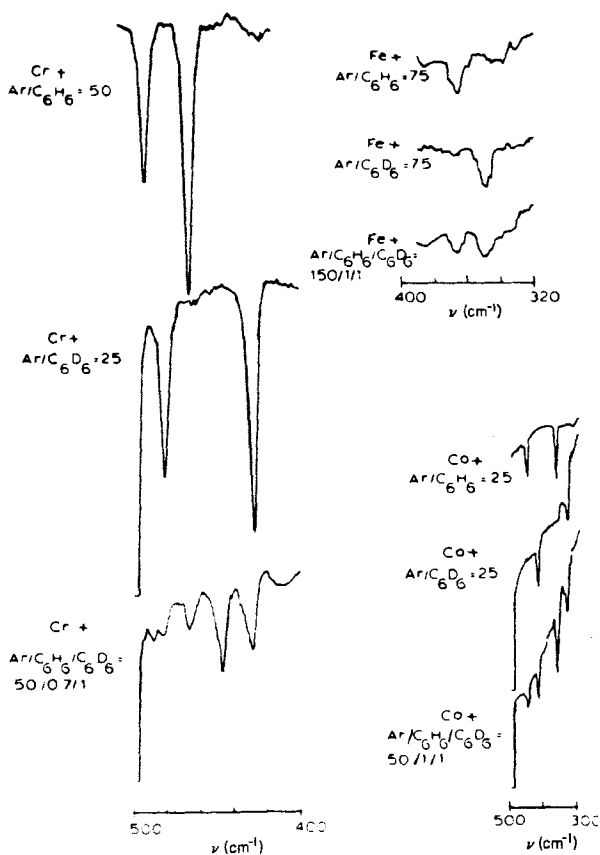


FIG. 37. Far-infrared spectra of chromium, iron, and cobalt atom reactions with benzene, benzene- d_6 and benzene/benzene- d_6 mixtures in argon matrices at 10–12K (171).

TABLE XV

FAR-INFRARED BANDS AND SHIFTS OF THE $\nu\text{C}=\text{C}$ STRETCHING AND $\delta\text{C}-\text{H}$ o.p. BENDING VIBRATIONS OF BENZENE UPON COMPLEXATION^a (171)

Complex	$\Delta\nu(\text{C}=\text{C})$ stretch ^b (cm^{-1})	$\delta(\text{C}-\text{H})$ o.p. bend ^b (cm^{-1})	Far-infrared (cm^{-1})
$(\text{C}_6\text{H}_6)_2\text{Cr}$	-49	+122	492, 466
$(\text{C}_6\text{H}_6)\text{Fe}$	-40	+89	485, ^c 366
$(\text{C}_6\text{H}_6)\text{Co}$	-39	+85	454, 366
$(\text{C}_6\text{H}_6)\text{Ni}$	-31	+75	445, ^c 346

^a Argon matrices at 10–12K, unless otherwise noted. ^b The symbols + and - indicate shifts to higher and lower wavenumbers, respectively, ^c Benzene matrix at 77 K.

Complexation with polyaromatic systems has also been observed. For instance, $\text{M}(\text{naphthalene})_2$, $\text{M} = \text{Cr}$ (88, 183), Mo (183), V (183), or Ti (183) may be synthesized in a solution reactor with the appropriate, metal vapors at liquid-nitrogen temperature. The $\text{Cr}/\text{naphthalene}$ complex is less stable (dec. 160°C) than $\text{Cr}(\text{C}_6\text{H}_6)_2$ (m.p. $283\text{--}284^\circ\text{C}$). In fact, the naphthalene ligand is sufficiently labile to allow reaction under mild conditions, to afford CrL_6 ($\text{L} = \text{CO}$ or Bu^iNC), or $\text{Cr}(\text{naphth})\text{L}_3$ [$\text{L} = \text{PF}_3$, $\text{P}(\text{OMe})_3$, or PMe_3]. The Mo , V , and Ti species are equally reactive. Analogous 1-methylnaphthalene complexes were also isolated (183). In addition, the complexes shown in Fig. 38 were synthesized by reaction, at the temperature of liquid nitrogen, of Cr atoms with 1,4-diphenylbutane (35, 201, 202). Analogous complexes were formed with 1,5-diphenylbutane (202).

Lagowski *et al.* (79) synthesized a very large series of bis(arene) $\text{Cr}(0)$ compounds, thereby providing a good example of the use of metal-atom chemistry in synthesizing homologous series of compounds

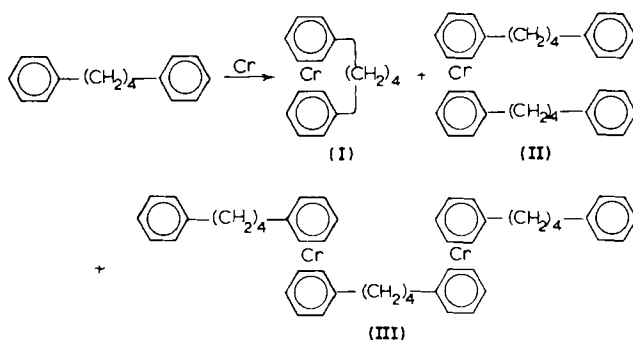


FIG. 38. Complexes synthesized by the reaction of chromium atoms with 1,4-diphenylbutane at the temperature of liquid nitrogen. From ref. (201).

in order to observe the evolution of various properties as a function of ligand and metal. In this case, the ^{13}C -NMR spectra were systematically recorded. For monosubstituted, bis(arene)Cr complexes containing substituents known (78) to perturb the resonance system of the arene (e.g., CH_3 , CO_2CH_3 , and $\text{N}(\text{CH}_3)_2$), an analysis of the C-4 chemical-shift indicated that there is no transmission of substituent effects between the complexed rings. The results were interpreted as meaning that a significant diminution of ring aromaticity occurs for complexation to chromium, an effect attributed to the donation of arene, π -electron density into vacant metal-orbitals. This lowering of aromaticity explains the failure of the compounds to undergo electrophilic, aromatic substitution. The availability of complexes having good leaving-groups, such as F and Cl, together with the lessened aromatic character of the ring, suggested that nucleophilic, aromatic substitution-reactions may be feasible.

As was suggested in the preceding discussion, most of the arene complexes isolated by metal-atom techniques are benzene derivatives. However, heterocyclic ligands are also known to act as 5- or 6-electron donors in transition-metal π -complexes (79), and it has proved possible to isolate heterocyclic complexes via the metal-atom route. Bis(2,6-dimethylpyridine)Cr(0) was prepared by cocondensation of Cr atoms with the ligand at 77 K (79). The red-brown product was isolated in only 2% yield; the stoichiometry was confirmed by mass spectrometry, and the structure determined by X-ray crystal-structure analysis, which supported a sandwich formulation.

Using an electron-gun source, tungsten atoms were reacted with benzene, toluene, or mesitylene at 77 K, to form the expected (arene) $_2\text{W}$ complex (42) in a yield of $\sim 30\%$, compared with the $\sim 2\%$ yield from the previously published, bis(benzene)W synthesis (32). These arene complexes are reversibly protonated, to give the appropriate $[(\eta\text{-arene})_2\text{WH}]^+$ species. By using the same technique, the analogous, niobium complexes were isolated (43).

Metal- σ -aryl complexes may also be generated via the metal-atom route. For example, the cocondensation of cobalt atoms with $\text{C}_6\text{F}_5\text{Br}$ yields $(\text{C}_6\text{F}_5)_2\text{Co}$ and CoBr_2 [70], both Co(II) species, although the mechanism for their formation was not elucidated. On adding toluene to the reaction mixture, the complex $(\text{C}_6\text{F}_5)_2\text{Co}(\text{toluene})$ was isolated (70). The X-ray structure of the compound showed a cobalt atom σ -bonded to two F-phenyl ligands and π -bonded to one toluene. According to the authors, this was the first example of an η^6 -arene complex of an R_2M compound. An isostructural complex was formed in the reaction of nickel atoms with toluene and bromopentafluorobenzene (71). These

materials are proving to be interesting arene hydrogenation catalysts (70, 71). An intermediate species, C_6F_5NiBr , observed to be stable to $-80^\circ C$, can be trapped by addition of PEt_3 . On warming this compound in the absence of toluene, decafluorobiphenyl was formed.

B. ALKENE AND ALKYNE COMPLEXES

1. *Mono-enes and Mono-yne*s

Nickel and palladium react with a number of olefins other than ethylene, to afford a wide range of binary complexes. With styrene (11), Ni atoms react at 77 K to form $tris(styrene)Ni(0)$, a red-brown solid that decomposes at $-20^\circ C$. The ability of nickel atoms to coordinate three olefins with a bulky phenyl substituent illustrates that the steric and electronic effects (54, 141) responsible for the stability of a tris (planar) coordination are not sufficiently great to preclude formation of a tris complex rather than a bis (olefin) species as the highest-stoichiometry complex. In contrast to the nickel-atom reaction, chromium atoms react (11) with styrene, to form both polystyrene and an intractable material in which chromium is bonded to polystyrene. It would be interesting to ascertain whether such a polymeric material might have any catalytic activity, in view of the current interest in polymer-supported catalysts (51).

The systematic synthesis and spectral examination of a large series of complexes, $M(ol)_n$, $n = 1-3$, $M = Ni$ or Pd , has been performed (140-142), with special reference to the optical spectra of the products, again affirming the usefulness of the technique for observing spectral trends as a function of substituent (see later). A number of interesting points emerged from this study, some of which have already been alluded to. The optical data for the nickel and palladium complexes respectively are reported in Tables XVI and XVII.

For all the olefins studied, alkyl-, fluoro-, or chloro-substituted, *three* binary, mononuclear species were observed. It now seems that it is a general property of Ni and Pd atom-olefin reactions at cryogenic temperatures to form complexes that have a maximum coordination of three olefin molecules per metal atom, regardless of the electronic or steric attributes of the substituent(s). As intimated previously, the absence of higher stoichiometry species, even for unsubstituted ethylene, is, most probably, the result of steric interactions (54).

As was the case for the Ni (123) and Pd/ C_2H_4 (140) systems, each of the binary olefin complexes isolated has associated with it a moderately intense, UV band, the bands for Pd complexes lying at higher energy than those of the nickel complexes; in addition, for each olefin sys-

TABLE XVI

OPTICAL SPECTROSCOPIC DATA FOR $\text{Ni}(\text{ol})_n$ (WHERE $n = 1, 2$, AND 3) (141)

Olefin	n	$\lambda_{\text{max}}(\text{cm}^{-1})$	$T_{\text{dec.}}(\text{K})^a$	$-\text{E}\pi^*(\text{eV})$
A C_2H_4 (ethylene)	1	31 350	35	2.91
	2	35 714	28	
	3	42 373	80	
B C_3H_6 (propene)	1	30 864	40	2.58
	2	34 843	35	
	3	41 152	67	
C C_4H_8 (1-butene)	1	30 675	49	2.48
	2	34 722	39	
	3	40 160	77	
D C_4H_8 (isobutene)	1	30 488	48	2.51
	2	35 088	36	
	3	39 370	80	
E C_4H_8 (<i>cis</i> -2-butene)	1	30 303	105	2.01
	2	34 483	36 ^b	
	3	41 152	105	
F C_4H_8 (<i>trans</i> -2-butene)	1	30 675	51	2.16
	2	34 722	25 ^b	
	3	39 682	80	
G C_6H_{12} (1-hexene)	1	30 650	38	2.29
	2	34 602	28	
	3	39 682	38	
H CH_2CHCl (vinyl chloride)	1	31 153	65	3.43
	2	35 714	25	
	3	41 841	225	
I CH_2CHF (vinyl fluoride)	1	31 056	37	3.08
	2	35 336	31	
	3	41 666	65	
J CClFCF_2 (chlorotrifluoroethylene)	1	31 056	25	2.44
	2	34 602	60	
	3	40 000	60	
K $\text{CH}_2\text{CHCH}_2\text{Cl}$ (allyl chloride)	1	30 864	100	
	2	35 461	100	
	3	43 290	100	
L C_2F_4 (tetrafluoroethylene)	1	30 675	35	1.68
	2	35 714	37	
	3	41 322	37	

^a Highest temperature at which a species absorbance was observed. This constitutes a lower limit for complex stability. ^b Estimated value, due to band-overlap difficulties in these spectra.

TABLE XVII
OPTICAL SPECTROSCOPIC DATA FOR Pd(ol)_n
(WHERE $n = 1, 2,$ AND 3) (141)

	Olefin (ol)	n	λ_{\max} (nm)
A	C ₂ H ₄	1	240
		2	221
		3	204
B	C ₃ H ₆	1	240
		2	221
		3	204
C	C ₂ H ₃ Cl	1	239
		2	221
		3	204
D	CH ₂ =CHCH ₂ Cl	1	238
		2	221
		3	203

tem, the transition energies move to higher energy with increasing olefin stoichiometry. The salient feature of the optical spectra is, however, the insensitivity of the UV-absorption energy as a function of olefin substituent (see Tables XVI and XVII). There is a suggested correlation between the value of λ_{\max} for Ni(ol) and the π^* orbital energy of the free olefin, as shown in Fig. 39; however, the fact that the shifts for λ_{\max} are so small, whereas the π^* orbital energy varies so much (see Table XVI) is inconsistent with the previous assignment (123) of these bands as metal-to-ligand charge-transfer (MLCT). GVB-CI-MO calculations for Ni(C₂H₄) (39, 191) suggested that these transitions might be better described as metal-localized, M(d) \rightarrow M(p_y), excitations, which would tend to be less sensitive to the olefin coordinated to the metal. Were this the case, the slight sensitivity of the transition to E $_{\pi^*}$ may be rationalized by observing that the M(p_y) orbital could mix somewhat with the olefin π^* orbital.

One other point to note in regard to this study (141) is that any evidence of oxidative addition, particularly with the chloro-olefins, was absent. The similarity of the spectra, coupled with the nonobservation of any bands in the visible region, as well as the observation of $\nu_{C=C}$ in the region commonly associated with π -complexation of an olefin (141, 142), all argue in favor of normal π -coordination, rather than oxidative insertion of the metal atom into, for example, a C-Cl bond. Oxidative, addition reactions of metal atoms will be discussed subsequently.

The cocondensation of iron atoms with styrene or phenylacetylene at 77 K produces (14) a low yield of polystyrene and a triphenylbenzene,

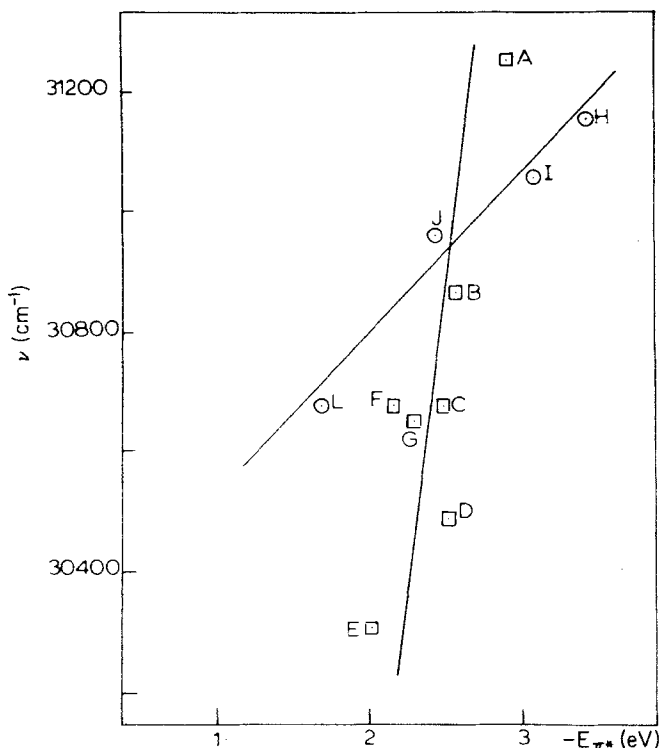


FIG. 39. Graphical representation of the correlation between $\bar{\nu}$ (cm $^{-1}$) for Ni(ol) and the energy ($E_{\pi^*}^*$) of the π^* orbital of the free olefin. The olefins are lettered as in Table XVI. Squares indicate hydrocarbon olefins, and circles, fluoro- or chloro-olefins (141).

respectively. However, warm-up in the presence of CO produced (styrene)Fe(CO) $_3$, (styrene)Fe(CO) $_4$, and Fe(CO) $_5$.

The reactions of the copper-triad metals with C $_2$ H $_4$ have also been studied, the copper-ethylene system (122, 124) having already been described. Silver and gold atoms behave somewhat differently from copper atoms, forming only M(C $_2$ H $_4$). The Ag(C $_2$ H $_4$) species was first reported by Kasai and McLeod (59) in an esr study of the reaction of Ag atoms with ethylene. Subsequent IR and UV-visible studies (143) confirmed the authenticity of this purple complex. The existence of Au(C $_2$ H $_4$) has also been demonstrated by the metal-atom route (143), this synthesis constituting the first example of a zero-valent, gold-olefin complex. A comparison of the gold and silver optical spectra is made in Fig. 40.

Moving from alkenes to alkynes, it was found that a variety of transition-metal atoms react with hexafluoro-2-butyne (HFB) to form new

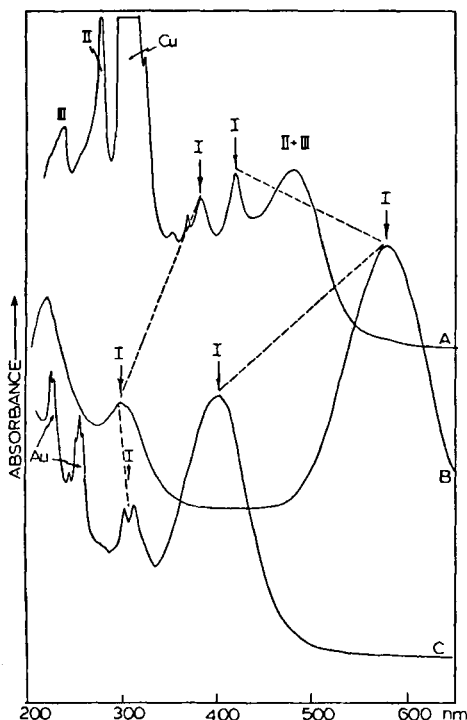
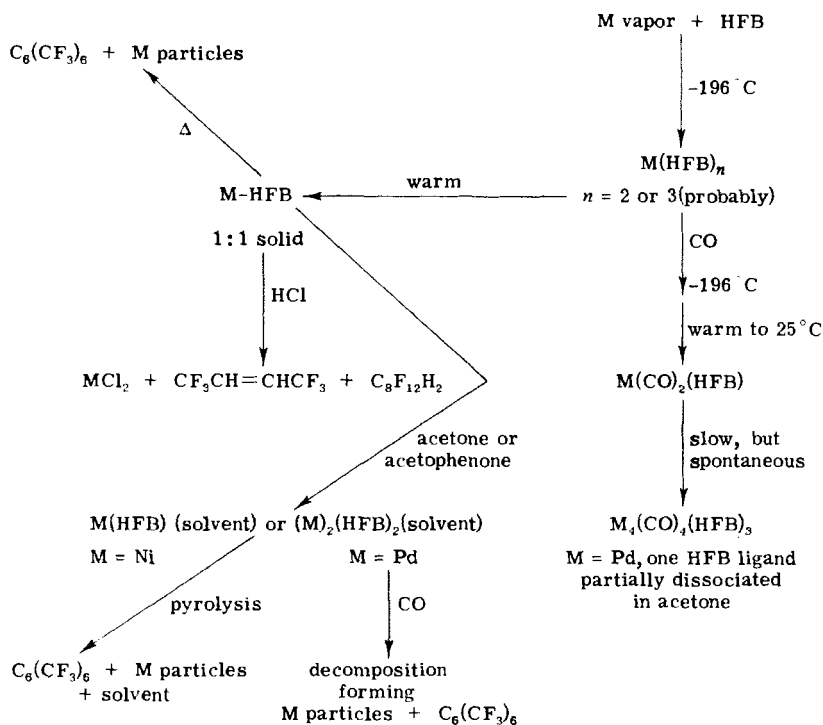


FIG. 40. Optical spectra of matrix-entrapped (A) $\text{Cu}(\text{C}_2\text{H}_4)_{1,2,3}$ in Ar, (B) $\text{Ag}(\text{C}_2\text{H}_4)$ in C_2H_4 , and (C) $\text{Au}(\text{C}_2\text{H}_4)$ in C_2H_4 at 10–12K where dotted lines indicate correlations between corresponding "low-energy" $6a_1 \rightarrow 3b_2$ and "high-energy" $5a_1 \rightarrow 6a_1$ excitations of $\text{M}(\text{C}_2\text{H}_4)$, where $\text{M} = \text{Cu}, \text{Ag}, \text{Au}$. Lines ascribed to free Cu and Au atoms in the matrix are indicated with arrows (143, 148).

chemical species (72). Nickel or palladium atoms dispersed in an excess of HFB and subsequently treated with CO at low temperatures yield labile $\text{M}(\text{CO})_2(\text{HFB})$ complexes that spontaneously form cluster systems on warming to near room temperature. The clusters formed are $\text{Ni}_4(\text{CO})_4(\text{HFB})$, which was already known (178), and the new species $\text{Pd}_4(\text{CO})_4(\text{HFB})_3$, in which the alkyne is very labile. The chemistry of these species, from metal-atom generation to ultimate decomposition, is illustrated in Scheme 5. Support for the postulated, binary, mononuclear, metal-alkyne species stems from Kasai and McLeod's esr characterization of $\text{Cu}(\text{C}_2\text{H}_2)_{1,2}$ (60), and unpublished, IR/UV-visible spectral results of Ozin and Power (144) which showed the formation of the species $\text{Ni}(\text{C}_2\text{H}_2)_n$, $n = 1$ or 2, as well as a species $\text{Ni}_2(\text{C}_2\text{H}_2)_m$ (where m is, most probably, unity). Attempts to make the analogous Au, Co, and Pt clusters in a similar way failed (72). However, it was

M-HFB and M-HFB-CO Chemistry (M = Ni or Pd)

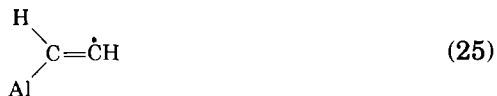


SCHEME 5 (72)

found that Co, Ni, Pd, Pt, Cu, and Au-HFB complexes lacking CO are stable (although the stoichiometries were not reported), and Ni-HFB(solvent) and Pd₂(HFB)₂(solvent) were prepared as thermally stable, soluble complexes that have a high propensity for the formation of hexa(trifluoromethyl)benzene, C₆(CF₃)₆ (a metal-atom-induced, trimerization reaction). In comparison, the main-group elements Ge and Sn interact with HFB (72) to form low-molecular-weight polymers incorporating a great deal of metal, quite reminiscent of the Cr/styrene reaction (11) already mentioned. The alkynes, 2-butyne and 1-propyne, form high polymers, and these reactions are, apparently, radical processes.

The copper atom-acetylene matrix-reaction, monitored originally by esr spectroscopy (60) has now been investigated by IR/UV-visible spectroscopy (144), and there is general agreement on the identification of two mononuclear species, Cu(C₂H₂)_{1,2}. The esr/IR/UV-visible

data are consistent with a π -complex formulation for both species, which is in sharp contrast with the Al atom-acetylene, cocondensation product (61), formulated as the radical species



which is also distinct from the Al atom-ethylene, cocondensation product formulated as π -bonded $\text{Al}(\text{C}_2\text{H}_4)$ (62).

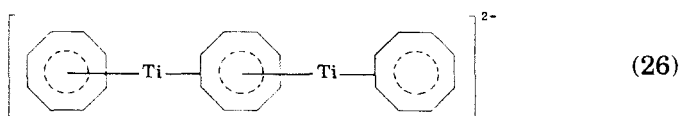
2. Dienes, Conjugated Dienes, and Cyclic Species

Cyclic dienes and conjugated dienes have also been fashionable systems in the metal-atom synthesis of organometallic complexes. Chromium atoms have been reacted with 1,3-cyclohexadiene at 77 K (12) and, upon subsequent treatment with an excess of PF_3 , the complex bis(η^4 -cyclohexadiene)-bis(trifluorophosphine)chromium was isolated. Reaction of chromium atoms with 1,4-cyclohexadiene did not afford the analogous complex (12); instead, a η^5 -cyclohexadienylhydridotris(trifluorophosphine)chromium(II) species, stable in solution to 50 °C in the absence of air, was formed. Chromium atoms react (13) at 77 K with cycloheptatriene in a hexane matrix to form a brown material which, upon warming to -20 °C, forms the known (33) species $[\text{Cr}(\text{C}_7\text{H}_7)(\text{C}_7\text{H}_{10})]$. That the low-temperature species contains only coordinated cycloheptatriene was confirmed by warming this species in the presence of PF_3 , which resulted in the formation of $[\text{Cr}(\text{C}_7\text{H}_8)(\text{PF}_3)_3]$.

Timms and Turney (184) studied the reactions at low temperatures of a wide range of transition-metal atoms with cycloheptatriene and cyclo-octatetraene. With C_7H_8 , the reactions are accompanied by extensive hydrogen-migration. Thus, cocondensation of C_7H_8 with the vapors of Ti, V, Cr, Fe, and Co affords $[\text{Ti}(\eta\text{-C}_7\text{H}_7)(\eta^5\text{-C}_7\text{H}_9)]$, $\text{V}(\text{C}_{14}\text{H}_{16})$, $[\text{Cr}(\eta\text{-C}_7\text{H}_7)(\eta^4\text{-C}_7\text{H}_{10})]$, $[\text{Fe}(\eta^5\text{-C}_7\text{H}_7)(\eta^5\text{-C}_7\text{H}_9)]$ or $\text{Fe}(\text{C}_{14}\text{H}_{18})$, and $\text{Co}(\text{C}_{14}\text{H}_n)$, $n = 15, 17$, or 19 , respectively. Where the mode of coordination of the cyclic triene is not specified, the data were not sufficiently conclusive to permit determining it. No reaction products were isolated with Mn, Ni, or Pd atoms. However, cocondensation of $\text{PF}_3/\text{C}_7\text{H}_8$ mixtures with vapors of Cr or Co affords $[\text{Cr}(\text{C}_7\text{H}_8)(\text{PF}_3)_3]$ or $[\text{Co}(\text{C}_7\text{H}_8)(\text{PF}_3)_3]$, respectively. In general, the complexes formed with C_7H_8 are new examples of sandwich complexes. Reaction of C_8H_8 with Ti, Fe, and Co atoms resulted in the formation of unidentified, intractable polymers; with chromium atoms, the complex $[\text{Cr}_2(\text{C}_8\text{H}_8)_3]$

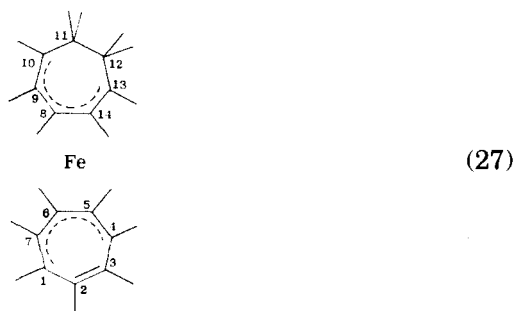
was obtained, an interesting observation in view of the fact that C_8H_8 complexes of these metals are well established (184).

In contrast, Skell and co-workers (169) demonstrated that there could be prepared, by the metal atom method, a reasonably well-defined, paramagnetic, yellow $Ti_2(C_8H_8)_3$ compound which, in THF, is rapidly reduced with potassium to yield a fairly stable, green solution of the diamagnetic dianion. The 1H -NMR spectrum and the analytical data were all consistent with the formulation of the green dianion shown, which appears to be the



first instance of such a "triple-decker" sandwich complex.

Reaction of iron atoms with cycloheptatriene to form $[Fe(\eta^5-C_7H_7)-(\eta^5-C_7H_9)]$ was confirmed by another group (15); these workers determined the crystal structure of the species, demonstrating a sandwich structure with the open faces of the two η^5 -systems skewed to each other. The temperature-dependent NMR spectrum of this species (16) indicated two types of fluxional behavior in solution. Evidence for a 1,2-shift mechanism of the 1-5- η -cycloheptatrienyl moiety in the structure shown,



with respect to the central, iron atom, as well as a low-temperature, rocking motion of both rings, was observed.

Fe atoms have been reacted with butadiene at liquid-nitrogen temperature (14). Upon warm-up in an atmosphere of CO or PF_3 , only bis(butadiene)Fe(CO) or bis(butadiene)Fe(PF_3) was isolated. One of the butadienes could be replaced by warming the species in $P(OMe)_3$, to form (butadiene)Fe $[P(OMe)_3]_3$. A similar reaction led to the formation of the analogous 2,3-dimethylbutadiene species. In addition, Fe atoms react with 1,5-cyclooctadiene to form $(1,5-COD)_2Fe$ (185, 189) which,

upon warming in the presence of phosphine (189), yields (1,3-COD)FeP₃, P = P(OMe)₃, P(OEt)₃, or P(O-*i*-Pr)₃. Again, hydrogen migration is evident in the isomerization of the COD ligand.

Lanthanide metal-atom chemistry has also become popular. Reaction of various lanthanide-metal atoms at 77 K with cyclo-octatetraene, with subsequent extraction of the reaction mixture with THF, resulted in a series of lanthanide complexes of formula [Ln(C₈H₈)₂](THF)₂[Ln(C₈H₈)₂], where Ln is La, Ce, Nd, or Er (24, 25). Reaction with Yb atoms yielded the known compound (51) Yb(C₈H₈). A crystal-structure determination of the neodymium compound was completed (25), and it showed that all of the C₈H₈ rings are present as the ten- π -electron, aromatic dianion. The structure was strikingly asymmetrical, in comparison to other lanthanide and actinide C₈H₈ complexes (25), as is illustrated in Fig. 41. All of these compounds are extremely sensitive to air and moisture, with traces of O₂ and H₂O causing decomposition. On exposure to air, they inflame spontaneously, often leaving a colored powder of Ln₂O₃.

A new class of organolanthanide complex has been reported from the metal-atom reaction of lanthanide atoms and butadiene (BD) or 2,-

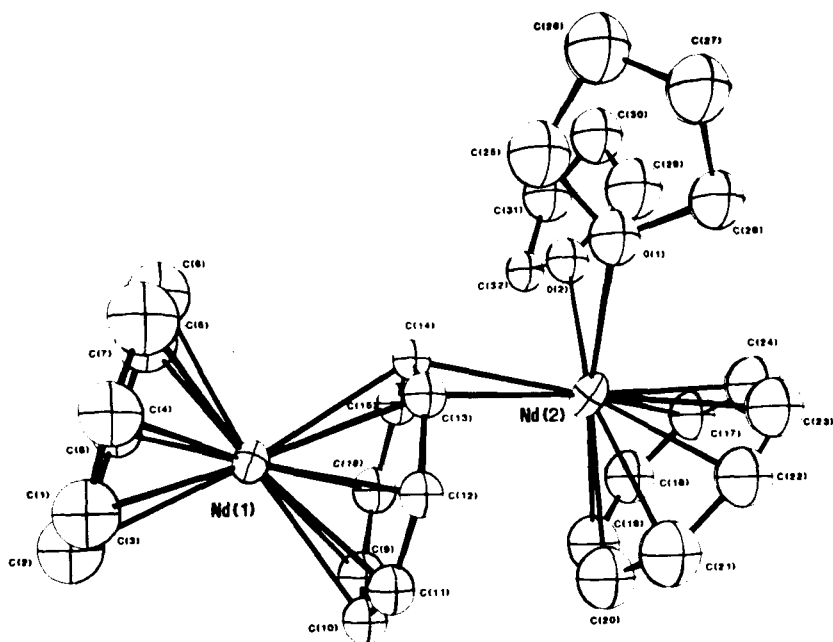
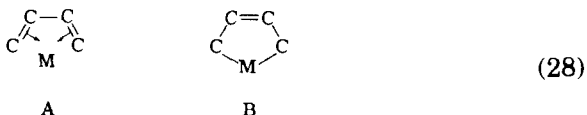


FIG. 41. An ORTEP drawing of [Nd(COT)(THF)₂][Nd(COT)₂], approximately along the *c* axis (25).

3-dimethyl-1,3-butadiene (DMBD) (31), with $M(\text{BD})_3$ resulting for $M = \text{Er, Ne, or Sm}$, and $M(\text{DMBD})_2$ for $M = \text{La or Er}$. Consideration of the spectral and analytical data suggested that the bonding in these species is best represented as intermediate between structures A and B.



C. OXIDATIVE ADDITION REACTIONS

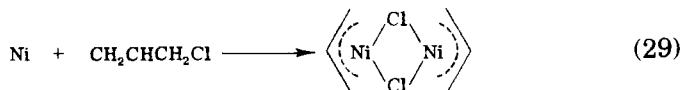
Although, as has already been mentioned, under matrix conditions between 10 and 77 K, there is no oxidative addition of a chloroolefin to nickel or palladium atoms (141), it is evident that this is simply a function of reaction and processing conditions, as it has been shown (68) that oxidative addition to C-C or C-H bonds by nickel atoms leads to "pseudocomplexes" having Ni:C:H ratios of 2-5:1:2. Klabunde and co-workers investigated the oxidative addition-reactions of palladium atoms with alkyl halides (73) and benzyl chlorides (74).

In the former (73), oxidative addition of palladium atoms to RX species resulted in formation of RMX compounds. Trapping experiments, free-radical scavenging experiments, and decomposition-product distributions suggested that the metal atom, C-X bond insertion occurs directly, via a caged, radical pair. A number of these RMX species, such as $(\text{CF}_3\text{PdI})_n$, $(\text{C}_2\text{F}_5\text{PdI})_n$, and $(n\text{-C}_3\text{F}_7\text{PdI})_n$, were isolable, whereas, with such organics as CH_3I , the products were not isolable. Without going into too much detail, a number of points had to be reconciled in order to predict a mechanistic pathway.

(1) Coupling and disproportionation reactions of R radicals are a minor process, usually not observed. Hence, these radicals, if formed, are not mobile in the matrix.

(2) Related to this, radical scavengers did not affect product yield or distribution, therefore minimizing the importance of a radical chain process.

(3) Photolysis from the vaporization source had no effect. [Interestingly, it is possible that such photolysis is responsible for the reaction (186)]



or, at least, the first step (141).]

(4) *tert*-Alkyl halides react as effectively as primary halides, indicating a nonbackside-attack mechanism, such as S_N2 .

(5) Vibrationally excited radicals are probably formed.

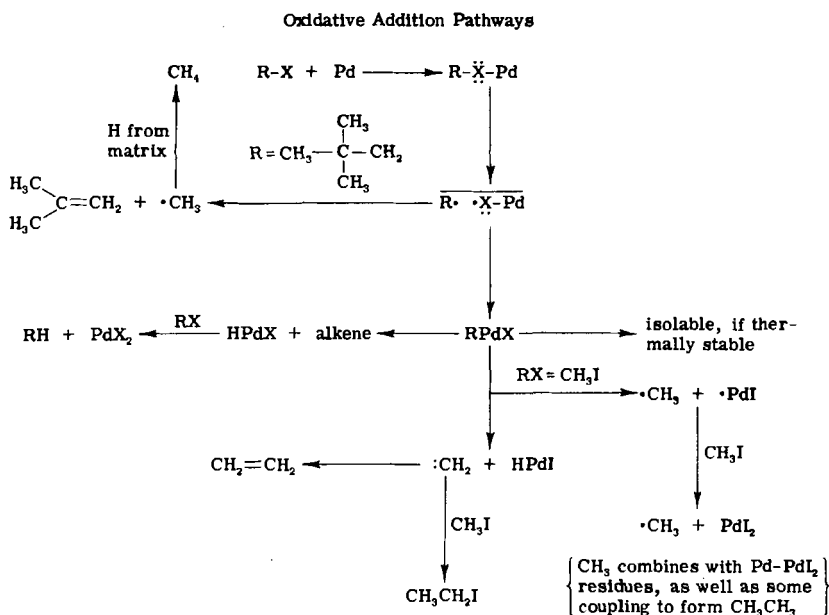
(6) $HPdX$ is an intermediate that can reduce $R-X$ to $R-H$.

(7) Gaseous products arise from the decomposition of $RPdX$, rather than from the process of formation of $RPdX$. Hence, if $RPdX$ is stable, it is the only organic product formed.

(8) Unsaturated alkyl halides react first by π -complexation (141), followed by $C-X$ oxidative addition, probably on matrix warm-up [but see the preceding point 3, and see ref. (81), which suggests that pyrolysis and radical production can occur on the crucible insulating material to cause reaction].

(9) It is likely that complexation to form $RX \cdots M$ occurs at 77 K, with oxidative addition occurring on warm-up (see point 8).

The mechanism shown in Scheme 6 is, for the most part, consistent with points (1) to (9). Thus, initially formed is a σ -complex that is stable only at low temperatures. Upon matrix warm-up, a caged, radical pair forms and, if the R portion possesses a sufficient excess of vibrational energy, decomposition processes may occur. The radicals combine to form $RPdX$, which may, or may not, be isolated.



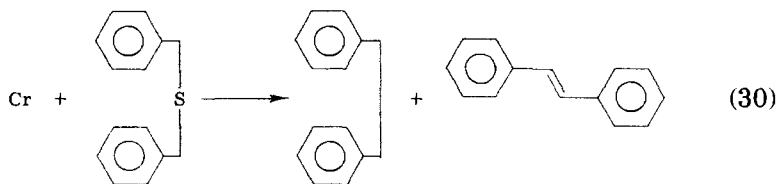
SCHEME 6 (73)

As far as the reactions with benzyl chlorides are concerned (74), the oxidative addition of benzyl chloride and substituted benzyl chlorides to palladium atoms yields η^3 -benzylpalladium chloride dimers. The parent compound, bis(1,2,3- η^3 -benzyl)di- μ -chloro-palladium(II), quantitatively adds four molecules of PEt_3 by first forcing the η^3 -benzyl- η^1 -benzyl transformation, with subsequent breakage of the Pd-Cl bridges to form *trans*-bis(PEt_3)(benzyl)chloroPd(II). The spectral characteristics of the parent molecule are indicative of the allylic type of bonding. Similar η^3 -benzyl compounds were formed from 4-methylbenzyl chloride, 2-chloro-1,1,1-trifluoro-2-phenylethane, and 3,4-dimethylbenzyl chloride.

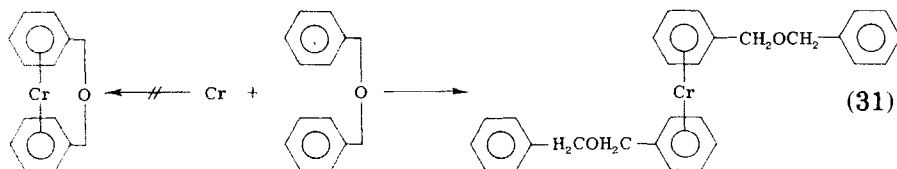
D. ORGANIC REACTIONS

In addition to complex-formation, the interaction of transition-metal atoms with organic substrates at low temperatures can result in rearrangement of the organic moiety without complexation. Two such reactions have already been briefly mentioned, namely, the polymerization of hexafluoro-2-butyne by Ge and Sn atoms (72) and the polymerization of styrene by Cr atoms (11). In this section we shall briefly summarize some of these transition-metal-atom-promoted, organic rearrangements.

Chromium atoms were cocondensed with benzyl sulfide at 77 K (35), the primary result being desulfurization to form bibenzyl and *trans*-stilbene. Coordination compounds were not characterized in this system.

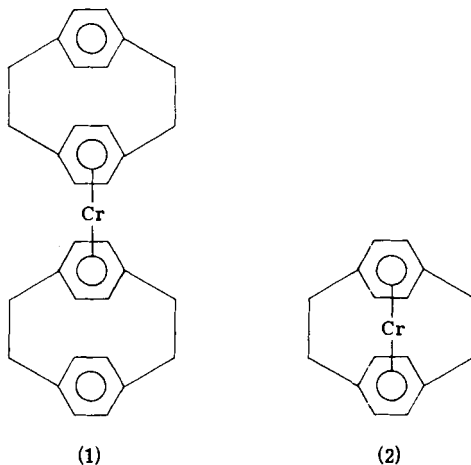


In contrast, when chromium atoms were reacted with benzyl ether, complexation to only one phenyl group of the ether was observed.

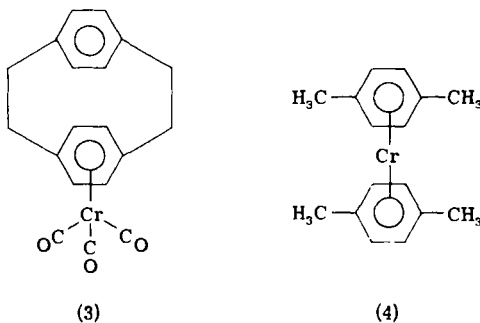


It has, however, proved possible to synthesize the following chromium complexes via a 77 K, Cr-atom, cocondensation reaction with 2,-

2-paracyclophane (202a). This is a significant discovery, in view of the fact that



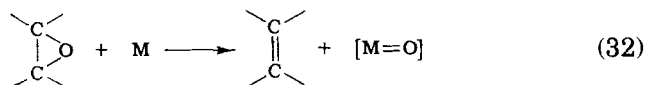
cyclophanes could hitherto be coordinated to transition metals only in combination with carbonyl ligands, an example (3) being shown.



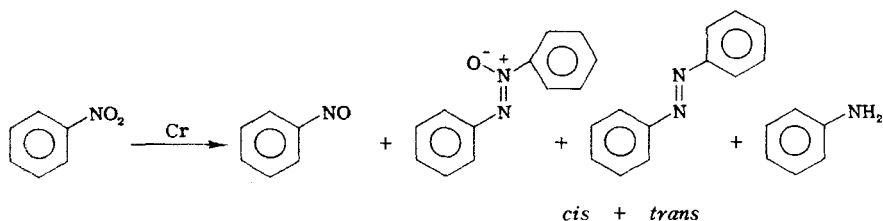
Binary complexes of types (1) and (2) are of special interest, as (1) represents a potential building-block for columnar structures of composition $[(\eta\text{-cyclophane})\text{-metal}]_n$, and (2) is expected to be kinetically very inert and should display a change from intramolecular, $\pi\text{-}\pi$ repulsion (free ligand) to bonding $\eta\text{-arene-metal}$ interaction (complex). Interestingly, complex (2) does, in fact, display compressed-sandwich properties, as seen from the esr, hyperfine coupling-constants for the ring protons and the ^{53}Cr site of the monocation of (2), which are increased and decreased, respectively, compared to the corresponding values for the monocation of (1) and (4). This finding pointed to a slightly more extensive $\text{Cr}(3d_z^2) \rightarrow \text{arene } (\sigma_{a_1})$ spin-delocalization in the monocation of (2), which is probably caused by a shorter metal-ligand distance than in the

cation of (1) and (4). The high stability of the cation of (2) [compared to either (1) or (4)] to solvolytic, metal–ligand cleavage has been explained in terms of the “concave sides” of the nonplanar, benzene rings of 2,2-paracyclophane functioning as a rigid, chelate ligand, oriented towards the central metal, thereby shielding the latter from solvolytic attack (202a). For the cation of (1), however, the cleavage can take place in two steps, via the half-sandwich complex $(\eta^6\text{-}2,2\text{-paracyclophane})\text{Cr}^+$, whereby the initial attack is easier than in, for example, the cation of (4), because coordination via the “convex sides” of the nonplanar, benzene rings leaves the central metal-atom exposed to attack by solvent. Thus, the observed order of reactivity $(1)^+ > (4)^+ > (2)^+$ may be understood (202a).

Transition-metal atoms have been shown to deoxygenate epoxides to alkenes (36). Chromium and titanium atoms emerged as the most effective species in this regard, abstracting over two equivalents of oxygen. By studying the reaction of a wide range of epoxides with chromium atoms, the reaction

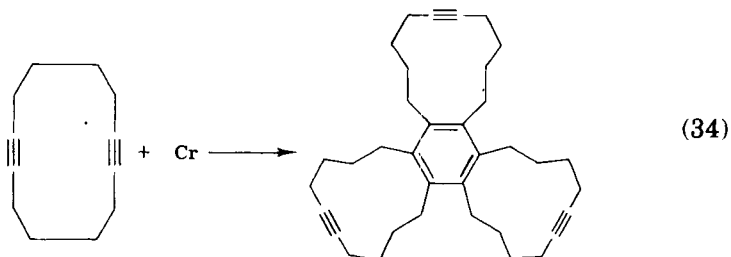


was found to be general. In addition, metal atoms also abstract oxygen from compounds containing nitrogen–oxygen multiple bonds (37). On cocondensing chromium atoms with nitrobenzene, a number of interesting organic moieties were observed.



The yields of the products were dependent on the metal:organic ratio. Similar reactions do not occur on preformed, chromium surfaces.

When chromium atoms were cocondensed at 77 K with 1,7-cyclodecadiyne (38), complexation was not observed; however, an organic trimer of the starting material was formed. Standard, organic characterization-techniques showed that this trimer is the one depicted, rather

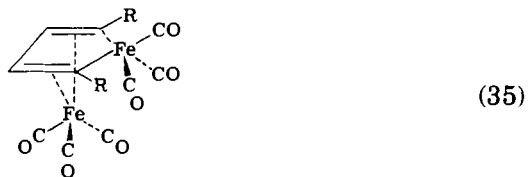


than a cage species [which, it had been supposed, a compound having identical physical properties might be (176)].

In addition, Lagowski and Simons showed (80) that the black, nickel-containing substances produced by the cocondensation of nickel atoms and alkynes are active, homogeneous catalysts for the oligomerization of terminal acetylenes under mild conditions. Table XVIII shows the yields of the oligomerization of propylene by these catalysts.

E. MISCELLANEOUS ORGANOMETALLIC SPECIES



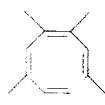
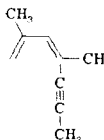
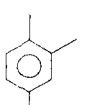
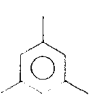
Somewhat related to the desulfurization reaction already discussed (35), the cocondensation of Cr and Fe atoms with thiophenes at 77 K leads to desulfurization of the thiophene (22, 187). Warm-up of the iron–thiophene cocondensate in a CO atmosphere produces tricarbonylferrocyclopentadiene–tricarbonyliron.



The cocondensation of nickel atoms and CS_2 at 12 K resulted in the formation of *three* binary, mononuclear, nickel/ CS_2 complexes, $\text{Ni}(\text{CS}_2)_n$, $n = 1-3$ (145). Mixed $^{12}\text{CS}_2/^{13}\text{CS}_2$ isotopes were used to identify the lowest stoichiometry species. An interpretation of the IR and UV–visible spectra, as well as normal-coordinate analyses (144), suggested that these species are best considered as normal π -complexes, with the nickel atom coordinated to the $\text{C}=\text{S}$ bond in a manner analogous to $\text{C}=\text{C}$ bond coordination (123).

An interesting reaction involves the cocondensation of transition-metal atoms with liquid methylphenylsiloxane polymers at -20 to 0°C

TABLE XVIII
 OLIGOMERS OF PROPYNE (80)

	Mol % of oligomer produced					
	10 ^a	30 ^a	15 ^a	34 ^b	6 ^b	5 ^b
Oligomer						
	I	II	III	IV		

^a Integration of the ¹H-NMR spectrum shows 55% of tetramer; proportions of individual isomers were estimated from GC/MS data. Tetramer mixtures show an asymmetrical, vinyl resonance centered at δ 5.40, and asymmetrical, methyl resonances centered at δ 1.70 (vs. Me₃Si in CS₂ solution). ^b Integration of the ¹H-NMR spectrum.

(188), a much higher temperature than is normally used in metal-atom work. Polymeric compounds (liquid at room temperature) in which two phenyl rings in the polymer are coordinated to each metal atom were formed with Ti, V, Cr, Mo, and W vapors. With chromium atoms, for example, reaction proceeded until about 50% of the available phenyl groups became coordinated to the metal.

An interesting study combining metal-atom chemistry with previously synthesized gold complexes resulted in the novel synthesis, and subsequent Mössbauer investigation, of gold cluster species (195). A typical experiment involved the evaporation of gold metal into an ethanol film (at -100°C) containing Au(PAr₃)X with the ratios of reactants being 8:3:4. The Mössbauer spectra of the products, Au₁₁(PAr₃)₇X₃ (Ar = C₆H₅, *p*-ClC₆H₄, X = SCN, I, or CN), showed different gold sites in the cluster. An interpretation involving five different gold sites (according to the crystal structure) was possible. The yield from the metal-atom route to these gold cluster complexes was 70%.

To conclude, we shall mention some metal-atom reactions with boranes (172) and carboranes (173). When cobalt atoms reacted with pentaborane(9) and cyclopentadiene, a number of new metalloborane clusters were formed (172), two of which were B₅H₅Co₃(η -C₅H₅)₃ and cyclopentyl-B₅H₄Co₂(η -C₅H₅)₃. Possible structures for the former are shown in Fig. 42. The reaction of cyclopentadiene, pentaborane(9), and 2-butyne with cobalt atoms yielded the metallocarborane species illustrated in Fig. 43 (173).

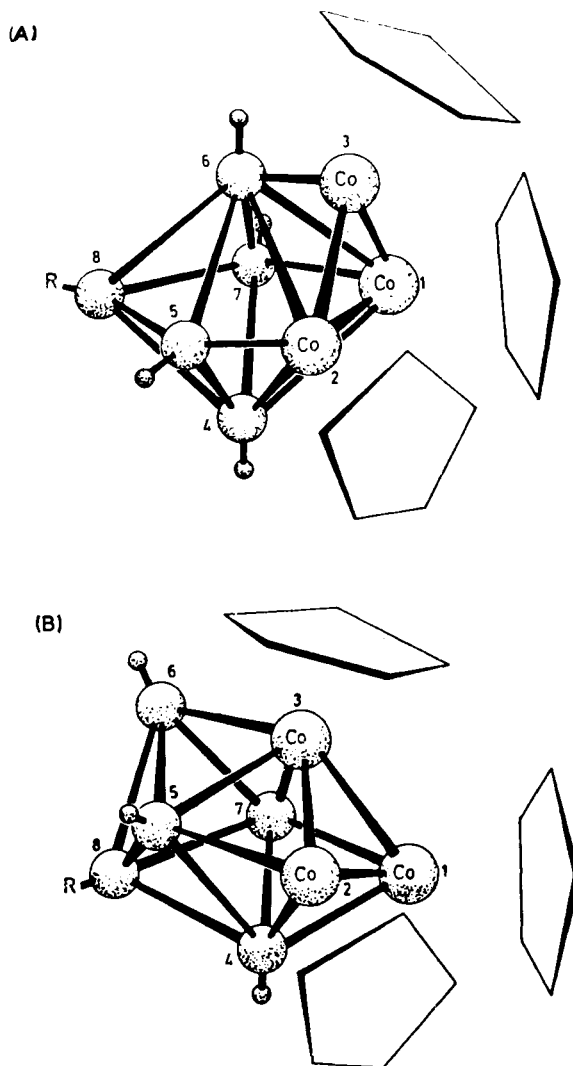


FIG. 42. Possible capped (A) and dodecahedral (B) structures for compound (I) ($R = H$) and compound (II) ($R = \text{cyclopentyl}$) (172).

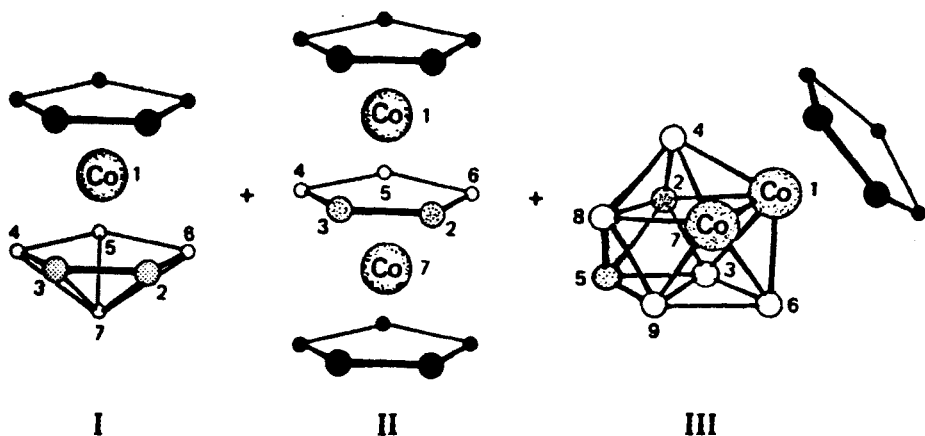


FIG. 43. Reaction of cyclopentadiene, pentaborane(9), and 2-butyne with cobalt atoms. Open circles, BH units; shaded circles, C-CH₃ units; and dark circles, C-H units. One cyclopentadienyl ring has been omitted on compound III, for clarity (173).

VII. Conclusion

It should be evident from this review that the fields of macro- and matrix-scale, metal-vapor chemistry are flourishing and are finding many unique applications in such areas as organic and organometallic synthesis, metal nucleation processes, photography, cluster model theory, surface-reaction intermediates, chemisorption models, alloy and bimetallic clusters, and heterogeneous catalysis. The interdisciplinary nature of the field is now apparent, and many new directions are expected to emerge in the near future. A logical move at this time would be a closer interaction between metal-vapor chemists and researchers in the fields of organometallic synthesis, homogeneous and heterogeneous catalysis, surface chemistry, and physics.

Addendum

The purpose of this section, added in proof, is to include certain references inadvertently omitted in the initial preparation of this article, as well as to update the review. We consider the literature coverage to be complete to about July 31, 1979. The papers referred to in this section will not be discussed in detail.

It is worth noting, prior to citing actual metal atom studies, the recent secondary ion mass spectrometry (SIMS)¹ on an argon matrix-isolated propene sample, demonstrating the applicability of SIMS analysis to the characterization of matrix-isolated species. The same group has reported the first ¹³C NMR spectra of organic molecules trapped in an argon matrix.¹

Further investigation of the optical spectra of Cu, Ag, and Au atoms isolated in H₂, O₂, N₂, and CH₄ matrices has been reported.²

Mössbauer spectra for the species Fe, Fe₂, Fe₂Mn, and Fe₃ have been investigated.³

The absorption spectra of Zr atoms isolated in a variety of matrices have been reported.⁴ In addition, the diatomic molecule ZrN, prepared using a hollow cathode source and N₂, was observed.⁴ Other work involving N₂ included the identification of ThN and Th(N₂),⁵ and TaN⁶ in various matrices.

Weltner *et al.*⁷ have performed an ESR and optical study of the high spin molecules MnH and MnH₂ (and possibly MnH₃) in Ar and Ne at 4K.

Three separate groups have recently published metal vapor-phosphine studies. Bowmaker⁸ isolated the series of complexes Ni(PH₃)_n (*n* = 1 → 4) and Cu(PH₃)_n (*n* = 1 → 3) via matrix isolation, the former series also having been investigated by Trabelsi and Loutellier.⁹ Co-condensation of (CH₃)₂NPF₂ with Cr, Fe, and Ni vapor at 77K gave the appropriate M(PF₂N(CH₃)₂)_n complexes,¹⁰ where M = Cr, *n* = 6; M = Fe, *n* = 5; and M = Ni, *n* = 4. Co-condensation of Cr, Fe, Co, and Ni vapors with CH₃N(PF₂)₂¹⁰ gave Cr[(PF₂)₂NCH₃]₂, Fe[(PF₂)₂NCH₃]₄, Co₂[(PF₂)₂NCH₃]₅, and {Ni[(PF₂)₂NCH₃]₂}_n. Mixed ligand co-condensations were also studied.¹⁰⁻¹²

With respect to CO complexes, the luminescence spectra of a series of Group VI metal carbonyls and substituted carbonyls were obtained in frozen gas matrices at 12K.¹³ In addition, the IR spectra of HCo(CO)₄ and HCo(CO)₃ (proposed as an intermediate in hydroformylation) were observed in an argon matrix.¹⁴

Recent organometallic studies have been reported. Mössbauer spectra have shown that the Fe₂ dimer reacts at 4K with CH₄ to oxidatively cleave the C—H bond to form HFe₂CH₃.¹⁵ Zirconium atoms have also been shown to oxidatively cleave the C—H and C—C bonds of alkanes to form discrete organometallic species.¹⁶

Co-condensation of Hf and Zr atoms from an electron-gun evaporation device, with P(Me)₃ and arenes at 77K gave good yields of the species [M(arene)₂P(Me)₃].¹⁷ Metal vapor synthesis led to Fe(η⁶-arene)L₂ and Fe(η⁶-arene)-(η⁴-diene),¹⁸ where L is a phosphorus ligand. In addition, complexes of stoichiometry Fe(η⁴-diene)L₃ (where L is again a

phosphorus ligand) were prepared for a variety of simple cyclic and acyclic dienes,¹⁹ and their NMR temperature dependence studied.

Ruthenium vapor, obtained by heating tungsten filaments coated with a mixture of ruthenium powder and epoxy resin, yielded $\text{Ru}(\text{Me}_2\text{NPF}_2)_5$ and $\text{Ru}(\text{C}_6\text{H}_6)_2$ on reaction with the appropriate ligand.^{20a} The atomic nature and purity of Ru vapor generated in this way were subsequently confirmed by matrix isolation optical spectroscopy.^{20b} In this study, other refractory metal atoms and clusters ($\text{Zr}_{2,3}$, $\text{Pd}_{1,2}$, $\text{Au}_{2,3}$, Hf, NbMo) were also investigated by matrix UV-visible methods. Bis(arene) complexes, including such species as bis(toluene)-molybdenum and bis(1-methylnaphthalene)molybdenum, can also be synthesized by condensing potassium atoms into THF solutions of the metal halides and arenes at 173K.²¹

Organic rearrangements have also been observed in metal atom chemistry. When nickel atoms were condensed with dimethylfulvene at 77K,²² the only observed product was a dimer of the starting organic, resulting from a formal [6 + 6] cycloaddition. Nickel atoms were also suggested to cyclodimerize norbornadiene via nickel-cyclopentane intermediates.²³ Metal atoms were also reacted with organocyclopropanes and spirocycles,²⁴ with the result that metal atoms reaggregated at a faster rate than they underwent reaction with the organic molecule, unless a functional group was present with which the metal atom could strongly interact.

A method has recently been described for wrapping polymers around metal atoms and very small metal clusters using both matrix and macro-scale metal vapor-fluid polymer synthetic techniques.²⁵ Significant early observations are that (i) the experiments can be entirely conducted at, or close to room temperature, (ii) the resulting "polymer stabilized metal cluster" combinations are homogeneous liquids which are stable at or near room temperature, and (iii) the methodology is easily extended to bimetallic and trimetallic polymer combinations.²⁵

ADDENDUM REFERENCES

1. H.T. Jonkman and J. Michl, *J. Chem. Soc. Chem. Commun.* 751 (1978); K.W. Zilm, R.T. Colin, D.M. Grant, and J. Michl, *J. Am. Chem. Soc.* **100**, 8038 (1978).
2. H. Abe, W. Schulze, and D.M. Kolb, *Chem. Phys. Lett.* **60**, 208 (1979).
3. W. Dyson and P.A. Montano, *J. Am. Chem. Soc.* **100**, 7439 (1979).
4. J.K. Bates and D.M. Gruen, *High Temp. Sci.* **10**, 27 (1978).
5. D.M. Gruen and G.T. Reedy, *J. Mol. Spec.* **74**, 423 (1979).
6. J.K. Bates and D.M. Gruen, *J. Chem. Phys.* **70**, 4428 (1979).
7. R.J. Van Zee, T.C. DeVore, J.L. Wilkerson, and W. Weltner, Jr., *J. Chem. Phys.* **69**, 1869 (1978).

8. G.A. Bowmaker, *Aust. J. Chem.* **31**, 2549 (1978).
9. M. Trabelsi and A. Loutellier, *J. Mol. Struct.* **43**, 151 (1978).
10. R.B. King and M. Chang, *Inorg. Chem.* **18**, 364 (1979).
11. M. Chang, M.G. Newton, and R.B. King, *Inorg. Chim. Acta* **30**, L341 (1978).
12. M. Chang, M.G. Newton, R.B. King, and T.J. Lotz, *Inorg. Chim. Acta* **28**, L153, (1978).
13. T.M. McHugh, R. Neurayanaswamy, A.J. Rest, and K. Salisbury, *J. Chem. Soc. Chem. Commun.* 208 (1979).
14. P. Wermer, B.S. Ault, and M. Orchin, *J. Organomet. Chem.* **162**, 189 (1978).
15. P.H. Barrett, M. Pasternak, and R.G. Pearson, *J. Am. Chem. Soc.* **101**, 222 (1979).
16. R.J. Remick, T.A. Asunta, and P.S. Skell, *J. Am. Chem. Soc.* **101**, 1320 (1979).
17. F.G.N. Cloke and M.L.H. Green, *J. Chem. Soc. Chem. Commun.* 127 (1979).
18. S.D. Ittel and C.A. Tolman, *J. Organomet. Chem.* **172**, C47 (1979).
19. S.D. Ittel, F.A. Van-Catledge, and J.P. Jesson, *J. Am. Chem. Soc.* **101**, 3874 (1979).
- 20a. P.L. Timms and R.B. King, *J. Chem. Soc. Chem. Commun.* 898 (1978).
- 20b. W. Klotzbücher and G.A. Ozin, *Inorg. Chem.* (in press).
21. P.N. Hawker, E.P. Kündig, and P.L. Timms, *J. Chem. Soc. Chem. Commun.* 370 (1978).
22. N. Hao, J.F. Sawyer, B.G. Sayer, and M.J. McGlinchey, *J. Am. Chem. Soc.* **101**, 2203 (1979).
23. J.R. Blackborow, V. Feldhoff, F.W. Grevels, R.H. Grubbs, and A. Mingashita, *J. Organomet. Chem.* **173**, 253 (1979).
24. J.A. Gladysz, J.G. Fulcher, R.C. Ugolick, A.J.L. Hanlan, and A.B. Bocarsly, *J. Am. Chem. Soc.* **101**, 3388 (1979).
25. G.A. Ozin and C.G. Francis, *Proc. EUCMOS Conf., Frankfurt, Sept. 1979*, in "Spectroscopy in Chemistry and Physics," Elsevier, New York, 1979, and *J. Mol. Struct.* (1979) (in press); C.G. Francis, G.A. Ozin, and H. Huber, *J. Am. Chem. Soc.* **101**, 6250 (1979); *Inorg. Chem.* **19**, 219 (1980); *Angew. Chem. Int. Ed. Engl.* (in press); C.G. Francis and G.A. Ozin, in "Organometallic Polymers" (E. Carraher, Jr., ed.). Academic Press, New York, 1980.

ACKNOWLEDGMENTS

G.A.O. acknowledges the invaluable collaboration of his students and colleagues whose names appear in the cited articles, and expresses his special indebtedness to Mr. Ted Huber for his invaluable technical assistance, Mr. Alex Campbell, Mr. Karl Molnar, Mr. Martin Mittelstadt, and Mr. Bob Torbet for their expert, machine-shop contributions, and Mrs. Elinor Foden for typing this manuscript. The financial assistance of the National Research Council of Canada New Ideas, Strategic Energy, and Operating Grant programmes, Imperial Oil of Canada, Atkinson Foundation, Connaught Fund, Lash Miller Chemical Laboratories, and Erindale College is all gratefully acknowledged. W.J.P. is indebted for an NRCC graduate scholarship throughout the tenure of his research.

REFERENCES

1. Abramowitz, S., Acquista, N., and Legin, I. W., *Chem. Phys. Lett.* **50**, 423 (1977).
2. Anderson, A. B., *J. Chem. Phys.* **66**, 5108 (1977).

3. Andrews, L., and Ozin, G. A. (Coblentz Award); Timms, P. L., Green, M. L. H., and Turner, J. J. (Corday-Morgan Award); Ozin, G. A., Burdett, J., and Poliakov, M. (Meldola Award).
- 3a. Andrews, L., and Smardzewski, R. R., *J. Phys. Chem.* **77**, 801 (1973).
- 3b. Andrews, L., Hwang, J. T., and Trindle, C. T., *J. Phys. Chem.* **77**, 1065 (1973).
4. Arai, H., and Tominaga, H., *J. Catal.* **43**, 131 (1976).
5. Baetzold, R. C., *J. Chem. Phys.* **55**, 4363 (1971).
6. Bando, H., Onishi, T., and Tamaru, K., *Chem. Lett.* p. 83 (1978).
7. Barrett, P. H., and Montano, P. A., *J. Chem. Soc., Faraday Trans. 2* p. 378 (1977).
8. Barrett, P., and Montano, P., *Ber. Bunsenges. Phys. Chem.* **82**, 30 (1978).
9. Barrow, R. F., and Griffiths, M. J., *J. Chem. Soc., Faraday Trans. 2* p. 943 (1977).
10. Bates, J. K., and Gruen, D. M., *Inorg. Chem.* **16**, 2450 (1977).
11. Blackborow, J. R., Grubbs, R., Miyashita, A., and Scrivanti, A., *J. Organomet. Chem.* **120**, c49 (1976).
12. Blackborow, J. K., Grubbs, R. H., Miyashita, A., Scrivanti, A., and von Gustorf, E. A. K., *J. Organomet. Chem.* **122**, c6 (1976).
13. Blackborow, J. R., Eady, C. R., von Gustorf, E. A. K., Scrivanti, A., and Wolfbeis, O., *J. Organomet. Chem.* **108**, c32 (1976).
14. Blackborow, J. R., Eady, C. R., von Gustorf, E. A. K., Scrivanti, A., and Wolfbeis, O., *J. Organomet. Chem.* **111**, c3 (1976).
15. Blackborow, J. R., Hildenbrand, K., von Gustorf, E. A. K., Scrivanti, A., Eady, C. R., Ehntolt, D., and Krüger, C., *J. Chem. Soc., Chem. Commun.* p. 16 (1976).
16. Blackborow, J. R., Grubbs, R. H., Hildenbrand, K., von Gustorf, E. A. K., Miyashita, A., and Scrivanti, A., *J. Chem. Soc., Dalton Trans.* p. 2205 (1977).
17. Bor, G., Dietler, U. K., and Noack, K., *J. Chem. Soc., Chem. Commun.* p. 914 (1976).
18. Brown, C. M., and Ginter, M. L., *J. Mol. Spectrosc.* **69**, 25 (1978).
19. Brown, T. L., and Sweany, R. L., *Inorg. Chem.* **16**, 415 (1977).
20. Brown, T. L., and Sweany, R. L., *Inorg. Chem.* **16**, 421 (1977).
21. Burdett, J. K., *Coord. Chem. Rev.* **27**, 1 (1978).
- 21a. Burdett, J. K., *J. Chem. Soc., Faraday Trans. 2* p. 1599 (1974).
22. Chivers, T., and Timms, P. L., *Can. J. Chem.* **55**, 3509 (1977).
23. Craddock, S., and Hinchcliffe, A. J., "Matrix Isolation." Cambridge Univ. Press, London and New York, 1975.
24. DeKock, C. W., Ely, S. R., and Hopkins, T. E., *J. Am. Chem. Soc.* **98**, 1624 (1976).
25. DeKock, C. W., Ely, S. R., Hopkins, T. E., and Brault, M. A., *Inorg. Chem.* **17**, 625 (1978).
26. DeKock, R. L., *Inorg. Chem.* **10**, 1205 (1971).
27. Demuth, J., Ibach, H., and Lehwald, S., *Surf. Sci.* (1978; in press), and personal communication.
28. DeVore, T. C., and Franzen, H. T., *Inorg. Chem.* **15**, 1318 (1976).
29. DeVore, T. C., *Inorg. Chem.* **15**, 1315 (1976).
30. Efremov, Y. M., Samoilova, A. N., and Gurvich, L. V., *Chem. Phys. Lett.* **44**, 108 (1976).
31. Evans, W. J., Engerer, S. C., and Neville, A. C., *J. Am. Chem. Soc.* **100**, 332 (1978).
32. Fischer, E. O., Scherer, F., and Stahl, H. O., *Chem. Ber.* **93**, 2065 (1960).
33. Fischer, E. O., Reckziegel, A., Müller, J., and Goser, P., *J. Organomet. Chem.* **11**, 13 (1968).
34. (a) Garland, C. W., and Yang, A. L., *J. Phys. Chem.* **61**, 1504 (1975); (b) Garland, C. W., Lord, R. C., and Troiano, P. F., *ibid.* **69**, 1188 (1965).

35. Gladysz, J. A., Fulcher, J. G., and Bocarsly, A. B., *Tetrahedron Lett.* p. 1725 (1978).
36. Gladysz, J. A., Fulcher, J. G., and Togashi, S., *J. Org. Chem.* **41**, 3648 (1976).
37. Gladysz, J. A., Fulcher, J. G., and Togashi, S., *Tetrahedron Lett.* p. 521 (1977).
38. Gladysz, J. A., Fulcher, J. G., Lee, S. J., and Bocarsly, A. B., *Tetrahedron Lett.* p. 3421 (1977).
39. Goddard, III, W. A., and Upton, T. H., *J. Am. Chem. Soc.* **100**, 321 (1978).
40. Green, D. W., and Reedy, G. T., *J. Chem. Phys.* **69**, 544 (1978).
41. Green, D. W., and Reedy, G. T., *J. Chem. Phys.* **69**, 552 (1978).
42. Green, M. L. H., Cloke, F. G. N., and Morris, G. E., *J. Chem. Soc., Chem. Commun.* p. 72 (1978).
43. Green, M. L. H., Cloke, F. G. N., and Price, D. H., *J. Chem. Soc., Chem. Commun.* p. 431 (1978).
44. Grinter, R., Barton, T. J., and Thomson, A. J., *J. Chem. Soc. Dalton Trans.* p. 608 (1978).
45. Grinter, R., Barton, T. J., and Thomson, A. J., *Ber. Bunsenges. Phys. Chem.* **82**, 131 (1978).
46. Grinter, R., Barton, T. J., and Thomson, A. J., *Chem. Phys. Lett.* **40**, 399 (1976).
47. Gruen, D. M., Green, D. W., and Hodges, R. V., *Inorg. Chem.* **15**, 970 (1976).
48. (a) Gruen, D., Carstens, D. H. W., Brashear, W., and Eslinger, D. E., *Appl. Spectrosc.* **26**, 185 (1972); (b) Guerra, C. R., and Schulman, J. H., *Surf. Sci.* **7**, 229 (1967).
49. Hanlan, A. J. L., Ph.D. Thesis, University of Toronto, 1978; unpublished work.
50. Harrod, J. F., Roberts, R. W., and Rissman, E. F., *J. Phys. Chem.* **71**, 343 (1967).
51. Hartley, F. R., and Vezey, P. N., *Adv. Organomet. Chem.* **15**, 189 (1977).
52. Hayes, L. G., and Thomas, J. L., *J. Am. Chem. Soc.* **91**, 6876 (1969).
53. Hoffman, R., and Elian, M., *Inorg. Chem.* **14**, 1058 (1975).
54. Hoffman, R., and Elian, M., *Inorg. Chem.* **14**, 375 (1975).
55. Ibers, J. A., Franz, B. A., and Enemark, J. H., *Inorg. Chem.* **8**, 1288 (1969).
56. Kasai, P. H., and McLeod, Jr., D., *J. Chem. Phys.* **55**, 1566 (1971).
57. Kasai, P. H., and McLeod, Jr., D., *Ber. Bunsenges. Phys. Chem.* **82**, 103 (1978).
58. Kasai, P. H., and McLeod, Jr., D., *J. Phys. Chem.* **82**, 1554 (1978).
59. Kasai, P. H., and McLeod, Jr., D., *J. Am. Chem. Soc.* **97**, 6602 (1975).
60. Kasai, P. H., and McLeod, Jr., D., *J. Am. Chem. Soc.* **100**, 625 (1978).
61. Kasai, P. H., McLeod, Jr., D., and Watanabe, T., *J. Am. Chem. Soc.* **99**, 3521 (1977).
62. Kasai, P. H., and McLeod, Jr., D., *J. Am. Chem. Soc.* **97**, 5610 (1975).
63. King, R. B., Chang, M., and Newton, M. G., *J. Am. Chem. Soc.* **100**, 998 (1978).
64. Klabunde, K. J., *Acc. Chem. Res.* **8**, 393 (1975).
65. Klabunde, K. J., and Murdock, T. O., *Chem. Tech. (Leipzig)* p. 624 (1975).
66. Klabunde, K. J., Efner, H. F., Murdock, T. O., and Ropple, R., *J. Am. Chem. Soc.* **98**, 1021 (1976).
67. Klabunde, K. J., Efner, H. F., Satek, L., and Donley, W., *J. Organomet. Chem.* **71**, 309 (1974).
68. Klabunde, K. J., and Davis, S. C., *J. Am. Chem. Soc.* **100**, 5975 (1978).
69. Klabunde, K. J., and Davis, S. C., *J. Catal.* **54**, 254 (1978).
70. Klabunde, K. J., Anderson, B. B., Behrens, C. L., and Radonovich, L. J., *J. Am. Chem. Soc.* **98**, 5390 (1976).
71. Klabunde, K. J., Anderson, B. B., Bader, M., and Radonovich, L. J., *J. Am. Chem. Soc.* **100**, 1313 (1978); Klabunde, K. J., *EUCHEM Conf., Venice, Nov. 1979*.
72. Klabunde, K. J., Groshens, T., Brezinski, M., and Kennelly, W., *J. Am. Chem. Soc.* **100**, 4437 (1978).
73. Klabunde, K. J., and Roberts, J. S., *J. Organomet. Chem.* **137**, 113 (1977).

74. Klabunde, K. J., and Roberts, J. S., *J. Am. Chem. Soc.* **99**, 2509 (1977).
75. Kolb, D. M., Forstmann, F., Leutloff, D., and Schulze, W., *J. Chem. Phys.* **66**, 2806 (1977).
76. Kolb, D. M., and Leutloff, D., *Chem. Phys. Lett.* **55**, 264 (1978).
77. Kolb, D. M., and Forstmann, F., *Ber. Bunsenges. Phys. Chem.* **82**, 30 (1978).
78. Lagowski, J. J., and Graves, V., *Inorg. Chem.* **15**, 577 (1976).
79. (a) Lagowski, J. J., Simons, L. H., Riley, P. E., and Davis, R. E., *J. Am. Chem. Soc.* **98**, 1044 (1976); (b) Lagowski, J. J., and Peer, W. J., *ibid.* **100**, 6262, (1978).
80. Lagowski, J. J., and Simons, L. H., *J. Org. Chem.* **16**, 3247 (1978).
81. Klabunde, K. J., Groshens, T., Efner, W. F., and Kramer, M., *J. Organomet. Chem.* **157**, 91 (1978).
82. Mann, D. M., and Broida, H. P., *J. Chem. Phys.* **55**, 84 (1971).
83. Maslowski, E., "Vibrational Spectra of Organometallic Compounds," Wiley-Interscience, New York, 1977.
84. McGlinchey, M. J., and Tan, T.-S., *J. Chem. Soc., Chem. Commun.* p. 155 (1976).
85. McGlinchey, M. J., Agarwal, A., and Tan, T.-S., *J. Organomet. Chem.* **141**, 85 (1977).
86. McLean, A. D., and Yoshimine, M., *IBM J. Res. Dev. Suppl.* **12**, 206 (1968).
87. Messmer, R. P., in "The Theoretical Basis for Heterogeneous Catalysis" (E. Drauglis and R. K. Jaffee, eds.), Plenum, New York, 1975.
88. Möckel, R., and Elschenbroich, C., *Angew. Chem. Int. Ed. Engl.* **16**, 870 (1977).
89. Montano, P. A., *J. Appl. Phys.* **49**, 1561 (1978); **49**, 4612 (1978); W. Dyson and P. A. Montano, *J. Am. Chem. Soc.* **100**, 7439 (1978).
90. Moore, C., *Natl. Bur. Stand. (U.S.) Circ.* **467**; Vol. I, 1949; Vol. II, 1952; and Vol. III, 1958.
91. Moskovits, M., and Ozin, G. A., "Cryochemistry," Wiley-Interscience, New York, 1976.
92. Moskovits, M., and Hulse, J. E., *J. Chem. Soc. Faraday Trans. 2* p. 471 (1977).
93. Moskovits, M., and Hulse, J. E., *J. Chem. Phys.* **66**, 3988 (1977).
94. Moskovits, M., and Hulse, J. E., *J. Chem. Phys.* **67**, 4271 (1977).
95. Moskovits, M., and Hulse, J. E., *Surf. Sci.* **57**, 125 (1976).
96. (a) Moskovits, M., and Hulse, J. E., *Surf. Sci.* **61**, 302 (1976); (b) M. Moskovits, *Acc. Chem. Res.* **12**, 229 (1979).
97. Nibler, J., Rohhantalab, H. M., and Allamandola, L., *Ber. Bunsenges. Phys. Chem.* **82**, 107 (1978).
98. Ogden, J. S., Darling, J. H., and Garton-Sprenger, M. B., *Faraday Symp. Chem. Soc.* **8**, 75 (1973).
99. Ozin, G. A., *Appl. Spectrosc.* **30**, 573 (1976).
100. Ozin, G. A., *Catal. Rev. Sci. Eng.* **16**, 191 (1977); *Coord. Chem. Rev.* **28**, 117 (1979); *Faraday Soc. Disc., Chem. Soc.* **14**, 1 (1980).
101. Ozin, G. A., Power, W. J., Upton, T., and Goddard, III, W. A., *J. Am. Chem. Soc.* **100**, 4750 (1978).
102. Ozin, G. A., Huber, H., McIntosh, D. F., Mitchell, S. A., Norman, Jr., J. G., and Noodleman, L., *J. Am. Chem. Soc.* **101**, 3504 (1979).
103. Ozin, G. A., *Acc. Chem. Res.* **10**, 21 (1977).
104. Ozin, G. A., and Power, W. J., *Inorg. Chem.* **16**, 212 (1977).
105. Ozin, G. A., and Power, W. J., *Ber. Bunsenges. Phys. Chem.* **82**, 93 (1978).
106. Ozin, G. A., Kündig, E. P., and Moskovits, M., *Nature* **254**, 503 (1975).
107. Ozin, G. A., Klotzbücher, W., and Busby, R., *J. Am. Chem. Soc.* **98**, 4013 (1976).
108. Ozin, G. A., Ford, T. A., Huber, H., Klotzbücher, W., Kündig, E. P., and Moskovits, M., *J. Chem. Phys.* **66**, 425 (1977).

109. Ozin, G. A., Klotzbücher, W. E., and Mitchell, S. A., *Inorg. Chem.* **16**, 3063 (1977).
110. Ozin, G. A., and Klotzbücher, W. E., *Inorg. Chem.* **16**, 984 (1977).
111. Ozin, G. A., and Klotzbücher, W. E., *Inorg. Chem.* **15**, 292 (1976).
112. Ozin, G. A., and Huber, H., *Inorg. Chem.* **17**, 155 (1978).
113. Ozin, G. A., Klotzbücher, W. E., Norman, Jr., J. G., and Kolari, H. J., *Inorg. Chem.* **16**, 2871 (1977).
114. Ozin, G. A., and Klotzbücher, W. E., *J. Mol. Catal.* **3**, 195 (1977/78).
115. Ozin, G. A., and Klotzbücher, W. E., *J. Am. Chem. Soc.* **100**, 2262 (1978).
116. Ozin, G. A., and Klotzbücher, W. E., *Inorg. Chem.* **18**, 2101 (1979).
117. Ozin, G. A., Huber, H., Kündig, E. P., and Moskovits, M., *J. Am. Chem. Soc.* **97**, 2097 (1975).
118. Ozin, G. A., McIntosh, D., and Moskovits, M., *Inorg. Chem.* **15**, 1669 (1976).
119. Ozin, G. A., and Hanlan, A. J. L., *Inorg. Chem.* **16**, 2848 (1977).
120. Ozin, G. A., and Hanlan, A. J. L., *Inorg. Chem.* **16**, 2857 (1977).
121. Ozin, G. A., Hanlan, A. J. L., and Power, W. J., *Inorg. Chem.* **17**, 3648 (1978).
122. Ozin, G. A., Huber, H., and McIntosh, D., *Inorg. Chem.* **16**, 3070 (1977).
123. Ozin, G. A., Huber, H., and Power, W. J., *J. Am. Chem. Soc.* **98**, 6508 (1976).
124. Ozin, G. A., Huber, H., and McIntosh, D., *J. Organomet. Chem.* **112**, c50 (1976).
125. Ozin, G. A., Ford, T. A., Huber, H., Klotzbücher, W., and Moskovits, M., *Inorg. Chem.* **15**, 1666 (1976).
126. Ozin, G. A., Hanlan, L., and Huber, H., *Inorg. Chem.* **15**, 2592 (1976).
127. Ozin, G. A., and Moskovits, M., in "Vibrational Spectra and Structure" (J. Durig, ed.), Elsevier, Amsterdam, 1975.
128. Ozin, G. A., and Lever, A. B. P., *Inorg. Chem.* **16**, 2012 (1977).
129. Ozin, G. A., Hanlan, L. A., Huber, H., Kündig, E. P., and McGarvey, B. R., *J. Am. Chem. Soc.* **97**, 7054 (1975).
130. Ozin, G. A., and McIntosh, D., *J. Am. Chem. Soc.* **98**, 3167 (1976).
131. Ozin, G. A., and McIntosh, D., *Inorg. Chem.* **16**, 51 (1977).
132. Ozin, G. A., Huber, H., and McIntosh, D., *Inorg. Chem.* **16**, 975 (1977).
133. Ozin, G. A., Huber, H., and McIntosh, D., *Inorg. Chem.* **17**, 1472 (1978).
134. Ozin, G. A., and McIntosh, D., *Inorg. Chem.* **16**, 59 (1977).
135. Ozin, G. A., and McIntosh, D., *Inorg. Chem.* **15**, 2869 (1976).
136. Ozin, G. A., and Huber, H., *Inorg. Chem.* **16**, 64 (1977).
137. Ozin, G. A., Huber, H., Klotzbücher, W., and Vander Voet, A., *Can. J. Chem.* **51**, 2722 (1973).
138. Ozin, G. A., Busby, R., and Klotzbücher, W., *Inorg. Chem.* **16**, 822 (1977).
139. Ozin, G. A., Huber, H., Ford, T. A., and Klotzbücher, W., *J. Am. Chem. Soc.* **98**, 3176 (1976).
140. Ozin, G. A., Huber, H., and Power, W. J., *Inorg. Chem.* **16**, 979 (1977).
141. Ozin, G. A., and Power, W. J., *Inorg. Chem.* **17**, 2836 (1978).
142. Ozin, G. A., and Power, W. J., *Inorg. Chem.* **16**, 2864 (1977).
143. Ozin, G. A., and McIntosh, D., *J. Organomet. Chem.* **121**, 127 (1976).
144. Ozin, G. A., and Power, W. J., unpublished data.
145. Ozin, G. A., Huber, H., and Power, W. J., *Inorg. Chem.* **16**, 2234 (1977).
146. Ozin, G. A., Huber, H., and McKenzie, P., *J. Am. Chem. Soc.* (in press).
147. Ozin, G. A., Kenney-Wallace, G., Farrel, J., Mitchell, S., and Huber, H., *J. Am. Chem. Soc.* (submitted).
148. Ozin, G. A., McIntosh, D., Mitchell, S., and Messmer, R. P. (to be published).
149. Ozin, G. A., and Mitchell, S., *J. Am. Chem. Soc.* **100**, 6776 (1978).
150. Ozin, G. A., Mitchell, S., Huber, H., Norman, J. G., and Noodleman, L., *J. Am. Chem. Soc.* **101**, 3504 (1979).

151. Ozin, G. A., and Mitchell, S., paper presented at the "Cluster Symposium," *Am. Chem. Soc. Meet.*, Anaheim, March 1977; and *Inorg. Chem.* **18**, 2932 (1979).
152. Ozin, G. A., Huber, H., and Mitchell, S. (to be published).
153. Ozin, G. A., and Hanlan, A. J. L., *J. Am. Chem. Soc.* **96**, 6324 (1974).
154. Ozin, G. A., and Hanlan, A. J. L., *Inorg. Chem.* **18**, 2091 (1979); **18**, 1781 (1979).
155. Pritchard, J., and Sims, M. L., *Trans. Faraday Soc.* **70**, 427 (1969).
156. Rehder, D., *J. Organomet. Chem.* **37**, 303 (1972).
157. Rest, A. J., and Taylor, D. L., *J. Chem. Soc., Chem. Commun.* p. 717 (1977).
158. Rieke, R. D., *Acc. Chem. Res.* **10**, 301 (1977).
159. Rieke, R. D., Wolf, W. J., Kujundžić, N., and Kavoluinas, A. V., *J. Am. Chem. Soc.* **99**, 4159 (1977).
160. Roberts, M. W., *Chem. Soc. Rev.* **6**, 373 (1977).
161. Roberts, M. W., and Kishi, K., *Surf. Sci.* **62**, 252 (1977).
162. Rothschild, W. G., and Yao, H. C., *J. Chem. Phys.* **68**, 4774 (1978).
163. Schulze, W., Becker, H. V., Minkwitz, R., and Marzel, K., *Chem. Phys. Lett.* **55**, 59 (1978).
164. Schulze, W., *Faraday Soc. Disc. Chem. Soc.* **14** (1980).
165. Seff, K., and Kim, Y., *J. Am. Chem. Soc.* **99**, 7055 (1977).
166. Sheppard, N., Prentice, J. D., and Lesuinans, A., *J. Chem. Soc. Chem. Commun.* p. 76 (1976).
167. Sinfelt, J., *Acc. Chem. Res.* **10**, 15 (1977); Sinfelt, J. H., Cusumano, J. A., Burton, J. J., and Garten, R. L., in "Advanced Material in Catalysis" (Burton, J. J., and Garten, R. L., eds.), Academic Press, New York, 1977.
168. Skell, P. S., Wescott, Jr., L. D., Goldstein, J. P., and Engerl, R. R., *J. Am. Chem. Soc.* **87**, 2829 (1965).
169. Skell, P. S., Kolesnikov, S. P., and Dobson, J. E., *J. Am. Chem. Soc.* **100**, 999 (1978).
170. Smardzewski, R. R., Efner, H. F., Fox, W. B., and Tevault, D. E., *Inorg. Chim. Acta* **24**, 193 (1977).
171. Smardzewski, R. R., Efner, H. F., Fox, W. B., and Tevault, D. E., *J. Organomet. Chem.* **146**, 45 (1978).
172. Sneddon, L. G., Hall, L. W., and Zimmerman, G. J., *J. Chem. Soc. Chem. Commun.* p. 45, 1977.
173. Sneddon, L. G., Zimmerman, G. J., and Wilczynski, R., *J. Organomet. Chem.* **154**, c29 (1978).
174. Somorjai, G., *Angew. Chem. Int. Ed. Engl.* **16**, 92 (1977).
175. Somorjai, G., *Acc. Chem. Res.* **9**, 248 (1976).
176. Stevens, R. D., *J. Org. Chem.* **38**, 2260 (1973).
177. Stone, F. G. A., Treichel, P. M., Pitcher, E., and King, R. B., *J. Am. Chem. Soc.* **83**, 2593 (1961).
178. Stone, F. G. A., King, R. B., Bruce, M. I., and Phillips, J. R., *Inorg. Chem.* **5**, 684 (1966).
179. Timms, P. L., and Turney, T. W., *Adv. Organomet. Chem.* **15**, 53 (1977).
180. Timms, P. L., and Atkins, R. M., *Spectrochim. Acta Part A* **33**, 853 (1977).
181. Timms, P. L., and Atkins, R. M., *Inorg. Nucl. Chem. Lett.* **14**, 113 (1978).
182. Timms, P. L., *J. Chem. Soc. Chem. Commun.* p. 1033 (1969).
183. Timms, P. L., and Kündig, E. P., *J. Chem. Soc. Chem. Commun.* p. 912 (1977).
184. Timms, P. L., and Turney, T. W., *J. Chem. Soc. Dalton Trans.* p. 2021 (1976).
185. Timms, P. L., and Mackenzie, R., *J. Chem. Soc. Chem. Commun.* p. 650 (1974).
186. Timms, P. L., and Piper, M., *J. Chem. Soc. Chem. Commun.* p. 52 (1972).
187. Timms, P. L., and Chivers, T., *J. Organomet. Chem.* **118**, c37 (1976).

188. Timms, P. L., and Francis, C. G., *J. Chem. Soc. Chem. Commun.* p. 466 (1977).
189. Tolman, C. A., English, A. D., and Jesson, J. P., *Inorg. Chem.* **15**, 1730 (1976).
190. Tolman, C. A., English, A. D., Ittel, S. D., and Jesson, J. P., *Inorg. Chem.* **17**, 2374 (1978).
191. Turner, J. J., Burdett, J. K., Perutz, R. N., and Poliakoff, M., *Pure Appl. Chem.* **49**, 271 (1977).
192. Turner, J. J., and Perutz, R. N., *J. Am. Chem. Soc.* **97**, 4791 (1975).
193. Turner, J. J., Burdett, J. K., Grzybowski, J. M., and Poliakoff, M., *J. Am. Chem. Soc.* **98**, 5728 (1976).
194. Verkade, J. G., Tolman, C. A., and Yarbrough, II, L. W., *Inorg. Chem.* **16**, 479 (1977).
195. Vollenbroek, F. A., Bouten, P. C. P., Trooster, J. M., van der Berg, J. P., and Bons, J. J., *Inorg. Chem.* **17**, 1345 (1978).
196. Wada, N., *J. Phys. (Paris)* **C2**, 219 (1977), and references cited therein.
197. Weltner, Jr., W., Ferrante, R. F., Wilkerson, J. L., and Graham, W. R. M., *J. Chem. Phys.* **67**, 5904 (1977).
198. Weltner Jr., W., Van Zee, R. J., and Seely, M. L., *J. Chem. Phys.* **67**, 861 (1977).
199. Wilke, G., Fischer, K., and Jonas, K., *Angew. Chem.* **85**, 620 (1973); *Angew. Chem. Int. Ed. Engl.* **12**, 565 (1973).
200. Wright, R. B., Bates, J. K., and Gruen, D. M., *Inorg. Chem.* **17**, 2275 (1978).
201. Zaitseva, N. N., Nesmeyanov, A. N., Domracher, G. A., Zinov'ev, V. D., Yur'eva, L. P., and Tverdokhlebova, I. I., *J. Organomet. Chem.* **121**, c52 (1976).
202. Zaitseva, N. N., Nesmeyanov, A. N., Yur'eva, L. P., Domracher, G. A., and Zinov'ev, V. D., *J. Organomet. Chem.* **153**, 181 (1978).
- 202a. Zenneck, U., Elschenbroich, C., and Möckel, R., *Angew. Chem. Int. Ed. Engl.* **17**, 531 (1978).
203. Zmbova, B., Ihle, H. R., and Langenscheidt, E., *J. Chem. Phys.* **66**, 5105 (1977).